

2001

The effect of valproic acid on motility and morphometry parameters, and actin and N-cadherin distribution in avian neural crest cells

Leah Christine Fuller
University of Northern Iowa

Copyright ©2001 Leah Christine Fuller

Follow this and additional works at: <https://scholarworks.uni.edu/etd>

Part of the [Developmental Biology Commons](#)

Let us know how access to this document benefits you

Recommended Citation

Fuller, Leah Christine, "The effect of valproic acid on motility and morphometry parameters, and actin and N-cadherin distribution in avian neural crest cells" (2001). *Theses and Dissertations @ UNI*. 598.
<https://scholarworks.uni.edu/etd/598>

This Open Access Thesis is brought to you for free and open access by the Graduate College at UNI ScholarWorks. It has been accepted for inclusion in Theses and Dissertations @ UNI by an authorized administrator of UNI ScholarWorks. For more information, please contact scholarworks@uni.edu.

THE EFFECT OF VALPROIC ACID ON
MOTILITY AND MORPHOMETRY PARAMETERS,
AND ACTIN AND N-CADHERIN DISTRIBUTION
IN AVIAN NEURAL CREST CELLS

An Abstract of a Thesis
Submitted
in Partial Fulfillment
of the Requirements for the Degree
Master of Science

Leah Christine Fuller
University of Northern Iowa
May 2001

ABSTRACT

All vertebrate species contain a transient ectodermal structure termed the neural crest from which a specific subpopulation of migratory cells, the neural crest cells (NCCs), is derived. Following an epithelial-mesenchymal transition, NCCs actively migrate throughout the developing embryo. Precise temporal and spatial cellular migration is essential for the formation of a diverse array of neural crest derived tissues and structures. Valproic acid (VPA) is a unique anti-convulsant drug that can produce craniofacial and neural tube defects in exposed infants. Alterations of NCC migration, proliferation, and cytoskeletal composition have been proposed as mechanisms of VPA's teratogenicity. To investigate this drug's effects on NCCs, trunk neural fold explants were microdissected from chick embryos and cultured in the presence of 0.75- 3.0 mM VPA. Computer assisted video image analysis, BrdU proliferation assays, and immunostaining with antibodies to F-actin and N-cadherin (A-CAM) were employed to investigate NCC behavior during VPA exposure. Overall cell area and width parameters were decreased compared to controls for all VPA-treated groups. Perimeter, length, elongation index, and migration velocity were not consistently changed from controls. Dynamic change in area and dynamic change in perimeter appeared to be negatively correlated with VPA concentration. This suggests inhibited cellular motile activity in the presence of VPA. VPA exposure increased the number of explants exhibiting a continuous epithelial layer of cells extending from the periphery of the attached explants, indicating a disturbed ability of the NCCs to complete the epithelial-mesenchymal transition necessary for proper migration. Proliferation assays revealed that 2.0 mM VPA

significantly lowered BrdU incorporation by 11.2% compared to controls. BrdU incorporation was inhibited 100% at 3.0 mM VPA. Immunostaining analysis of VPA exposed explants revealed A-CAM positive cell-cell junctions within attached epithelial sheets. Independent NCCs within the same cultures were not positive for A-CAM. This suggests VPA altered A-CAM regulation, inhibiting the ability of NCCs to break free of their adherens junctions. F-actin staining revealed dose-dependant decreases in the staining intensity of stress fibers and cortical areas of independent NCCs. In a small proportion of 2.0 mM VPA exposed NCCs there was an irregular, globular distribution of intense (bright) staining not seen in any other concentrations. This pattern was also seen in many rounded cells at this concentration. Within explant attached epithelial sheets, only cortical areas of NCCs were stained positively. Stress fiber staining was absent. Alteration of neural tube integrity and NCC motile capabilities through increased cell-cell adhesion, and lowered or terminated cell proliferation could promote the development of NTDs such as spina bifida. Other VPA induced defects might consequently be produced through lowered number of NCCs available to contribute to neural crest derivatives.

THE EFFECT OF VALPROIC ACID ON
MOTILITY AND MORPHOMETRY PARAMETERS,
AND ACTIN AND N-CADHERIN DISTRIBUTION
IN AVIAN NEURAL CREST CELLS

A Thesis

Submitted

in Partial Fulfillment

of the Requirements for the Degree

Master of Science

Leah Christine Fuller


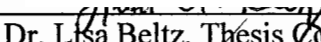
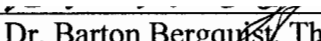
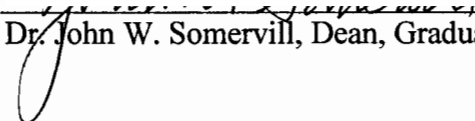
University of Northern Iowa

May 2001

This Study By: Leah Christine Fuller

Entitled: THE EFFECT OF VALPROIC ACID ON
MOTILITY AND MORPHOMETRY PARAMETERS,
AND ACTIN AND N-CADHERIN DISTRUBUTION
IN AVIAN NEURAL CREST CELLS

Has been approved as meeting the thesis requirement for the
Degree of Master of Science

<u>12-11-00</u> Date	 Dr. Darrell Wiens, Chair, Thesis Committee
<u>12/11/2000</u> Date	 Dr. Lisa Beltz, Thesis Committee Member
<u>12/11/2000</u> Date	 Dr. Barton Bergquist, Thesis Committee Member
<u>2/1/2001</u> Date	 Dr. John W. Somervill, Dean, Graduate College

DEDICATION

This thesis is dedicated to my father, who taught me that if a thing is worth doing, it's worth doing well; and to my husband, without whose continued support and patience this work would not have been completed.

ACKNOWLEDGEMENTS

Funding for this research was provided by the University of Northern Iowa Graduate College and The American Heart Association. Thank you to Dr. Darrell Wiens for your excellent teaching, guidance, and advice in all areas of this project. Thank you to Dr. Lisa Beltz and Dr. Barton Bergquist for your comments and review of this manuscript. Thank you to Shannon Cornelius for your assistance with the fluorescence microscopy. Finally, thank you to my husband, Don, for data entry assistance.

TABLE OF CONTENTS

	PAGE
LIST OF TABLES	vii
LIST OF FIGURES	viii
CHAPTER 1. INTRODUCTION	1
Problem	1
Objectives	7
Literature Review.....	7
Neural Crest Cells	7
Morphogenesis of the Neural Crest	11
Cell Motility.....	24
Neural Tube Defects: Spina Bifida	28
Cell Migration and NTD Formation	31
Role of Cell Proliferation in NTD Formation.....	32
Valproic Acid.....	33
Mechanism of Action.....	34
Evidence for Weak Teratogenicity	37
Mechanisms of Teratogenesis.....	42
VPA Effects Cell Motility and the Cytoskeleton.....	48
CHAPTER 2. MATERIALS AND METHODS	52
Isolation and Culture of NCCs.....	52
Image Capture.....	53

	PAGE
Motion Analysis.....	54
Statistical Analysis.....	57
Immunohistochemistry.....	57
Proliferation Assay.....	59
CHAPTER 3. RESULTS.....	61
The Effect of Valproic Acid on NCC Emigration and Explant Morphology	61
The Effect of Valproic Acid on Cell Morphometry and Cell Morphology.....	67
The Effect of Valproic Acid on Cell Proliferation	83
The Effect of Valproic Acid on N-Cadherin (A-CAM) Expression.....	85
The Effect of Valproic Acid on Stress Fiber Distribution	93
CHAPTER 4. DISCUSSION	103
The Effect of VPA on Explant Attachment	104
The Effect of VPA on NCC Morphology in Culture.....	104
The Effect of VPA on NCC Motility in Culture	105
The Effect of VPA on the Actin Cytoskeleton.....	106
The Effect of VPA on Epithelial Sheet Morphology.....	108
The Effect of VPA on Cell-Substratum and Cell-Cell Contacts.....	108
The Effect of VPA on Cell Proliferation.....	111
Summary	112
LITERATURE CITED	113

LIST OF TABLES

TABLE	PAGE
1 The effects of VPA on explant attachment rates and cell emigration rates after 24 hours in culture.....	63
2a The effect of 0.75mM VPA on NCC morphometry parameters.....	71
2b The effect of 1.5 mM VPA on NCC morphometry parameters.....	72
2c The effect of 2.0 mM VPA on NCC morphometry parameters.....	73
2d The effect of 3.0 mM VPA on NCC morphometry parameters.....	74
3a The effect of 0.75mM VPA on NCC motility parameters.....	75
3b The effect of 1.5 mM VPA on NCC motility parameters.....	76
3c The effect of 2.0 mM VPA on NCC motility parameters.....	77
3d The effect of 3.0 mM VPA on NCC motility parameters.....	78
4 Proliferation assay results of BrdU incorporation into nuclei of dividing NCCs in culture.....	84

LIST OF FIGURES

FIGURE	PAGE
1 Structural formula of VPA.....	33
2 Stage 10 embryo as seen for microdissection.....	52
3 Computer generated image of migratory NCCs cultured in the control condition.....	55
4 The effects of VPA on explant attachment and cell emigration rates after 24 hours in culture.....	64
5a Control explant as seen with a phase contrast microscope.....	65
5b 2.0 mM VPA-treated explant as seen with a phase contrast microscope.....	66
6a Example of control cells ready for video image analysis with Optimas.....	69
6b Example of 2.0 mM VPA-treated cells just prior to video image analysis with Optimas.....	70
7 Mean percent increase or decrease from control in median value for morphometry parameters \pm standard error.....	81
8 Mean percent increase or decrease from control in median value for motility parameters \pm standard error.....	82
9a Phase contrast image of explant cultured in 0.75 mM VPA.....	87
9b Explant cultured in 0.75 mM VPA, primary antibody to A-CAM detected with a Cy-3 fluorescent label.....	88
10a Phase contrast image of explant cultured in 1.5 mM VPA.....	89
10b Explant cultured in 1.5 mM VPA, immunostained with primary antibody to A-CAM and detected with a Cy-3 fluorescent label.....	90
11a Phase contrast image of explant cultured in 2.0 mM VPA.....	91
11b Explant cultured in 2.0 mM VPA, immunostained with primary antibody to A-CAM and detected with a Cy-3 fluorescent label.....	92

FIGURE	PAGE
12 NCCs cultured in control condition, immunostained with FITC-conjugated phalloidin.....	95
13 NCCs cultured in 0.75 mM VPA, immunostained with FITC-conjugated phalloidin.....	96
14 NCCs cultured in 0.75 mM VPA, immunostained with FITC-conjugated phalloidin.....	97
15 NCCs cultured in 1.5 mM VPA, immunostained with FITC-conjugated phalloidin.....	98
16 NCCs cultured in 1.5 mM VPA, immunostained with FITC-conjugated phalloidin.....	99
17 NCCs cultured in 1.5 mM VPA, immunostained with FITC-conjugated phalloidin.....	100
18 NCCs cultured in 2.0 mM VPA, immunostained with FITC-conjugated phalloidin.....	101
19 NCCs cultured in 3.0 mM VPA, immunostained with FITC-conjugated phalloidin.....	102

CHAPTER 1

INTRODUCTION

Problem

All vertebrate species contain a transient ectodermal structure termed the neural crest from which a specific subpopulation of migratory cells, the neural crest cells (NCCs), emerges. Individual NCCs are multipotent and have demonstrated limited ability to self renew, such as do stem cells (LaBonne and Bronner-Fraser 1998). The interaction between the neural tube/plate and the ectodermal epidermis induces formation of the NCC population as the apical tips of the neural folds appose. In the cranial portions of the tube, detachment of NCCs begins prior to fusion of the folds, whereas in the trunk, they detach after the neural folds have fused. NCCs will migrate into the extracellular matrix facilitated by the breakdown of the basal lamina, loss of intercellular junctions, loss of neural cell adhesion molecules (CAMs), an increase in fibronectin, and an extension of cellular processes (Campbell and others 1986).

The three subprocesses of neural crest morphogenesis are initiation of migration, dispersion of NCCs away from the neural tube, and termination of migration as cells reach their final destination (Erickson and Perris 1993). As the surface ectoderm closes above the neural tube, the NCCs emerge from the dorsal portion of the neural tube through an epithelial-mesenchymal transition induced by interactions of the neural plate and the epidermis. Many specific cell changes within the neural tube have been recorded during initiation of migration. These include a reduction in cell-cell adhesion, and increase in cell-matrix-adhesion, a general increase in motility correlated with

cytoskeletal reorganization and an increase in protease activity. The mechanism and regulatory cues coordinating the classic epithelial-mesenchymal transition for NCC migration are largely a mystery. The loss or destruction of adhesion proteins involved in the junctions may be responsible for this transition. Protein kinase-C inhibitors have been demonstrated to have the ability to induce an epithelial-mesenchymal transition (Minichiello and others 1999). The basement membrane of the dorsal neural tube is discontinuous prior to and during NCC migration initiation, a necessary step for proper emigration (Erickson and Perris 1993). Cell adhesion molecules (CAMs) of the cadherin superfamily, typically E-cadherin or N-cadherin (A-CAM), are localized principally in differentiated adherens junctions (Duband and others 1988). They also can mediate adhesion independent of their incorporation into junctions (Gumbiner 2000). The adhesion molecules N-CAM, L-CAM and T-cadherin, known to mediate cell-cell attachment, are seen in the neural tube. Transmission electron microscopy analysis has revealed well-developed adherens junctions at the apical surface of the dorsal neural tube. These cadherin-based junctions must be broken before NCC detachment can take place.

The prominent scenario depicting NCC migration is that of active migration based on a balanced environment of promoting and inhibitory signals from a variety of molecules within the extracellular matrix. There have been several matrix components identified along the dorsolateral side of the neural tube as strong promoters of migration including fibronectin, laminin, and collagen types I, III, IV, and VI. Focal adhesions (or contacts or adhesion plaques) are found on the underside of a migrating cell. They are rich in the structural proteins vinculin, paxillin, talin, and α -actinin, in addition to

integrins, which are responsible for cell attachment to the matrix. Tyrosine kinases including focal adhesion kinase (FAK), c-Src, and c-Csk are also associated with these structures and are believed to play critical roles in cell-substrate adhesion and promotion of motility (Schaller and others 1992; Bergman and others 1995; Burridge and others 1992; Ilc and others 1995; Kornberg and others 1992; Lipfert and others 1992; Richardson and Parsons 1995; Cary and others 1996; Klemke and others 1994).

The final stage of migration involves the cells reaching their target location and ceasing migration. The extracellular signals directing this may be the opposite of those responsible for initiation of migration (Erickson and Perris 1993). NCCs contribute to facial cartilage, connective tissue, and bone; sensory neurons and glia; Schwann cells; brachial, mandibular, and hyoid arches; melanocytes; smooth muscle; and chromaffin (adrenal) cells (Bronner-Fraser 1993).

The crawling movements of cells can be broken down into three steps: extension of a leading edge, attachment of this edge to the substratum, and retraction of the rear of the cell into the cell body. These cell movements are produced by the cytoskeleton, a complex cohesive network of filaments and proteins in conjunction with the cortical layer of actin filaments associated with a diverse collection of actin-binding proteins.

Crawling cells have a leading lamella, a flat anterior end, and narrow tail, creating an observable polarity. The term “cortical flow” encompasses movements of the lamellar substance. A dynamic cycle of actin assembly and disassembly operates throughout the entire lamella. This complex internal scaffolding is useless without the accessory proteins that link the filaments to each other and to other parts of the cell. They

strengthen the cytoskeleton by crosslinking and forming bundles within it, and allow generation of internal movements of organelles using the filaments like tracks.

All pregnancies carry a three percent risk for a major birth defect independent of any intrinsic or extrinsic factors (Buehler and others 1994). Neural tube defects (NTDs) are malformations affecting the brain and/or spinal cord that may or may not result from abnormal neural tube closure (DeSesso and others 1999). Spina bifida and anencephaly account for 50% and 40%, respectively, of NTD cases (Lewis and others 1998). Spina bifida includes all abnormalities in which vertebral arches fail to close dorsal to the spinal cord to form the vertebral canal, and may or may not involve the spinal cord itself. There are several types of spina bifida ranging from no impairment to severe impairment.

The etiology of NTDs is multifactorial. Fetal drug exposure is one of many important factors in NTD development. At least 221 teratogenic agents have been associated with the production of NTDs in at least one species (DeSesso and others 1999). Valproic acid (VPA), a weak human teratogen, is a simple eight carbon, branched-chain fatty acid. It is mainly indicated as prevention or cure for myoclonic seizures, partial seizures, status epilepticus, and tonic-clonic seizures, mania, and migraine (Browne 1980). The exact mechanism of VPA's beneficial effects as well as its teratogenic potential is poorly understood. Multiple reports since 1976 have shown VPA to be a potent teratogen in the rabbit, mouse, rat, hamster, axolotl, and chick. The most common NTD seen in human infants exposed to VPA is spina bifida. Spina bifida has been shown to result from lowered cellular proliferation in the neuroepithelium.

Numerous studies have demonstrated that when it is altered, NTDs can result (Copp 1988, 1990; Bennett and others 2000).

Matrix and cell adhesion molecules, when disturbed at the time of neurulation, can also be involved in the generation of NTDs by altering cell adhesion dependant morphogenic events (Newgreen and others 1997). When the extracellular matrix molecules laminin, fibronectin, and chondroitin sulfate proteoglycan and the cell adhesion molecules E- and N- cadherin, and N-CAM were examined in quail embryos with spontaneous NTDs, it was determined that these molecules are disturbed in spontaneous NTDs during neurulation (Newgreen and others 1997).

Several hypotheses are being investigated to identify the mechanism(s) of VPA's teratogenicity. These hypotheses include interference with embryonic lipid metabolism, interference with zinc metabolism, and interference with neurotransmitter metabolism (Clarke and Brown 1987; Wegner and others; Nau 1994). Another hypothesis examines alteration of intracellular pH, which is an important parameter of numerous cellular functions and seems to be a promising area of study because the early mammalian embryo has a relatively high intracellular pH and may then accumulate acidic compounds such as VPA via ion trapping (Scott and others 1990 cited in Nau 1994). Lastly, interference with embryonic folate metabolism is currently being investigated (Nau 1994).

VPA has been shown to inhibit the proliferation of neuronal cells in culture and recent studies have been carried out to determine the explanation. Transcriptional activities of genes coding for several growth factors, receptors and neurotrophic factors

was investigated by Bennett and associates (2000). They used two VPA sensitive strains of mice, LM/Bc (less) and SWV (more), and found that transcriptional activity of neurotrophic and growth factor genes were altered during neurulation in the presence of VPA.

VPA and VPA-analogues have been demonstrated to increase mean cell area of cultured fibroblastoid L-cells in correlation with the teratogenic potential of each analogue tested (Berezin and others 1996). Walmod and others (1999) demonstrated that after treating L929 cells with 3mM there was increased flattening and spreading of the cells compared to control. Overall, the cells were larger and had more and/or longer processes. Relative F-actin per cell was calculated and found to be significantly higher (23%) for treated cells. F-actin distribution was altered indicated by an increase amount of stress fibers, and a decrease in cortical F-actin and lower numbers of membrane ruffles. VPA treatment induced an increase of phosphotyrosine, paxillin, vinculin, and focal adhesion kinase (FAK). This supports the hypothesis that VPA might cause a decrease in cell motility through increased cell-substratum adhesion (Walmod and others 1999). Walmod and others (1998) performed experiments on fibroblastoid L-cells in 3.0 mM VPA, and found that cellular migration was inhibited in a dose dependant manner. Confocal micrographs of fluorescence staining of microtubules, F-actin, and selected focal adhesion proteins demonstrated that VPA-exposure caused an enhanced focal adhesion formation accompanied by a rearrangement of F-actin reflected by an increase in stress fiber formation (Walmod and others 1998). In addition, treated cells seemed to be devoid of microspikes, which were observed in great numbers in control cells.

Objectives

Left and right neural folds will be dissected from chick embryos of Hamburger-Hamilton stages 10⁻ - 10⁺ (Hamburger and Hamilton 1951). One fold will be cultured as a control. The other will be cultured in the presence of 0.75, 1.5, 2.0, or 3.0 mM VPA. The neural fold explants and migratory NCCs will be analyzed after 24 hours of culture.

The objectives of this study were: (1) to assess the effect of VPA on overall morphology in culture of both the neural fold explants and associated migratory NCCs using computer-assisted video image analysis; (2) to evaluate VPA's effect on motile behavior of the cultured migrating NCCs using computer-assisted video image analysis; (3) to determine VPA's effect on the proliferation rate of NCCs; and (4) to reveal the effect of VPA on the cellular distribution of N-cadherin (A-CAM), and filamentous actin in both control and drug-treated groups.

Literature Review

Neural Crest Cells

Towards the end of gastrulation there are three layers of cells, the ectoderm, endoderm, and mesoderm. Each layer gives rise to specific structures in the developed embryo. The entire nervous system and the epidermis are derived from the ectoderm (Bronner-Fraser 1998). All vertebrate species contain a transient ectodermal structure termed the neural crest from which a specific subpopulation of migratory cells, the neural crest cells (NCCs), emerges. Traditionally, NCCs have been thought of as a segregated population of cells within the neural plate, bordered by presumptive epidermis and central nervous system. Recent cell lineage analyses, however, have indicated a common

origin within the neural folds for epidermal, neural crest and neural tube derivatives. Individual NCCs are multipotent and have demonstrated limited ability to self renew, such as do stem cells (LaBonne and Bronner-Fraser 1998).

In the chick, neurulation comprises several phases and has distinct patterns. During neural induction, the medial ectoderm thickens and then invaginates into a neural groove. The paired crests of the neural groove rise and come into contact initially in the head region at several different locations. The first closure site is in the future mesencephalon at approximately 30 hours post incubation at Hamburger-Hamilton stage 8 (Hamburger and Hamilton 1951). Within 4 hours, a second closure site is seen at the rhombocervical level in the form of multisite contacts of the neural folds. The folds continue to meet and close caudally in a zipperlike manner as the apical tips of the neural folds appose and numerous contact points are made. The folds fuse mainly in a posterior direction to form a complete tube open at both ends that separates from the adjacent ectoderm.

The interaction between the neural tube/plate and the ectodermal epidermis induces formation of the NCC population as the apical tips of the neural folds appose. Evidence points to the proteins dorsalin-1, BMP-4 and BMP-7, all members of the transforming growth factor β superfamily, to be involved with this interaction (Basler and others 1993; Liem and others 1995). These proteins are expressed in the epidermal ectoderm at the time of neural crest induction in the chick and are sufficient to substitute for the non-neural ectoderm in inducing NCCs *in vitro* (Liem and others 1995). When

BMP4 and BMP7 activity is blocked, the epidermal ectoderm is unable to induce NCCs (Liem and others 1997).

In the cranial portions of the tube, detachment of NCCs begins prior to fusion of the folds, whereas in the trunk, they detach after the neural folds have fused. NCCs migrate into the extracellular matrix facilitated by the breakdown of the basal lamina, loss of intercellular junctions, loss of neural cell adhesion molecules (CAMs), an increase in fibronectin, and an extension of cellular processes (Campbell and others 1986). Within the neural folds, individual precursor cells have the potential to contribute to the epidermal, neural tube, or neural crest lineages. Currently it is not understood exactly what causes only specific cells to leave, or when during their migration these cells become committed to a certain fate. Timing of emigration appears to restrict the range of possible NCC derivatives (Serbedzija and others 1994).

Cranial derived NCCs of the caudal forebrain populate the cardiac ganglion and the enteric ganglia of the gut. Those of the midbrain contribute to most of the facial cartilage and bone, facial connective tissues, ciliary and trigeminal ganglion, and Schwann cells. Hindbrain NCCs migrate to form the mandibular and hyoid arches, genticulate and vestibular ganglia, brachial arches, peripheral ganglia, cardiac ganglia, enteric ganglia, melanocytes, and chromaffin (adrenal) cells. Trunk derived NCCs form melanocytes, sensory neurons and glia, sympathoadrenal cells, smooth muscle, and Schwann cells (Bronner-Fraser 1993).

There are two models to explain the considerable differences in the fates of these seemingly identical cells. The environment-directed model maintains that most NCCs

are multipotent when they leave the neural tube, and the timing of their departure depends on the environmental cues encountered at dispersion. Differentiation occurs as exposure to local environmental cues changes along each particular path. In a number of studies, single avian NCCs have been isolated and allowed to proliferate into a colony of clones in the presence of differing growth factors. Melanocytes, sympathetic neuroblasts, and sensory neurons were all observed in the different cultures. Similar *in vitro* studies with rat and mouse NCCs resulted in a trio of differing cell types for each respective experiment (Stemple and others 1992; Ito and others 1993; and Shah and others 1996) supporting the environment-directed model.

In the phenotype-directed model, NCCs are specified as a particular lineage around the time of emigration from the neural tube. This specification results in molecular changes in NCC subpopulations, thus directing the specific migratory path to be taken. There is much less evidence for this type of specification (Bronner-Fraser 1995; Erickson and Reedy 1998).

It has also been suggested that escape from the neural tube may be responsible for the separation of the NCC lineage. Fate-mapping studies have demonstrated that large numbers of NCCs must be destroyed to effect the final derived structures. Ablation of a small portion of the mesencephalic, occipital, or cervical dorsal neural tube does not result in an abnormal embryo (Bronner-Fraser 1995). Ablation of cardiac NCCs frequently generates abnormal heart, great vessel, and parasympathetic nerve development. Following ablation of NCCs, replacement cells migrate into the gap from both anterior and posterior positions. Increased cell division or decreased cell death near

the extirpation site may also contribute to cell replacement, but evidence is currently lacking (Vaglia and Hall 1999). It is clear that in a normal embryo, the region that actually becomes neural crest is only a portion of the overall potential region (Bronner-Fraser 1995; Selleck and Bronner-Fraser 1996).

Because migrating NCCs are morphologically indistinguishable from other embryonic cell types, specific markers had to be developed in order to study them. HNK-1 (NC-1) antibody has been very effective, especially in avian studies. It does not appear to label mouse or amphibian NCCs however. Lipophilic fluorescent dyes have been used to inject both single cells and cohorts of presumptive NCCs with excellent results (Selleck and Bronner-Fraser 1996). Because NCC migration routes are so intimately linked to the cell's final fate, it is essential to understand pathway establishment and guidance mechanisms underlying their migration.

Morphogenesis of the Neural Crest

The three subprocesses of neural crest morphogenesis are initiation of migration, dispersion of NCCs away from the neural tube, and termination of migration as cells reach their final destination. Continuous cell-cell and cell-matrix interactions are known to govern each particular step of morphogenesis, but the specific mechanisms involved in NCC detachment from the neural epithelium as well as the onset of migration are poorly understood (Erickson and Perris 1993). As the surface ectoderm closes above the neural tube, the NCCs emerge from the dorsal portion at the region of the most newly formed somite through an epithelial-mesenchymal transition induced by interactions of the neural plate and the epidermis. The ability of the neural plate to respond to inductive cues

appears to depend on the age of the embryo. NCCs emerge in a wave that begins in the anterior of the embryo and proceeds posteriorly. A number of factors have been proposed to be critical at this step including: (1) basement membrane disruption permitting NCC escape; (2) deposition of suitable migratory substratum for NCC migration along the dorsal neural tube; (3) acquisition of motile capabilities; and (4) loss of high affinity cell-cell adhesions with an increase in cell-matrix adhesion. The molecular event(s) that are responsible for triggering initial emigration is still largely a mystery, but many specific cell changes within the neural tube have been recorded. These include a reduction in cell-cell adhesion, and increase in cell-matrix-adhesion, a general increase in motility correlated with cytoskeletal reorganization and an increase in protease activity (Erickson and Perris 1993).

The basement membrane of the dorsal neural tube is discontinuous prior to and during NCC migration initiation. It is continuous in the remaining portions where NCCs are not seen. Before the fusion of the neural folds, one of the first morphogenic events seen during head NCC migration is disruption of the neural epithelial basement membrane that envelops them. In addition, early migrating NCCs seem unable to penetrate intact basement membranes *in vivo* or when challenged in culture with a placental membrane. Taken together, this supports the idea that lack of intact basement membrane is a necessary step for proper emigration (Erickson and Perris 1993).

NCCs are recognizable as a separate population once they have emerged from the neural tube. The mechanism and regulatory cues coordinating this classic epithelial-mesenchymal transition for NCC migration are largely a mystery. One theory implies

that NCCs are able to generate enough tractional force (based on increased NCC affinity for fibronectin and laminin just prior to migration) to simply pull away from the adherens junctions anchoring them to the luminal surface. NCCs are known to produce a number of proteases and their production increases about the time of emigration.

Another theory states that the loss or destruction of adhesion proteins involved in the junctions is responsible for the transition. In all solid tissues, cadherins are major cell-cell adhesion molecules involved in development and maintenance. Cadherins form tight complexes with catenins, believed to link the cadherins functionally to the actin cytoskeleton. Cell adhesion molecules (CAMs) of the cadherin superfamily, typically E-cadherin or N-cadherin (A-CAM), are localized principally in differentiated adherens junctions (Duband and others 1988). They also can mediate adhesion independent of their incorporation into junctions (Gumbiner 2000). Transmission electron microscopy analysis has revealed well-developed adherens junctions at the apical surface of the dorsal neural tube. The adhesion molecules N-CAM, L-CAM and T-cadherin, known to mediate cell-cell attachment, are also seen in the neural tube. These cadherin-based junctions must be broken before NCC detachment can take place. In some studies, lower levels of A-CAM have been seen in the dorsal neural tube just prior to NCC migration. There is other evidence, however, that supports the loss of function of A-CAM instead. It has been suggested that the state of phosphorylation of junctional proteins regulates A-CAM function by adjusting cadherin connection to the cytoskeleton of the NCCs (Erickson and Perris 1993; Selleck and Bronner-Fraser 1996; Erickson and Reedy 1998). It has been discovered that A-CAM and E-cadherin both are lost from the NCCs prior to

or shortly after detachment from the neural tube as they initiate migration. In mice with abnormally high levels of N-CAM, NCCs fail to migrate from segments of the neural tube, and the resulting embryos display spina bifida (Moase and Trasler 1990, 1991). It is known that chick NCCs also downregulate cadherin-B6 and upregulate cadherin-7 while losing their neuroepithelial morphology (Akitaya and Bronner-Fraser 1992; Nakagawa and Takeichi 1995).

Protein kinase-C inhibitors can also induce epithelial-mesenchymal transitions. Conventional, novel and atypical isoforms of protein kinase-C are found in embryonic neural tissues. Immunolocalization has shown atypical isoforms enriched at the apical margin of the neural epithelia, overlapping with A-CAM and F-actin. Because atypical protein kinase-C isoforms are present at the appropriate developmental stage and subcellular site, they may contribute to the epithelio-mesenchymal transition of neural cells (Minichiello and others 1999).

A-CAM's role as an adhesion molecule is also involved in the establishment of embryonic asymmetry. It is one of the earliest proteins to be asymmetrically expressed in the chick embryo. For proper establishment of the left-right axis, it must be expressed during gastrulation. Blocking A-CAM function randomizes heart looping and alters the expression of later components of the molecular cascade resulting in left-right asymmetry (Garcia-Castro and others 2000).

Bone morphogenic protein (BMP) family members are strong candidates for specification of NCC fate (Shah and others 1996). Identification of genes induced by bone morphogenic proteins (BMPs) might help elucidate the mechanism of induction. In

chick, the zinc finger transcription factor *slug* is expressed in both the dorsal folds of the neural plate and neural tube, and later in migrating NCCs (Liem and others 1995). A reorganization of the cytoskeleton, and cell surface adhesion molecules and receptors accompanies the onset of NCC migration. Little is known about the extent of regulation of expression of cell surface proteins by BMP signaling. In a screen for molecules participating in early steps of NCC differentiation via BMP induction, *rhoB* was identified. This molecule is a member of the *rho* gene family, which code for small GTP-binding proteins of the *ras* superfamily. The three major members of this family, rho, rac, and cdc42 appear to be involved in adhesion, morphology, motility, and cell cycle progression (Hall 1998; Van Aelst and D'Souza-Schorey 1997). *RhoB* is expressed selectively by cells in the dorsal neural tube upon induction by BMPs. It also is transiently expressed in migrating NCCs. They are prevented from delamination of the dorsal neural epithelium when rho activity is blocked by C3 endotoxin, suggesting a role for *rhoB* in this step. NCCs have a more elongated morphology overall when rho activity is blocked, but no significant changes are noted in migration (Liu and Jessell 1998).

NCC emigration does not appear to be triggered by the main extracellular matrix molecules present in migratory pathways. Premigratory NCCs have reduced adhesion and locomotion capabilities on ECM molecules compared to migratory crest cells. During the transition from premigratory to migratory, NCCs gradually acquire the ability to adhere to substratum. Extracellular matrix molecules failed to induce premature migration from premigratory NCCs, therefore a soluble factor may be present in the extracellular environment that may induce emigration. Transforming growth factor β is a

leading candidate. It is expressed early during embryogenesis, it's involved in a variety of morphogenic processes, and it regulates integrin expression. Delannet and Duband (1992) found that transforming growth factor β is able to induce premature emigration from the neural tube and enhance fibronectin adhesion of NCCs *in vitro*. It does not, however, seem to affect the cell-cell adhesion, proliferation, or locomotory behavior of NCCs. Potentially it may modify either the expression pattern or binding specificities of integrins on the surface of these cells (Delannet and Duband 1992).

Once out of the tube, all NCCs are morphologically similar, but migrate along distinct pathways and differentiate into a variety of cell types. In general, active NCCs appear to migrate without the guidance of long-range chemical or physical cues, using instead the heterogeneity of the extracellular matrix substratum (Henderson and Copp 1997). The prominent scenario depicting NCC migration is that of active migration based on a balanced environment of promoting and inhibitory signals from a variety of molecules within the extracellular matrix. There have been several matrix components identified along the dorsolateral side of the neural tube as strong promoters of migration including fibronectin, laminin, and collagen types I, III, IV, and VI. Functional cell-matrix receptors on the cell surface are also required to interact with the matrix, and appropriate cell markers are needed to mediate attachment. Integrins comprise a family of cell surface heterodimeric glycoproteins capable of binding both matrix molecules and cell surface receptors. Recruitment of integrins by their ligands induces the formation of focal adhesion sites where complex signaling machinery is established between integrin clusters and the cytoskeleton. NCCs express a minimum of eleven distinct heterodimers

of integrin. At least five $\alpha 1$ and three $\beta 1$ integrins are implicated in the interaction of NCCs with fibronectin and laminin (Henderson and Copp 1997). Not all integrins expressed are involved in adhesion and migration however; they may have additional functions relating to cell proliferation, survival, and differentiation. Such a diversity of receptors is believed to allow migrating cells to adapt to multiple changes of environment as they populate various areas of the embryo (Testaz and others 1999). Laminin, a major component of basal laminae, functions in NCC adhesion, migration and differentiation. Receptors for laminin include at least nine members of the integrin family. In NCCs, the $\alpha 1 \beta 1$ member binds a unique fragment of laminin compared to other cell types, and this may be responsible for some of the differing adhesive responses for the different cell types (Desban and Duband 1997). Other matrix receptors may be involved in the onset and early NCC migration, but data is limited due to lack of immunological and molecular probes for avian receptors (Erickson and Perris 1993).

Focal adhesions (or contacts or adhesion plaques) are found on the underside of a migrating cell. They are patches of the cell membrane that interact with the extracellular matrix, remaining in a fixed position on the substratum while the cell passes over. If a cell is rapidly displaced such as with a blast of fluid, the focal adhesions are left behind, indicating they were anchored to the substratum. They are rich in the structural proteins vinculin, paxillin, talin, and α -actinin, in addition to integrins. Integrins are found embedded in the plasma membrane with a site for fibronectin attachment on the exterior of the cell, and site for talin attachment inside. Talin is then connected to vinculin, which is associated with α -actinin and cortical actin filaments of the cytoskeleton (Bray 1992).

Tyrosine kinases including focal adhesion kinase (FAK), c-Src, and c-Csk are also associated with these structures and are believed to play critical roles in cell-substrate adhesion and promotion of motility (Schaller and others 1992; Bergman and others 1995; Burridge and others 1992; Illic and others 1995; Kornberg and others 1992; Lipfert and others 1992; Richardson and Parsons 1995; Cary and others 1996; Klemke and others 1994).

The receptors for epidermal growth factor and hepatocyte growth factor, soluble factors that can induce epithelial-to-mesenchymal transition (EMT) are protein tyrosine kinases (PTKs) (Komada and Kitamura 1993). Tyrosine kinase inhibitors have been shown to elevate cadherin levels at cell adhesions and increase NCC-cell adhesion (Monier-Gavelle and Duband 1995). Because NCCs can be influenced by protein tyrosine kinase-derived signals (also see below), it is reasonable to hypothesize that protein tyrosine phosphatases (PTPases) co-regulate these events via phosphotyrosine signals. Numerous cytoplasmic and transmembrane PTPase genes have been identified and have been found to be receptor-like molecules structurally related to cell adhesion molecules (CAMs). Scant information is available concerning the potential cooperative influences of PTPases and PTKs over NCC motility. Brennan and others (1999) however have demonstrated that the activities of these molecules are both required for the maintenance of NCC motility on culture. PTPases contribute to NCC locomotion by influencing cell-cell adhesion and focal adhesion dynamics. If PTPases are inhibited with vanadate or herbimycin-A, NCCs migrating on fibronectin show a significant dose-dependant decrease in migration rate as well as layering pattern changes. Instead of

forming a haphazard layer of overlapping cells with a leading edge of freely migrating cells, NCCs migrated as a compact cohesive sheet with few separated cells. Within this sheet, the extensive borders between cells were cadherin-rich; A-CAM represented at least some of this cadherin population. In contrast, the addition of a different inhibitor, genistein, showed no enhancement of cadherin concentration in cell-cell borders. Using PTK inhibitors, PTPase and PTK-dependant signaling pathways were demonstrated to cooperate to promote NCC migration on fibronectin. PTKs also are a prerequisite for focal adhesion formation. Without herbimycin A-sensitive PTK activity, focal adhesions largely fail to form. PTPase inhibition induces large aberrant aggregates of focal adhesion proteins, suggesting a key role for PTPases in focal adhesion distribution. There is also a novel function for genistein-sensitive PTKs in abrogating a contact-mediated inhibition of movement, which is latent in these cells. Overall, the maintenance of cell migration is controlled in at least three ways by PTPases and PTKs: (1) upregulation of expression or enzyme activity of particular PTPases and PTKs; (2) maintenance of low cell-cell adhesion and dynamic substrate adhesion by these enzymes; and (3) abrogation of latent contact-mediated inhibition (Brennan and others 1999).

At Hamburger Hamilton stage 12-13, the first of two waves of migration find NCCs migrating ventrally between the neural tube and somites. Interestingly, NCCs invade only the anterior portion of the somites and tend to stay in a dorsal position. As NCCs are precursors to ganglia, this patterned distribution results in the segmental organization seen in sensory and sympathetic ganglia later. Several inhibitory molecules have been found in the posterior halves of somites, but until recently molecules

promoting cellular migration into the anterior portion of the somite had not been discovered. Tucker and others (1999) have recently identified that thrombospondin-1, originally identified as a protein secreted from platelets, may promote the migration of NCCs through the anterior portion of the somites. It was immunolocalized to the extracellular matrix where NCCs migrate in early development (Tucker and others 1999). Many of these early NCCs are pluripotent, having the ability to generate progeny of more than one cell type. The sensory and sympathetic ganglia, glial cells and portions of the adrenal medulla are a few of the final structures to which these early NCCs contribute.

Evidence suggests that environmental factors and not predisposition are responsible for directing this early wave of NCCs. Neurotrophins, stem cell factor, and other growth factors have been demonstrated to affect NCC proliferation, survival, and differentiation in several lineages. Stem cell factor is a survival factor for pluripotent NCCs, and promotes differentiation of NCCs into cells of the sensory neuron lineage. Transforming growth factor β 1 is a mitogen inducing neurotrophin dependency, and is a powerful anti-mitotic signal for all NCCs. Neurotrophin-3 specifically promotes high affinity uptake of norepinephrine, potentially playing a role in the differentiation of sympathetic neuroblasts. Various combinations of these growth factors also have specific effects differing from the action of each as an individual. Pluripotent NCCs have been found even at sites of terminal differentiation, further supporting the idea that cues originating from the microenvironment, at least in part, direct NCC type specification (Sieber-Blum and Zhang 1997).

Twenty-four hours later in the second migration wave, NCCs invade the dorsolateral space between the somites and ectoderm. Melanocytes are the only NCC derivatives found exclusively along this path. The cells travel uniformly across the top of the somite, unlike earlier cells. These presumptive melanocytes enter the epidermis where basement membrane is disrupted within 24 hours after invading the dorsolateral path. A possible explanation for the exclusivity of melanoblasts to this pathway may be that they need to differentiate from the rest of the NCC population by acquiring the ability to overcome inhibitory molecules found along this specific path. This may be accomplished through the loss of receptors for the inhibitor cues. Alternatively, they may be the only subpopulation sensitive to unknown positive migration cues. Overall, early evidence suggests that the migration of these potential pigment cells is made possible by gaining the ability to exploit an inhibitory matrix coincident with overall changes in the matrix composition (Erickson and Perris 1993; Erickson and Reedy 1998).

Evidence is emerging of various embryonic tissues acting as barriers to NCC migration, such as the caudal part of the sclerotome, the dermomyotome, and the perinotochordal mesenchyme. In areas where NCCs do not migrate, several molecules have been discovered that inhibit NCC migration such as collagen IX, chondroitin sulfate proteoglycans, and the peanut-agglutinin (PNA)-binding molecules aggrecan and versican (Ring and others 1996; Landolt and others 1995; Henderson and others 1997; Perris and others 1991; and Kerr and Newgreen 1997). Aggrecan, strongly inhibitory to avian NCC migration, is thought to be responsible for the repulsive effects of the notochord (Perris and others 1996). Versican, less inhibitory than aggrecan, is expressed

in the caudal sclerotome and notochord as well. When it is over expressed along NCC migration pathways, as in murine *spotch* mutants, a variety of developmental defects are observed, including deficiency of NCC derivatives and spina bifida (Landolt and others 1995). Mutations in the endothelin-B receptor cause an overabundance of laminins, collagen type IV, and proteoglycans, resulting in abnormalities of pigmentation and absent or diminished innervation of the gut (Baynash and others 1994; Tennyson and others 1990).

Members of the Eph family of receptor tyrosine kinases (RTKs) and their ligands, the ephrins, appear to play an inhibitory role in directing segmental migratory pathways in both the trunk and hindbrain regions. EphB RTKs and ephrin-B1 are expressed in striking non-overlapping patterns during trunk neural crest migration. It turns out that ephrin-B1 affects NCCs directly by inducing a typical avoidance response, conferring the rostrocaudal polarity to trunk neural crest migration (Krull 1998). In neurites, the interaction of the chondroitin sulfate proteoglycan neurocan with its receptor coordinately inhibits both A-CAM and β 1-integrin-mediated adhesion and neurite outgrowth. This may prevent cell and neurite migration across specific boundaries within the embryo (Leung and others 2000). Collapsin-1, belonging to the Semaphorin family of molecules, is expressed within the somites and the cranial neural tube along the borders of NCC migratory pathways coincident with the onset of NCC migration. Neurophilin-1, an essential part of a neuronal receptor complex for collapsin-1, is expressed in migrating NCCs. *In vitro* assays have shown explanted NCC avoidance of substratum areas containing collapsin-Fc, suggesting a role for this molecule in migration route patterning

(Eickholt and others 1999). F-Spondin is also expressed in somite areas that NCCs avoid during migration (Debby-Brafman and others 1999).

The final stage of migration involves the cells finding their target location and ceasing migration. The extracellular signals directing this may be the opposite of those responsible for initiation of migration. Around the dorsal root ganglia, for example, a basement membrane containing the characteristic components laminin, collagen type IV and VI, and perlecan appear soon after the coalescence of the NCCs.

Chondroitin/keratan sulfate proteoglycans and decorin, linking matrix molecules inhibitory for NCC movement, are found intimately associated with subepidermal basement membrane potentially connecting it to the interstitial matrix. The overabundance of these typical matrix components and their macromolecular arrangement in the matrix surrounding NCCs may transform the substratum into one that inhibits migration. Changes are also seen in the surface components possibly responsible for the cell's interaction with the matrix. The down regulation of hyaluronan, which interferes with cell-cell adhesion, also occurs potentially increasing the stability of the cell in its final location. Finally, reexpression of adhesion molecules such as N-CAM, A-CAM, and E-cadherin suggest increased cell-cell affinity (Erickson and Perris 1993). The control of A-CAM may rely directly on the activity of integrins involved in the process of cell motion. As NCCs end migration aggregating into peripheral ganglia, A-CAM is reexpressed on their surfaces coincidentally with the disappearance of fibronectin. In *in vivo* studies, an inverse correlation between the expression of A-CAM and the migratory behavior of NCCs has been established. This suggests a precisely

regulated negative control system for the expression and function of A-CAM molecules during migration. Consistently, *in vitro* NCCs do not establish extensive intercellular contacts during migration despite having A-CAM molecules on their surfaces. In these cells, A-CAM is excluded from regions of cell-cell contact. When serine-threonine kinases, tyrosine kinases, and phosphotyrosine phosphatases are inhibited, aggregates of cells form with tight cell-cell cohesion among cells accompanied by A-CAM accumulation in the areas of intercellular contacts. This indicates a complex cascade of intracellular signals involving kinases and phosphatases elicited by surface receptors as a mechanism of A-CAM mediated interactions. The receptors that would regulate these A-CAM junctions are not yet known. Because integrins constitute major receptors for extracellular matrix molecules involved in NCC migration, a question is raised related to whether or not they might be a part of the regulatory mechanism of A-CAM activity. Agents that interfere with fibronectin-to-integrin interactions cause rapid A-CAM-mediated cell-cell aggregations. This process is mediated by A-CAM molecules being incorporated from cytoplasmic pools into adherens junctions that are associated with cytoskeletal elements (Monier-Gavelle and Duband 1997).

Cell Motility

The crawling movements of cells can be broken down into three steps: extension of a leading edge, attachment of this edge to the substratum, and retraction of the rear of the cell into the cell body. These cell movements are produced by the cytoskeleton, a complex cohesive network of filaments and proteins in conjunction with the cortical layer of actin filaments associated with a diverse collection of actin-binding proteins. Three

principle protein filaments make up the cell's internal scaffolding. Microtubules are the largest at 25 nm diameter, and are constructed of tubulin heterodimers. They are found forming a polarized lattice throughout the cytoplasm. Focal complex dynamics responsible for formation, maintenance, and removal of focal adhesions are in part regulated by microtubules. Depolymerization of microtubules in fibroblasts leads to a decrease in the turnover of focal complexes, resulting in reduced cell spreading, large peripheral focal adhesions, and reduced protrusive activity. Adhesions dissociate upon direct contact with microtubules, and either the cell retracts or a new protrusion forms. These relaxing signals are likely regulated by members of the Rho family, but the exact nature of the signals is unclear. Migratory defects that manifest as inhibited focal adhesion turnover have been reported in cells lacking the focal adhesion components calpain, focal adhesion kinase, and SRC family kinases (Klinghoffer and others 1999; Sieg and others 1999; Huttenlocher and others 1997). These cells show inhibited cell spreading and strong focal adhesions predominately at the cell periphery perhaps due to an inability to recycle adhesive components (Horwitz and Parsons 1999).

Intermediate filaments have a distribution similar to microtubules, but have a smaller diameter of 10 nm. They are made of a unique family of proteins often distinctive of a particular cell type, such as keratin in epithelial cells, desmin in muscle cells, or vimentin in fibroblastoid cells (Bray 1992).

Actin filaments are the smallest type (eight nm diameter) and are composed of the protein actin. Cortical actin filaments interact with a diverse array of actin-binding proteins to produce movement. Cell process extension, anchorage, and contraction is

facilitated by actin polymerization and depolymerization. The actin network is stabilized through the formation of adhesion complexes or focal adhesions. Integrin receptors, actin filaments, and associated proteins gather within the plasma membrane in these regions. Cooperation of actin filaments, cross-linking proteins such as α -actinin, actin fragmenting proteins such as gelsolin, and various forms of myosin are responsible for motile behavior. As the cells migrate, focal complexes (small nascent adhesion complexes) at the front grow and strengthen into more organized focal adhesions that serve as points of traction over which the body of the cell moves. In stationary fibroblasts, it has been discovered that these adhesions are highly motile, while in migrating cells they are stationary, suggesting the existence of a molecular clutch coupling traction and contractile forces. The mechanism that regulates formation and release of these complexes remains unclear (Horwitz and Parsons 1999). Surface stimulation by various soluble or substrate-bound proteins, peptides, lipids and small molecules initiates crawling behavior.

Crawling cells have a leading lamella, flat anterior end, and narrow tail, creating an observable polarity. Multiple organelle free lamellae are produced, but only those that contact the surface in focal contacts are capable of generating locomotion. Typically, an actively crawling cell will have one dominant lamella, and others retract coordinately. Cell type and external environment affect lamellar advancement. Forming extensions of the leading lamella are cylindrical spikes called filopodia, or expansions of small blebs that flatten and cluster. Ruffling is also seen, where the leading edge of the lamellar veil lifts upward from the substrate and bends backward perpendicular to the adherent portion

of the lamella. This ruffle then migrates rearward toward the cell body while retracting and dissipating over it.

The term “cortical flow” encompasses movements of the lamellar substance. The leading lamella is elastic, and is stiff enough to deform or push objects out of its way (Stossel 1993). The association between actin polymerization and membrane protrusion had been well established, but the actual driving force for membrane extension of the leading lamellae is unclear. A dynamic cycle of actin assembly and disassembly operates throughout the entire lamella. Actin has intrinsic self-association properties resulting in polarized filaments. Supporting these filaments are regulatory proteins, some of which function in response to transmembrane signals. To switch off actin assembly, ion-activated control proteins such as gelsolin, severin and fragmin bind to the sides of filaments, sever bonds and cap filament ends to inhibit growth. Ponticulin and diacylglycerol have been implicated in helping to induce actin nucleation. Filament crosslinking molecules help incorporate actin into a three-dimensional network as the filaments elongate. In addition, tropomyosin and caldesmon bind to the groove of actin filament helix and stabilize it against spontaneous fragmentation.

Both myosin I and II cause actin filaments to slide past one another *in vitro*. In a locomoting cell, they probably have distinct roles. Myosin I is located primarily at the front of the cell and is responsible for movement of vesicles and the plasma membrane associated with membrane ruffling. Myosin II is mainly concerned with contraction of the cortex (Bray 1992). This complex internal scaffolding is useless without all of the accessory proteins that link the three types of filaments to each other and to other parts of

the cell. They strengthen the cytoskeleton by crosslinking and forming bundles within the cytoskeleton, and allow generation of internal movements of organelles using the filaments like tracks.

Neural Tube Defects: Spina Bifida

All pregnancies carry a three percent risk for a major birth defect independent of any intrinsic or extrinsic factors (Buehler and others 1994). Neural tube defects (NTDs) are malformations affecting the brain and/or spinal cord that may or may not result from abnormal neural tube closure (DeSesso and others 1999). These defects occur in 1.3 to 2.0 human fetuses per 1000 live births, representing the second most frequent congenital anomaly behind cardiac malformations (Wenstrom 1996). The range of prevalence is from 8 per 1000 for the British and the Sikhs, to 1 per 1000 in Lagos, Nigeria (Campbell and others 1986).

The etiology of neural tube defects is multifactorial. The greatest risk factor for having an NTD-affected fetus is a previous pregnancy resulting in a NTD, increasing to 10 times that of the general population. In women with two NTD pregnancies, the recurrence rate is approximately 10%, suggesting a genetic susceptibility (Lewis and others 1998). When studied, the inheritance pattern does not fit a single gene inheritance; the model is one of multigenic inheritance influenced by environment. Using a mouse model polymorphic for positioning of cranial neural tube closure site two, it was demonstrated that variation in the pattern of closure at this site is a genetically determined factor with the ability to influence the susceptibility of the embryo to cranial NTDs (Fleming 2000).

Maternal illness and fetal drug exposure are also important factors in NTD development. At least 221 teratogenic agents have been associated with the production of NTDs in at least one species (DeSesso and others 1999). Other extrinsic factors that correlate to higher incidences of NTDs are geographic region, maternal age and birth order, influence of socioeconomic class, and overall nutrition of the mother (Campbell and others 1986).

Spina bifida and anencephaly account for 50% and 40%, respectively, of NTD cases (Lewis and others 1998). Spina bifida includes all abnormalities in which vertebral arches fail to close dorsal to the spinal cord to form the vertebral canal, and may or may not involve the spinal cord itself. There are several types of spina bifida ranging from no impairment to severe impairment.

Spina bifida occulta is the most common and least severe type of defect. Below the skin, there is a localized gap in one or more vertebral arches, but the spinal cord and meninges remain entirely within the vertebral canal. The overlying skin may be normal, dimpled, pigmented, contain a lipoma, or have a tuft of hair. This usually does not present a neurological disorder as neural tissue is not directly involved, and the individual may not ever realize there is a defect unless an X-ray reveals it. Typical symptoms including muscle weakness and abnormal posture or gait are observed at the time when an affected child begins to walk; and bladder and bowel control problems are noted during toilet training (Buta 1975; Lewis and others 1998).

Spina bifida cystica involves the neural tissue in the vertebral defect. There are two types. In meningocele, the dura mater and arachnoid mater protrude through the

defect in the vertebral arches forming a cystic swelling, but the cord and nerves stay within the vertebral canal. In meningocele there is a cystic swelling, however the spinal cord is raised from the canal and is closely apposed to the wall of the swelling or its apex. Both meningocele and meningocele are most common in the lower thoracic lumbar and sacral regions where the position and extent of defect determine the degree of neurological impairment.

In spina bifida aperta (myeloschisis), the spinal cord takes the form of an open neural plate exposed to the external surface. This is the most common form of spina bifida seen in valproic acid exposed fetuses. In the more serious cases of spina bifida, there is partial or complete paralysis of the lower half of the body, partial or complete loss of bladder control, and absence of reflexes (Lewis and others 1998).

The final form of spina bifida is anencephaly, caused by failure of the cephalic part of the neural tube to close. This lethal defect results in missing cerebral hemispheres and/or forebrain, with acrania always present. Other NTDs include encephalocele, protrusion of the brain through the cranium; and iniencephaly, failure of the occipital part of the cranium and upper spinal regions to close about the neural tube permitting exposure of cord and brain tissue (Lewis and others 1998).

No animal model has been found that models human NTDs convincingly. The chick and mouse are used most often for studies because of the similarities during the process of neurulation between them and humans. Typically, animal studies utilize naturally occurring defects to help us understand the normal closure mechanisms. They are also treated with known or potential human teratogens in order to elucidate their

mechanisms as well as furthering our understanding of the overall process of neurulation. The chick embryo has helped to show that the process of neural tube closure is a flexible process and NTDs may form by several different mechanisms within just one model. Campbell, Dayton, and Sohal's studies used the whole chick *in ovo* (1986) to show that 47% of chicks with abnormally open neural tubes in the embryo develop neural tube defects when mature, that 14% with delayed neural tube closure developed NTDs, and, interestingly, that 3% of chicks with apparently normally closed neural tubes developed NTDs when mature. Overall, animal studies have given us many other clues about the causes of NTDs. Naturally occurring or teratogenically produced failure of the neural tube to close may lead to NTDs. Single agents may increase or decrease the incidence of NTDs dependant on the time of treatment. Also, neural tube closure can be affected by agents with many different mechanisms of action (Campbell and others 1986).

Cell Migration and NTD Formation

Many types of cells must interact to correctly form an embryo, and these cells rely on signals from each other and from the environment in which they reside. Matrix and cell adhesion molecules, when disturbed at the time of neurulation, could be involved in the generation of NTDs by altering cell adhesion dependant morphogenic events (Newgreen and others 1997). The extracellular matrix molecules laminin, fibronectin, and chondroitin sulfate proteoglycan as well as the cell adhesion molecules E- and N-cadherin, and N-CAM were examined in quail embryos with spontaneous NTDs. HNK-1 was also used to label NCCs. In open NTDs, the early stages of normal primary neurulation with a sharp separation between E- and A-CAM expressing regions were

noted. Intervening matrix labeled less intensely for chondroitin sulfate proteoglycan relative to laminin and fibronectin when compared to control embryos. In closed NTDs, a band of matrix did not separate the dorsal superficial layer from the neural tube as in control embryos, and A-CAM and N-CAM were co-expressed with E-cadherin. In normal embryos, A-CAM and N-CAM are not found at this stage. The overlap region resembled the mid-dorsal tissue at earlier stages in normal secondary neurulation in the tail bud. Matrix molecules were found not around, but within the neural and epidermal epithelia in all of the defects. Lastly, unlike controls, HNK-1-labeled NCCs were frequently absent in regions of NTDs. The authors concluded that matrix and cell adhesion molecules are disturbed in spontaneous NTDs during neurulation (Newgreen and others 1997).

Role of Cell Proliferation in NTD Formation

Normal cellular proliferation in the neuroepithelium plays an important role in proper neural tube closure. Numerous studies have demonstrated that when it is altered, NTDs can result (Copp 1988, 1990; Bennett and others 2000). For example, in the mouse mutant curly tail, 60% of *ct/ct* mutants develop spinal NTDs as a result of delayed neurulation (the other 40% develop normally). It is frequently used as a model system for neurulation investigations. When independent measurements of cell proliferation such as mitotic index, and median length of S-phase were studied, reduced rates of cell proliferation in gut endoderm and notochord cells in the neuropore region were indicated when compared to normally developing embryos. The incidence of cell death was not

consistently different from controls. This suggests the lowered rate of cell proliferation in these tissues is a mechanism of NTD pathogenesis in curly tail embryos (Copp 1988).

Valproic Acid

Valproic acid, (2-propylpentanoic acid or dipropylacetic acid, VPA) is a simple eight carbon, branched-chain fatty acid (Figure 1). It is an anticonvulsant chemically unrelated to any other anticonvulsant drugs in that it lacks a nitrogen molecule or a heterocyclic functional group.

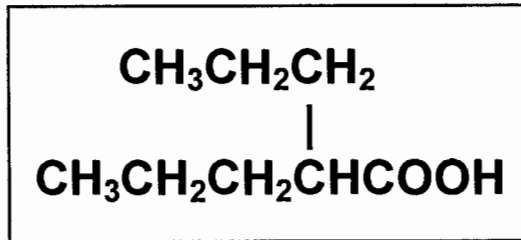


Figure 1 Structural formula of VPA

The discovery of VPA as an anticonvulsant was unusual in that it was being used as a solvent to test other potential anticonvulsant compounds. All of the compounds seemed to have the same effect indicating that VPA itself had the ability to prevent seizures. It was released for use in 1967 in Europe, and was licensed in the United States by the FDA in 1978 for the treatment of absence seizures (Lammer and others 1987). By 1988, one million patients worldwide were on VPA therapy (Walmod and others 1998). It is known under the trade names Depakene (valproic acid), Depakote (divalproex sodium, sustained release form), and Depacon (intravenous form of valproate sodium). A popular drug because of its broad range of uses and relatively low occurrence of sedative and

behavioral side effects (Clayton-Smith and Donnai 1995), it has been mainly indicated as prevention or cure for myoclonic seizures, partial seizures, status epilepticus, tonic-clonic seizures, mania, and migraine (Browne 1980). Valproate also has been studied as treatment for anxiety, depressive, and psychotic disorders; alcohol withdrawal and dependence; tardive dyskinesia; agitation associated with dementia; and borderline personality disorder (Davis and others 2000). Approximately 35% of patients with schizophrenia received VPA as treatment in 1998 making it one of the most commonly prescribed for this disorder, second to lithium which had been the longstanding treatment (Citrome and others 2000).

Bipolar disorder has been treated with lithium for over 30 years. Unfortunately this treatment has numerous negative side effects. For those patients requiring alternative treatment, recent data indicates that valproate is a well-tolerated and effective agent (Lennkh and Simhandl 2000; Mitchell 2000). A preliminary study using Divalproex treatment for explosive temper and mood lability in disruptive children and adolescents showed eight out of ten subjects respondent to the drug, and zero of ten respondent to placebo (Donovan and others 2000). Two elderly women suffering from Charles Bonnet syndrome (pseudohallucinations in elderly people frequently suffering from reduced visual acuity) recently were successfully treated with valproate (Hori and others 2000).

Mechanism of Action

The exact mechanism of VPA's beneficial effects is poorly understood. VPA has been shown to increase total brain and cerebellar levels of the inhibitory neurotransmitter gamma-aminobutyric acid (GABA) in the central nervous system. This inhibition has

been shown to correlate with the antiepileptic effect of VPA in some animal models of epilepsy (Browne 1980). VPA directly inhibits GABA transaminase, resulting in inhibition of GABA catabolism and decreases in sodium channel activity. It also blocks the reuptake of GABA into glia and nerve endings. It has demonstrated activation of glutamic acid decarboxylase (GAD), a major enzyme in GABA synthesis, and strong inhibition of succinic semialdehyde dehydrogenase, an enzyme in the GABA degradation pathway (Loscher 1993; Johannessen 2000). When GABA levels within the medial preoptic area in mice exposed to VPA were sampled, and it was found that: (1) VPA had regional specificity upon GABA levels, (2) a sex difference was present in the effects of VPA on GABA levels within the medial preoptic area, and (3) GABA levels increased in the afternoon of all days of the female estrous cycle, with VPA attenuating the rise seen on the afternoon of proestrous (Dodge and others 2000). Evidence also exists that suggests VPA reduces neurotransmission mediated by excitatory amino acids such as aspartic acid and gamma-hydroxybuteric acid. However, concentrations of VPA greater than 5 mM enhanced rather than inhibited epileptiform activity induced by veratridine in rat hippocampal CA1 pyramidal neurons (Otoom and Alkadhi 1999).

VPA may also work by suppressing repetitive neuronal firing through inhibition of voltage sensitive sodium channels (Tunnicliff 1999). When high concentrations (5 to 30 mM/L) of the drug were applied to *Aplysia* neurons, an increase in membrane potassium conductance developed, leading to an increase in membrane potential (Davis and others 1994). *In vitro* studies have shown that VPA is a potent inhibitor of succinate semialdehyde dehydrogenase, which is related to the tricarboxylic acid (TCA) cycle.

VPA might also inhibit the TCA cycle at the alpha-ketoglutarate dehydrogenase step.

The effect of VPA on excitatory neurotransmission and on excitatory membranes is likely to be responsible for the mood stabilizing effect as well as in the treatment of migraine (Johannessen 2000).

Dysregulation of central norepinephrine (NE) neuronal systems might be involved in the expression and development of major affective disorders, including bipolar disorder. The noradrenergic neurons of the locus coeruleus represent the source of noradrenergic terminals innervating many limbic and forebrain regions. These neurons are ideally placed to exert global modulatory or state-related changes in brain activity, and thus present potential targets for mood stabilizing drugs such as VPA (Sands and others 2000). It is important to note that the antiepileptic effects of VPA are seen quickly, whereas the antimanic effects may take up to three weeks to be observed. This implies different mechanisms of action for the two effects. Sands and others (2000) suggest that gene expression of components of brain neurotransmitter systems, such as tyrosine hydroxylase (TH) are altered by VPA as it is with tricyclic antidepressants based on results of past studies. Adult male Sprague-Dawley rats were exposed to acute and chronic valproate treatment, and changes in the TH gene expression in the locus coeruleus were noted. Both treatments induced increases specifically in TH mRNA expression, with acutely treated responses less robust and inconsistent (Sands and others 2000). It is possible that VPA exerts a direct pharmacological effect on gene expression in the NE system through stimulation of cellular effector processes and subsequent

activation of transcription factors. It is also possible that this is an indirect result exerted by changes in the GABAergic neurotransmission in the brain (Sands and others 2000).

Several reports have indicated that anti-epileptic drugs including VPA affect the immune system. NF-kappaB is essential to the expression of the kappa light chain of immunoglobulin and proinflammatory cytokines. VPA inhibits NF-kappaB activation induced by lipopolysaccharide. VPA significantly inhibited lipopolysaccharide-induced production of TNF-alpha and IL-6 production via inhibition of NF-kappaB activation. These findings are consistent with the idea that VPA suppresses TNF-alpha and IL-6 production via inhibition of NF-kappaB activation (Ichiyama and others 2000).

Evidence for Weak Teratogenicity

Of the approximately 2.8 million Americans with epilepsy, 680,000 to 1.1 million afflicted women are of childbearing age (Yerby 1994). Pregnant women with epilepsy constitute 0.5% of all pregnancies (Nulman and others 1999). Dickinson and others (1979) showed that VPA crosses the placenta and the umbilical cord, resulting in newborn serum concentrations higher than found in maternal serum. Additional supporting evidence was provided by Nau and others in 1984. Embryonic mouse neuroepithelium showed higher uptake of VPA than maternal blood, amniotic fluid and other embryonic tissues when ^{14}C -VPA was administered to pregnant mice (Dencker and others 1990). Maternal plasma concentrations exceeding 1.6 mM have been shown to be necessary to produce exencephaly in the mouse (Nau 1986a). Human plasma concentrations after therapeutic application of VPA vary from 0.36 to 0.6 mM (Kratke

and Kirschbaum 1996). It is currently unclear exactly what level fetal serum concentrations are during embryogenesis.

The first adverse report of a human fetus exposed to the drug was in 1980. The exposed infant was born with low birth weight, hypoplastic nose, fronto-orbital ridges, and levocardia (Dalens and others 1980). In 1982, Robert and Guibaud reported from the Rhone Alps region that VPA was the cause of neural tube defects in children born to epileptic mothers on VPA therapy. Their data suggested a causal relationship between VPA and neural tube defects when administered during the first trimester of pregnancy. The estimated increased risk of a valproate-exposed fetus having spina bifida is 1-2% (Bjerkedal and others 1982). Clayton-Smith and Donnai described fetal valproate syndrome (FVS) in 1995. They defined a set of anomalies associated with VPA exposure. They are neural tube defects (spina bifida), congenital heart defects, oral clefts, genital abnormalities, and limb defects. Other less frequent abnormalities included abdominal wall defects, tracheomalacia, and strabismus. The most common neural tube defect was spina bifida with a predisposition for very low lumbar or sacral defects suggesting that valproate affects primarily the lowest closure site of the neural tube (Clayton-Smith and Donnai 1995). Congenital heart defect incidence is estimated to be around four times that of the general population. Both septal defects and valvular problems have been reported. These reports are not as consistent as with the neural tube defects. Oral clefts have also been observed in children of mothers on valproate monotherapy (Clayton-Smith and Donnai 1995).

Multiple reports since 1976 have shown VPA to be a potent teratogen in the rabbit, mouse, rat, hamster, axolotl, and chick. The fact that VPA affects so many species makes a causal relationship in humans more biologically plausible (Lammer 1987). A review of nine studies using whole embryo rat and mouse culture by Gofflot and others (1995) reported a series of macroscopic malformations. The list in order of high to low incidence included: unfused brain folds, irregular brain structure, abnormal curvature, stunted forebrain, irregular segmentation of the somites, decreased yolk sac vasculature, abnormal otic system, abnormal optic system, irregular shape of the head, underdeveloped branchial bars, and posterior neuropore closure defects. In both rats and mice exposed to VPA during organogenesis, developmental defects of the digits and axial skeleton were produced. Exencephaly was also produced, but only in mice (Narotsky and others 1994).

Although spina bifida is the primary NTD seen in humans, in animal models VPA induces exencephaly (an anterior neural tube defect) much more frequently (Lammer 1987; Nau 1994). VPA administration during embryogenesis in the mouse also results in oral clefts, increased embryolethality, and reduction of fetal weight (Nau 1986b). Lumbosacral spina bifida aperta with accompanying tail malformations and spina bifida occulta can be produced in mice at a significant rate when exposed to VPA. Specifically, the closure of the lumbar and sacral/coccygeal vertebrae is inhibited. Developmental delay was not a factor in these malformations (Nau 1994). The spina bifida aperta morphology and period of sensitivity are different for VPA and retinoic acid in the mouse fetus. It is possible that there are differing mechanisms of spina bifida induction between

these two teratogens (Ehlers and others 1992). There are also strain differences noted concerning VPA-induced formation of neural tube defects, indicating a clear genetic link to VPA susceptibility in the mouse (Nau 1994).

When the histological structure of the murine hindbrain neuroepithelium is observed after treatment with VPA, two modifications are noted. In all treated embryos, there appeared to be a dilation of the area characterized by increases in surface and lateral bulges on both sides of the neuroepithelium. These bulges sometimes presented two or three irregular disorganized lobes. Other alterations included increased number of cells or cell debris in the lumen of the brain vesicles and optic stalks, and an increase of the protruding cell contour on the ventricular surface of the neuroepithelium. More abnormalities were noted. Irregular suture line was observed at all levels of the caudal neural tube. The wavy, zigzag or irregular types of sutures were not random, and had not been previously described (Gofflot and others 1994). A survey of nine studies using whole embryo culture demonstrated that VPA affects rat neural tube and brain development as well. Asymmetric layers of neural epithelium, incomplete neural fold fusion, general neural tube irregularities, and incomplete and irregular segmentation of brain vesicles occurred when embryos were exposed to VPA (Gofflot and others 1994).

Somites in the chick embryo are affected by VPA. The Pax family of pattern forming genes, specifically Pax-1, have been demonstrated to be regulators of axial skeletal patterning at the somite level. VPA causes malformations in chick somite development in a dose dependent manner. Large somite disorganization patterns, mis-segmentation of the somites, or fusing of somites together are seen. In these embryos,

Pax-1 expression was lowered according to Northern Blot analysis. *In situ* hybridization revealed that areas of malformed somites corresponded to areas of low Pax-1 expression. Embryos with Pax-1 gene expression altered using an anti-sense oligoneucleotide exhibited similar malformations when compared to VPA treated embryos (Barnes and others 1996).

In the amphibian *Ambystoma mexicanum*, VPA caused retarded development, heart malformations, and neural tube defects, some of which resembled exencephaly. Continuous treatment resulted in more consistent and serious developmental disturbances than did pulse treatment. Neurulation was retarded and neural fold closure was disturbed. The neural epithelium was disorganized and its cells were less elongated than normal. Intercellular spaces in neural epithelium as well as in connective tissue were enlarged and cell adhesion seemed to be disturbed in both tissues. Oversized somites appeared with treatment, periodically filling the space between the notochord and notoplate, while the notochord itself seemed undisturbed. During 2.0mM continuous exposure, NCC derivatives were not detectable in the embryos. The nature of these disturbances may indicate an interaction between the drug and components of the extracellular matrix and the cytoskeleton in non-mammalian cells (Kratke and Kirschbaum 1996).

Nau and Spielmann in 1983 showed similar doses of VPA can have unique fetal effects depending on the administration schedule. Peak concentrations of VPA can be related to the teratogenicity in the mouse in that a particular threshold concentration, approximately 230-250 μ g/ml (1.67 mM) mouse serum, must be reached before neural tube defects are formed (Nau 1985).

Four metabolites of VPA, 2-en-VPA, 4-OH-VPA, 5-OH-VPA, and 3-keto-VPA were administered to pregnant mice to determine the teratogenic potential of each. Metabolite concentrations were much lower than VPA. Metabolite/VPA ratios were generally between 0.001 and 0.02. Further, the metabolites did not accumulate in embryonic tissues, unlike VPA. It was determined that the parent drug, and not one of the four metabolites tested, was the principle teratogen in mice (Nau 1986b). 2-en-VPA, VPA's main pharmacodynamically active metabolite, had a particularly low teratogenic potential. Heinz Nau (1986a) demonstrated that the low teratogenic and embryotoxic potential of this metabolite is due to intrinsic activity of the compound, and not just lower peak concentrations found in mother and embryo. The peak maternal serum concentrations for VPA were only slightly higher than 2-en-VPA. They concluded this difference was clearly not enough to account for the large difference between the teratogenicity of the two compounds (Nau 1986b). With further study, this compound may become an acceptable substitute for VPA in female patients trying to conceive.

Mechanisms of Teratogenesis

The mechanisms of neurulation and spontaneous NTD formation have not been entirely understood. In addition, the exact biochemical mechanism of most teratogens, including VPA, is not known. Several hypotheses are being investigated to identify the mechanism(s) of VPA's teratogenicity. These hypotheses include interference with embryonic lipid metabolism, interference with zinc metabolism, and interference with neurotransmitter metabolism (Clarke and Brown 1987; Wegner and others 1990; Nau 1994). Another hypothesis examines alteration of intracellular pH, which is an important

parameter of numerous cellular functions and seems to be a promising area of study because the early mammalian embryo has a relatively high intracellular pH and may then accumulate acidic compounds such as VPA via ion trapping (Scott and others 1990 cited in Nau 1994). Lastly, interference with embryonic folate metabolism is currently being investigated (Nau 1994). It has been widely documented that folate taken before and during pregnancy reduces the risk of neural tube and neural crest defects including failure of neural tube closure, orofacial defects and heart septation anomalies. Folate concentrations decrease during pregnancy, and treatment with antiepileptic drugs such as VPA can intensify this effect (Hendel and others 1984). Teratogenic doses of VPA induced a characteristic dose-dependant alteration of embryonic folate metabolism. The amounts of formylated folates decreased, while the amount of tetrahydrofolic acid (THF) increased. This relative change in folate metabolite concentrations suggests that the interconversion between THF and 5-CHO-THF may have been inhibited by VPA. These results indicate that interference with embryonic folate metabolism may be involved in some aspects of VPA teratogenesis (Nau 1994). The protective mechanism of folic acid is unknown at the cellular level.

Increased homocysteine levels are detected with folate deficiency, and it has been hypothesized that homocysteine *per se* might be the teratogenic agent. Indeed folic acid supplementation is effective in preventing neural tube and other defects only when homocysteine levels are concomitantly reduced (Rosenquist and others 1996). Induction of neural crest and neural tube defects is a general effect of N-methyl-D-aspartate (NMDA) receptor antagonists. Proteins involved in functional NMDA receptors are

present as early as stage 10 in the chick. There is evidence from later stages of development that the NMDA receptor is a regulator of neuronal cell migration, cell-cell adhesion, and apoptosis (Komuro and Rakie 1993; Rashid and Cambray-Deakin 1992; Balazs and others 1989). The NMDA receptor antagonists ethanol and VPA have been identified as possibly contributing to NTDs by competitive inhibition. Homocysteine has also been found to act as an NMDA receptor antagonist in avian embryos. Homocysteine induced neural tube, conotruncal, and orofacial malformations in a dose and time dependant manner. Rosenquist and others (1999) have demonstrated that of three agonists introduced in combination with homocysteine, glycine is the most effective, significantly reducing defects at two different doses. Due to the similarity of deformations between these three antagonists, similar teratogenic mechanisms involving the NMDA receptor may be at work.

In addition to folate supplementation, methionine supplementation appears to inhibit NTD formation, indicating it may also play a role in NTDs. A study by Hishida and Nau (1998) demonstrated that in mice, 30 minutes after VPA treatment, significant, dose dependant decreases in serum methionine and serine levels are noted, while homocysteine and cysteine were increased via accelerated conversion of methionine to homocysteine. There was also an inhibition of homocysteine remethylation due to folate metabolism deficiencies, an increase of aminothiols, and a depression of (chemically) reduced glutathione. They suggest that alteration of amino acid metabolism could contribute to VPA's teratogenicity in at least four ways: (1) deficiency of methionine, which is requisite for neural tube closure shown by *in vitro* studies; (2) increased levels

of homocysteine becoming toxic through production of reactive oxygen species; (3) increased levels of cysteine, known for its radioprotective and antioxidant roles, becoming toxic when redox metal ions are present resulting in reactive oxygen species; and (4) reduction in the reduced form of glutathione (GSH) which is an important protector against reactive oxygen species during early development. They hypothesize that folate supplementation may prevent NTDs via elevation of homocysteine remethylation to methionine (Hishida and Nau 1998). In a study of 62 patients on AED monotherapy however, only seven had hyperhomocysteinemia, and none of these was on valproate therapy. However, in 54% of those on valproate there were lower than normal (12.0 nmol/l) plasma folate concentrations. Serum vitamin B-12 concentrations were significantly elevated only in patients on valproate therapy in this study, supporting several other studies' findings. The mechanism of this elevation is currently unknown (Tamura and others 2000).

In 1995, Sato, Shirota, and Nagao reported the first evidence that pantothenic acid (PTA), when coadministered with VPA, significantly decreased exencephaly in the mouse. PTA is essential for a developing animal; deficiency results in neural tube defects and growth retardation. VPA induced a dose dependent increase in exencephaly as well as a significant rate of rib, thoracic, and sternebral malformations when compared to controls. PTA coadministration resulted in significant decrease in exencephaly rates, but did not appear to decrease any types of skeletal malformations. Conversely, folic acid has been demonstrated to reduce rib and sternebral abnormalities. This may indicate

two differing mechanisms of protecting against neural tube defects (Sato and others 1995).

Several lines of investigation have led to evidence that the mammalian neural tube closure initiates in at least four discrete locations. Failure of closure in any of the sites I through IV may result in the differing types and locales of spina bifida. Disrupted closure site-specific genetic processes may contribute to some NTDs. There are few genes identified as having roles in these closure sites that may be affected by teratogens. One of these, coding for the cell cycle enzyme ribonucleotide reductase subunit R1 (*rnr-r1*), has recently been identified as a VPA-sensitive gene. Using the inbred mouse strain SWV/Fnn, which has a high susceptibility to VPA-induced NTDs in closure site II, a VPA-sensitive closure site II-specific clone was identified and confirmed to code for *rnr-r1*. VPA drug treatment significantly increased the amount of *rnr-r1* mRNA along with a significant decrease in cellular proliferation in the closure site II neural tube region of the embryos. *Rnr-r1* appears to play a critical role in exencephaly induced by VPA (Craig and others 2000).

Neurulation in the early chick embryo is also affected by VPA. Concentrations of 0.5-1.5 mM VPA caused a dose dependent increase in the incidence of open anterior and posterior neuropores. Greater concentrations increased the number of complete disruptions of the neural tube along its entire length. These defects do not appear to be related to developmental delay and they were not repaired with continued incubation time (Kelly and Regan 1992).

In older chick embryos, the noncytotoxic effects of VPA on vertebral chondrocytes during spine formation were investigated (Basu and Wezeman 2000). VPA significantly lowered expression of type IX collagen and aggrecan core protein mRNA levels. This alteration in these critical genes expressions during vertebral chondrogenesis may be related to the failure of neural arch development in lumbar spina bifida (Basu and Wezeman 2000).

While studying the genetic basis for VPA teratogenicity in mice, Failla and others (2000) discovered that parental factors influence fetal susceptibility to induced malformations. Results of reciprocal crosses between teratogen susceptible and resistant strains of mice suggested that the maternal genotype was more strongly associated with VPA-induced teratogenicity than was the paternal genotype. The nature of this paternal factor is unknown. Morphological analysis of the VPA-treated fetuses revealed the presence of homeotic transformations generally in the lower thoracic and lumbar regions, but not the cervical or upper thoracic segments. Penetrance and localization of VPA-induced malformations varied among six strains tested. Malformations seen in the lumbar, sacral, and appendicular regions of treated embryos were consistent with those expected after dysregulation of the 5' *Hox* genes during early development. This altered gene expression may disturb positional cues for closure of the posterior neuropore (Failla and others 2000).

VPA has been shown to inhibit the proliferation of neuronal cells in culture and recent studies have been carried out to determine the explanation. The proliferative rate of C6 glioma cells has been inhibited in a dose dependant manner using a 1 mM

concentration to achieve 50% inhibition. This effect was reversible and, at the concentration utilized, could not be attributed to cytotoxicity. When present, VPA interrupted the cell cycle 5 hours into the G1 phase, 6-6.5 hours prior to S phase. S-phase entries by cells past this restriction point were not affected by VPA exposure (Martin 1991).

To determine the potential mechanism of the antiproliferative effect of VPA, transcriptional activities of genes coding for several growth factors, receptors and neurotrophic factors was investigated by Bennett and associates (2000). They used two VPA sensitive strains of mice, LM/Bc (less) and SWV (more), and found that transcriptional activity of neurotrophic and growth factor genes were altered during neurulation in the presence of VPA. The pattern of alterations suggested that the high incidence of teratogenicity in the SWV strain of mice might be due to suppression of proliferation in the neuroepithelium. Interestingly, they also found that these two strains behaved differently under control conditions, supporting the multifactorial explanation of NTD formation.

VPA Effects Cell Motility and the Cytoskeleton

Walmod and others (1998) performed experiments on L-cells in 3.0 mM treatment of VPA and two analogues, (E)-2-en-VPA and (\pm)-4-en-VPA. The migration of the cells was tracked for 10 hours using video recordings and it was found that cellular migration was inhibited in a dose dependant manner for all three compounds, inversely correlated to each compound's teratogenicity. The inhibition was not dependent on the clone of L-cells and was independent of the culture substratum.

To determine to what extent VPA was inducing migratory inhibition, RGD-containing peptide rescue treatment was carried out. Treatment with an RGD-containing peptide, reducing integrin binding to components of the extracellular matrix, partially reverted the motility inhibition induced by VPA. It was therefore shown that increased attachment was contributing to decreased motility, but it was not the sole cause (Walmod and others 1999). It was shown that the actomyosin cytoskeleton of VPA-treated cells was capable of contraction upon exposure to ATP, indicating that the reduced motility was not caused by inhibition of actomyosin contraction. Gelsolin is an essential protein involved in F-actin dynamics responsible for severing and capping actin fibers. It was found that long term exposure to 3 mM VPA lead to redistribution of gelsolin from the peripheral membrane ruffles (control) to a diffuse perinuclear localization (treated). When control cells were incubated with a decapeptide containing one of the phosphatidylinositol biphosphate (PIP₂) binding motifs of gelsolin, leaving the gelsolin in a potential actin binding state, a strong rounding response was seen, resulting in brighter cells. In contrast, VPA treated cells exposed to the peptide were not significantly more rounded, and insignificant changes in brightness were noted. VPA appears to leave L-cells in an unresponsive state to a PIP₂ binding motif. Walmod and others suggest that the VPA-induced alteration in gelsolin regulated dynamics of actin filaments contribute to the reduced motile behavior and altered morphology of VPA treated cells and, therefore, possibly to the teratogenic potential of the compound (Walmod and others 1999). Confocal micrographs of fluorescence staining of microtubules, F-actin, and selected focal adhesion proteins demonstrated that VPA-exposure caused an enhanced

focal adhesion formation accompanied by a rearrangement of F-actin reflected by an increase in stress fiber formation (Walmod and others 1998). In control cells, F-actin was mainly present as a cortical mesh, whereas in the treated cells, there were numerous stress fibers often with a perinuclear distribution. Organization patterns of the cytoskeleton are a major factor in cellular morphology. Both treated and untreated cells demonstrated a well-developed scaffold of microtubules whose organization did not seem to be affected by VPA. In addition, treated cells seemed to be devoid of microspikes, which were observed in great numbers in control cells. Mechanical tension generated within the cytoskeleton and transmitted to the exterior via cell-cell and cell-ECM interactions have been demonstrated to effect cellular morphology, motility, and morphogenesis (Ingber and others 1994).

It has been revealed that VPA causes alterations in the focal adhesions and actin cytoskeleton of fibroblastoid L-cells. VPA and VPA- analogues have been demonstrated by Berezin and others (1996) to increase mean cell area of cultured fibroblastoid L-cells in correlation with the teratogenic potential of each analogue tested. Walmod and others (1999) demonstrated that after treating L929 cells with 3mM VPA or sodium valproate for 48 hours there was increased flattening and spreading of the cells compared to control. Overall, the cells were larger and had more and/or longer processes. Relative F-actin per cell was calculated and found to be significantly higher (23%) for treated cells. F-actin distribution was altered indicated by an increase amount of stress fibers, and a decrease in cortical F-actin and lower numbers of membrane ruffles. Treated cells also had more pronounced focal adhesion proteins at the ventral surface, indicating more

pronounced adhesion. In focal adhesion complexes, VPA treatment induced an increase of phosphotyrosine, paxillin, vinculin, and focal adhesion kinase (FAK). When these were visualized with appropriate antibodies, they were found in oblong patches more strongly manifested in treated than control cells, where cytosol staining was more diffuse (Walmod and others 1998, 1999). This indicated that a higher proportion of these proteins had been directed to the focal adhesion sites. This supports the hypothesis that VPA might cause a decrease in cell motility through increased cell-substratum adhesion (Walmod and others 1999).

It has been reported that expression of the neuronal cell adhesion molecule N-CAM is upregulated in human neuroblastoma cells upon exposure to VPA (Cinatl Jr. and others 1996) while other cell adhesion molecules such as ICAM-1, VCAM-1, ELAM-1, and LFA-3 were not. The effect may reflect changes in the cell adhesion mechanism (Walmod and others 1988). Increased cell-cell adhesion may additionally contribute to VPA induced NTDs. VPA has been demonstrated to induce expression of a collagen type IV receptor in C6 glioma cells and astrocytes in primary cultures (Martin and Regan 1988). It has also been shown that VPA modifies the extracellular matrix in a three dimensional agarose gel culture of human chondrocytes, reducing the amount of collagen type II and increasing the deposition of collagen type I (Aulthouse and Hitt 1994).

CHAPTER 2

MATERIALS AND METHODS

Isolation and Culture of NCCs

Fertilized Red Rock hen eggs (Whelp, Inc., Bancroft, IA) were incubated 30-35 hours at 37° C with high humidity to obtain embryos at Hamburger-Hamilton stages 10⁻ through 10⁺ (Hamburger and Hamilton 1951). Embryos were located and removed from the egg using a ring of *Whatman* 3MM chromatography paper (Whatman Int. LTD, Maidstone, UK). The adhered embryo was immersed in Earle's Balanced Salt Solution (EBSS) (Sigma, St. Louis, MO) and warmed to 38° C for microdissection with glass needles as previously described (Wiens and others, 1992; Orris and Wiens, 1998). Trunk neural fold explants were obtained by making incisions midsagittally between neural folds, lateral to each, and then across the entire neural tube at the cranial end and at the eighth intersomitic groove (Figure 2).

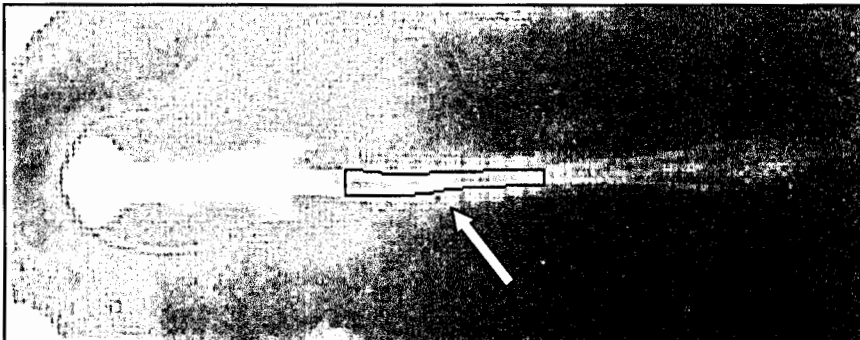


Figure 2 Stage 10 embryo as seen for microdissection. Black rectangle indicates area of trunk neural folds to be removed for culture. White arrow indicates somites used for stage identification. Magnification: 10x.

Neural tubes were removed from the embryos and placed into a fresh dish of EBSS. The notochords were dissected away leaving the left and right neural folds. Each was separated into 2-4 pieces approximately the length of two somites. One neural fold was cultured in Medium 199 with HEPES modification, pH 7.35 (Sigma, St. Louis, MO), supplemented with 1% antibiotic/antimycotic (Sigma, St. Louis, MO), 10% fetal bovine serum (Sigma, St. Louis, MO), and 5% donor horse serum (Atlanta Biologicals, Nacross, GA). The other was cultured in the same medium but with either 0.75, 1.5, 2.0, or 3.0 mM valproic acid (Sigma, St. Louis, MO) added from a stock of 0.75M or 1.0 M solution. This corresponds to a range found to be experimentally effective in previous studies and corresponds to serum concentrations found in human plasma after therapeutic VPA dosage (Gofflot et al. 1995; Kratke and Kirschbaum 1996; Walmod et al. 1998). Both were incubated in 35 mm Falcon *Primaria* culture dishes (Falcon, Becton-Dickenson, Lincoln Park, NJ) for 24-48 hours. For experiments intended for immunostaining, the same procedure and media were utilized. During this time, explants adhered to the culture surface, and NCCs migrated outward from them in all directions.

Image Capture

In order to collect motility and morphometry data, after 24 hours of culture, the dishes were removed from the incubator and immediately placed in a preheated aluminum block stage warmer on an Olympus CK2 inverted phase contrast microscope equipped with a Hitachi 3 CCD video camera. A field of 15-50 isolated migratory NCCs were identified at 100x and 14 sequential images were captured with an MVC PCI frame capture board (Imaging Technology, Bedford, MA) at three minute intervals using

Optimas imaging software, version 6.0 (Optimas Corporation Inc., Bothell, WA). Dish temperature was maintained at 38° C throughout the image capture period for optimum NCC migration capability. The images files were stored on the hard drive of a Gateway P5-166 computer, with copies on Iomega 100MB Zip disks (Iomega Corporation, Roy, Utah).

In order to determine total cell counts; proportions of flat, rounded, clustered, and independent cells, and assess overall explant morphology, single 40X images of the explants were also captured as before the dishes were fixed for immunocytochemistry.

Motion Analysis

The Optimas program was utilized to extract area morphometry and motion analysis data from each series of control or VPA-treated images. Each series of frames was opened in Optimas version 6.0 (Optimas Corporation Inc., Bothell, WA) and 12-14 isolated, flattened migratory cells were selected for analysis. Those that were rounded, had migrated out of the field of view, or were not clearly visible in any one of the frames were excluded from analysis. Each individual cell chosen for analysis was manually assigned a unique label to maintain correct data collection and export throughout data collection. The program was calibrated to take all measurements in micrometers. Using the computer mouse, each cell border was traced by hand for maximum accuracy (Figure 3).



Figure 3 Computer generated image of migratory NCCs cultured in the control condition. The periphery of the cell has been traced for morphometry and motion analysis. Image captured at 100x.

Optimas calculated the area, perimeter, circularity, maximum length, maximum width, velocity, and distance traveled between frames for each of the 10-14 individual traced cells for the fourteen frames. These values were then exported to the spreadsheet program Microsoft Excel. Area was defined as total area of an object within the perimeter outline. Perimeter was defined as total length of the perimeter of the area object. Centroid (center point) position was found by averaging all X and Y coordinates of pixels within the traced area, and using the single mean X and Y coordinates to define the centroid of the object. Circularity of each traced area was calculated as the ratio of the perimeter length squared, divided by the area (a minimum value of four π would only be obtained by true circles). Maximum length was defined as the longest axis of the outlined area. Width was the greatest distance measured perpendicular to the longest

axis. Distance traveled between frames was defined as the distance the cell's centroid had been displaced between successive frames. Velocity was defined as the displacement of the cells centroid between frames divided by the time between frames. For statistical analysis of area, perimeter, circularity, maximum length, maximum width, velocity, and distance traveled between frames, the mean parameter value was found per frame for all cells traced within that frame, resulting in 14 values for corresponding to the 14 frames in the 'movie'.

Elongation index, total distance migrated, dynamic change in area, and dynamic change in perimeter were manually calculated using the original exported data from Optimas, then added to the Excel spreadsheet for analysis. Elongation index was calculated in Microsoft Excel by dividing the width by the length of the cell. For statistical analysis, the mean elongation index value was found per frame for all cells traced within that frame, resulting in 14 values for corresponding to the 14 frames in the 'movie'. Total distance traveled was the sum of the distance traveled between successive frames for each cell. This resulted in 10-14 values, depending on the total number of cells selected for analysis in each particular movie. Dynamic change in area was calculated by finding the absolute value of the difference in area for each cell from frame to frame. The mean dynamic change in area was figured for all cells between each frame, resulting in 13 values for the 14 frame series. Dynamic change in perimeter was similarly calculated by finding the mean absolute value of the difference in perimeter for all cells in each frame resulting in 13 dynamic change in perimeter values.

Statistical Analysis

Measurements taken using the Optimas program were exported to Microsoft Excel for management, comparison, and descriptive statistics. For area, perimeter, circularity, width, length, and elongation index, the mean values for all cells were found per frame resulting in 14 values for either drug or control series. The differences between control and drug-treated cells were tested for significance utilizing the Wilcoxon rank sum test for nonparametric data. Velocity, total distance, change in distance migrated between frames, total distance migrated, total dynamic change in area and dynamic change in perimeter were all found for each individual cell for fourteen frames, resulting in 10-14 values based upon number of cells traced. The differences between control and drug-exposed cells were then tested for significance utilizing the Wilcoxon rank sum test for nonparametric data. For all tests, the approximate normal deviate $|Z|$ with a corresponding P value less than or equal to 0.05 was considered to be significant.

Immunohistochemistry

Monoclonal Anti-A-Cell Adhesion Molecule (A-CAM) antibody (Sigma, St. Louis, MO) was used to visualize N-cadherin at the cell junctions. This antibody localizes a 135 kD calcium-dependant adhesion molecule associated with intercellular adherens junctions in several species including chicken (Volk and others 1990). This antibody reacts with the N-terminal half of the extracellular domain of A-CAM (Volk 1984, 1990). Cultured explants were washed in PBS at 37°C and then fixed in 20% DMSO in methanol for 30 minutes. After PBS washing, 0.1% Triton X-100 in PBS was added for 3 to 5 minutes to permeabilize the cells. Blocking was done by incubating for

30 minutes in serum blocking solution, reagent 1A in the Zymed Histostain SP kit (Zymed Laboratories Inc., San Francisco, California). Incubation with Monoclonal Anti-A-CAM antibody (Sigma, St. Louis, MO) was performed for 30 minutes at 37° C with 100% humidity or overnight at 9°C with high humidity. Primary antibody was then removed, and the cultures were washed three times in PBS. Biotinylated secondary antibody, Biotin-Goat Anti-mouse IgG, (reagent 1B from the Zymed kit), was added for 30 minutes. Then the cultures were washed in PBS as before. In the dark, CY3-Streptavidin (Zymed Laboratories Inc., San Francisco, CA) was added to the cultures for 10 minutes at room temperature. The cultures were thoroughly washed with PBS and mounted in antifade mounting media, 5% n-propyl gallate (Sigma, St. Louis, MO), 25% 0.5M Tris pH 9.0, and 70 % glycerol. After drying overnight in the dark, the edges of the coverslips were sealed with Permount (Fischer Scientific, Fair Lawn, NJ). Images of the explants were captured both with phase-contrast optics and fluorescence on an Olympus BX40 microscope equipped with a 3 CCD video camera system (Optronics Engineering, Goleta, CA) for low light image capture. The fluorescence images were captured with a manual shutter speed of 2. The images files were stored on the hard drive of a Gateway P5-166 computer, with copies on Iomega 100MB Zip disks (Iomega Corporation, Roy, Utah).

Fluorescein isothiocyanate (FITC)-labeled phalloidin (Sigma, St. Louis, MO) was used to reveal the filamentous actin in cells. This phalloidin binds and stabilizes filamentous actin (Wulf and others 1976). Explants were washed in PBS at 37°C then fixed in 3.7% formaldehyde for 10 minutes. After PBS washing, 0.1% Triton X-100 in

PBS was added for 3-5 minutes with gentle agitation to permeabilize the cells. In the dark at room temperature, 100 μ l of a 5 μ g per ml solution of FITC-phalloidin was added to each dish for 60 minutes. The cultures were thoroughly washed with PBS and mounted in antifade mounting medium (33% w/v glycerol, 13.3% w/v Mowiol (Aldrich, Milwaukee, WI), 0.13 M Tris buffer, pH 8.5). All slides were kept in the dark at 4°C until images were taken of the cells. Images of the explants were captured with fluorescence optics on the Olympus BX40 microscope equipped with a 3 CCD video camera system (Optronics Engineering, Goleta, CA) designed for low light image capture using a manual shutter speed of 1. The images files were stored as above.

Proliferation Assay

Neural fold explants were cultured as described for 24 hours. At that time the initial culture medium was replaced with media containing a 10⁻² M solution of bromodeoxyuridine (BrdU) diluted 1:1000. After 2 hours of incubation, cultures were washed 2 times with 38°C PBS and visualization of BrdU incorporated nuclei was performed using reagents and methods from the Zymed BrdU staining kit (Zymed Laboratories, San Francisco, California). The dishes were mounted with a plastic coverslip in Gelmount from the kit and allowed to dry overnight. The total number of cells that had migrated from the explants was counted with a hand-held counter while viewing on an AO binocular microscope at 150x magnification. The number of emigrated NCCs positive for BrdU, indicated by purple-brown stained nuclei, was counted and a percent of total positive emigrated cells was then calculated. A Student's T-test was used to determine if percent stained was significantly different between

control and VPA-treated cultures. Using Optimas imaging software (Media Cybernetics, Bedford, MA), images were captured with a Hitachi 3 CCD video camera from an Olympus CK2 inverted phase contrast microscope and stored as before.

CHAPTER 3

RESULTS

The Effect of VPA on NCC Emigration and Explant Morphology

Neural fold tissues were dissected from embryos and placed into *Primaria* culture dishes for a 24-27 hour incubation period during which the explants adhered and cells began to migrate outward. At that time computer images were taken of some explants at 40X and 100X and stored on Iomega Zip disks and on the hard drive of a Gateway P5-166 computer. Control explants adhered to the *Primaria* surface and migrating cells were noted around the explant in at least 95% of cases. Explants cultured in the presence of 0.75 mM, 1.5 mM, and 2.0mM VPA had a 75-90% attachment rate with emigrating cells apparent after 24 hours. Explants cultured in the presence of 3.0 mM VPA had an attachment rate of about 50%, and of those approximately 40% had any cells migrating outward.

In control dishes scored for number of emigrated cells, an average of 275 cells per explant (range, 74-998) was found. The vast majority of these cells were independent, flat and demonstrated typical motile cell morphology (Figure 5a). Approximately 2-5 % were rounded and 5-10% were in clusters or sheet-like groups. The explant in the center of the carpet of cells was easily distinguished, having a distinct border and round or curved morphology. Approximately 5% of the control explants had 25% or less of their cells in an epithelial sheet formation extending from the explants edge.

In 0.75mM VPA-treated explants scored for number of emigrated cells, there was an average of 218 cells emigrated per explant with a range of 45-718. Slightly less than

half of the emigrated cells were independent, with 2-5% of those rounded, and the rest contained in epithelial sheets extending from the explant. The sheet comprised 25-75% of the explant's border; with the remaining portion a distinct boundary between explant and culture surface. Not every explant displayed some epithelial sheet morphology; 20-25% were similar to controls.

In 1.5 mM VPA-treated dishes scored for number of emigrated cells, an average of 247 per explant (range, 24-920) was calculated. In 2.0 mM VPA-treated dishes, an average of 133 cells per explant was recorded (range, 61-215). For both 1.5 and 2.0 mM VPA-treated groups, the number of explants displaying the epithelial sheet morphology around at least half of the explant was 70-75%. Some of the explants had two sheets on opposing sides, and some of these sheets curved around the explant in a wing shape (see Figure 11a). The remaining explant border was distinct and may or may not have had independent migratory cells around it. Also, seen in some 1.5 and 2.0 mM VPA-treated dishes, were completely flattened explants totally surrounded by an epithelial sheet, having no distinguishable border between the edge of the explant and the beginning of the sheet (Figure 5b). These explants had no independent cells outside of the sheet at all.

In 3.0 mM VPA-treated dishes that had attached explants with emigrated cells, an average of 121 cells per explant (range 0-321) were found. The occurrence of an epithelial sheet around the explant was seen in only 5-10% of cases. Most explants with migrating cells resembled control cells morphologically, although the overall density of cells in the carpet surrounding the explant seemed less. Half of the attached explants had zero to twenty cells. The few cells leaving the explant were rounded up, blebby, and

tended to be in clusters. Data describing the proportions of migrating cells are summarized in Table 1 and Figure 4. Typical appearances of the cultures are shown by photomicrographs in Figures 9a, 10a, and 11a.

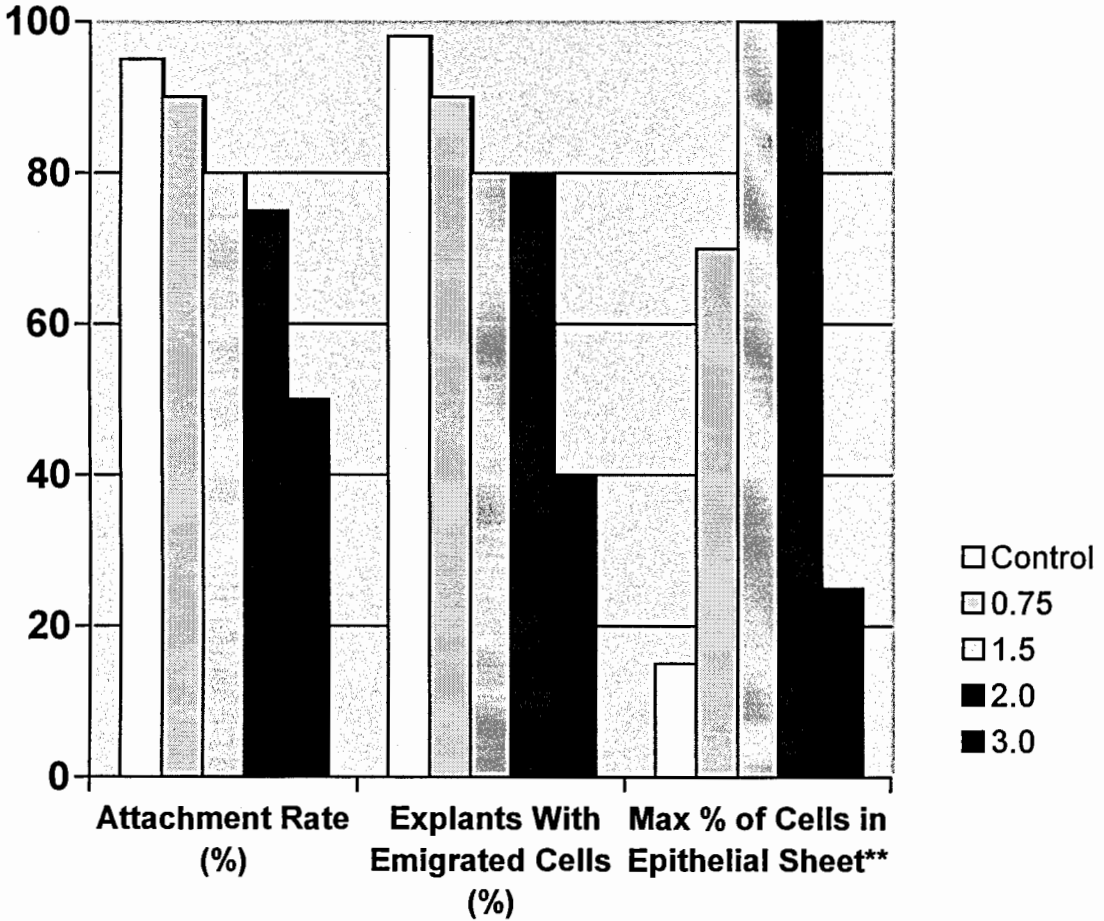
Table 1 The effects of VPA on explant attachment rates and cell emigration rates after 24 hours in culture *

	Explant Attachment Rate After 24 Hours	Percent of Explants With Emigrated Cells After 24 Hours	Mean Number of Emigrated Cells per Explant, Range	Percent of Emigrated Cells Incorporated Into Epithelial Sheet
Control	95% +	98%+	275, 74-998	0-15%
0.75 mM	90%	90%+	218, 45-718	0-70%
1.5 mM	80%	80%	247, 24-920	0-100%
2.0 mM	75%	80%	133, 61-215	0-100%
3.0 mM	50%	40%	121**, 0-321	0-25%

*N = 20-45 explants per treatment level.

**explants with less than 10 emigrated cells excluded (approximately one third of explants with emigrated cells apparent).

Figure 4 The effects of VPA on explant attachment and cell emigration rates after 24 hours in culture*



*N = 20-45 explants per treatment level.

**Explants with no cells incorporated into an epithelial sheet formation were seen in all treatment levels.

Figure 5a Control explant as seen with a phase contrast microscope, 40X. Cells are independent of one another as they leave the explant (A), center far left. The white arrow indicates a flattened cell displaying typical properties of a migrating cell, flattened against the culture surface with multiple filopodia extended. The black arrow indicates a rounded cell typical of a nonmigratory cell, possibly preparing for mitosis.

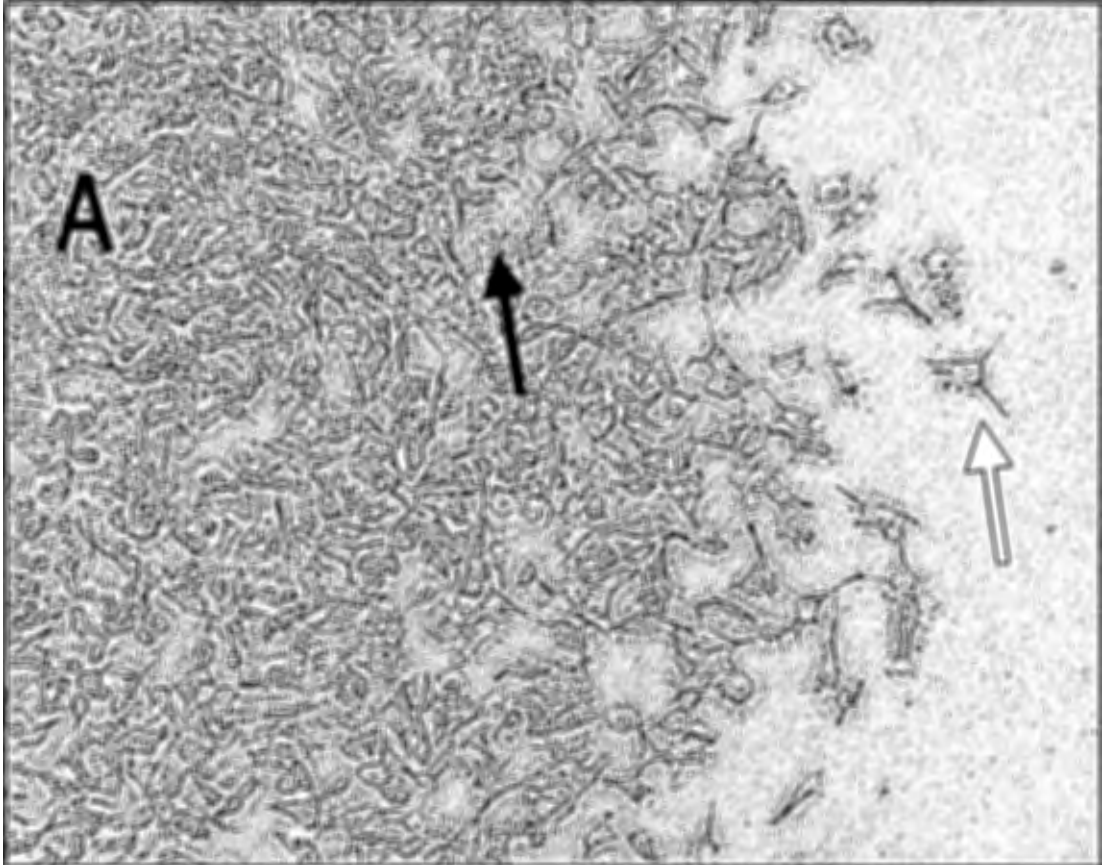
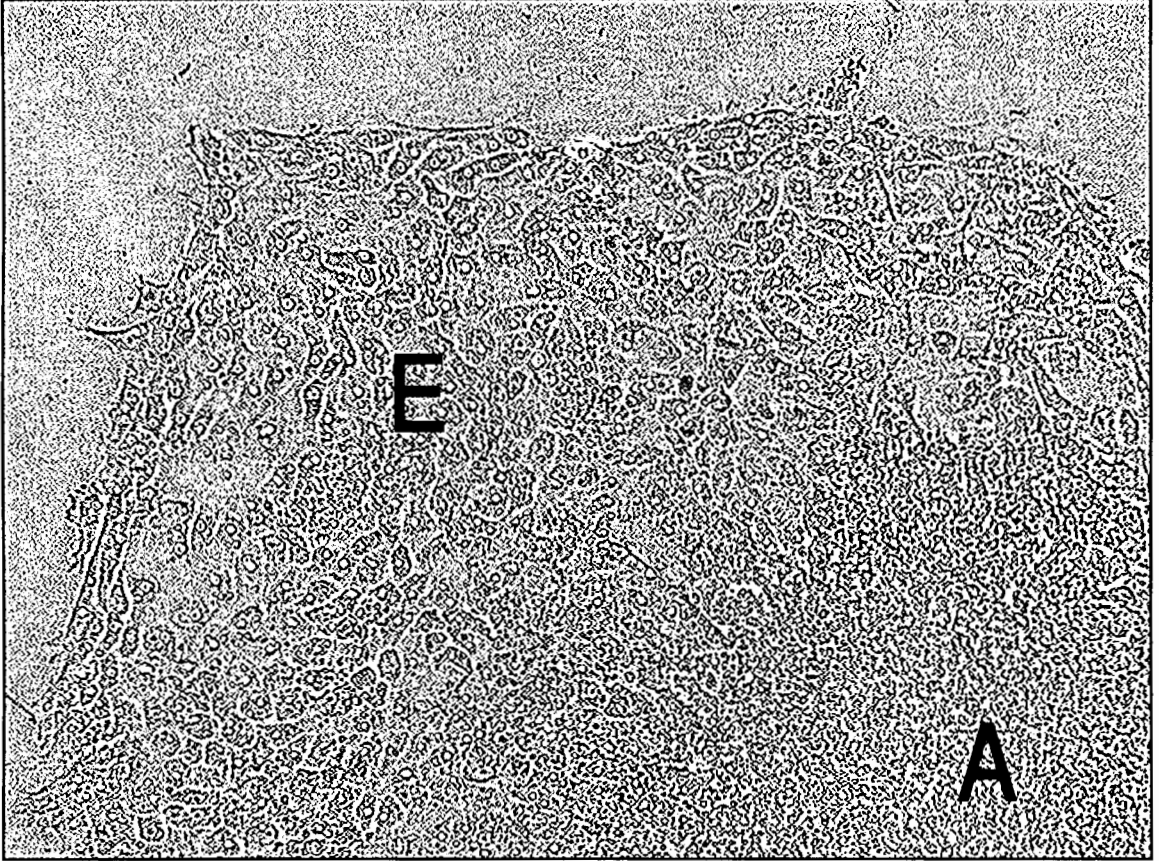


Figure 5b 2.0 mM VPA-treated explant as seen with a phase contrast microscope, 40X. The cells are not independent of one another when they leave the explant (A, lower right corner) but remain in an epithelial sheet (E).



The Effect of VPA on Cell Morphometry and Cell Morphology

To reveal the effect that VPA had on NCC morphology and motile behavior, explants were cultured in the presence of the drug and then 14 frame “movies” of the cells migrating on the culture surface were captured. Each dish was placed in an aluminum block stage warmer and once every three minutes for a total of 39 minutes an image was captured of a section of the cell carpet surrounding the explant with individual flattened migratory cells (Figure 6a). Depending on the number of migrated cells in the microscopic field of view, 6-14 were selected to analyze. Each of these cells was hand traced with the computer mouse through the complete series of frames (Figure 6b). The Optimas program was then commanded to generate a set of area morphometry data and a set of motion analysis data. These were exported to Microsoft Excel. There the appropriate parameters in the spreadsheet were selected for descriptive statistics, producing the mean, standard deviation, median, standard error, and range for each cell throughout the “movie.” This data was then averaged for all cells and tested for significance with a Wilcoxon rank Sum test using the SAS statistical package (SAS Institute, Cary, NC) running on the university mainframe computer.

Tables 2a-2d display the mean \pm standard deviation, median, and range for the morphometry parameters area, perimeter, circularity, elongation index, maximum length, maximum width, and statistical significance for each of the four drug treatments. Tables 3a-3d display the mean \pm standard deviation, median, and range of the motility parameters migration velocity, dynamic change in area and dynamic change in perimeter for each of the four drug treatments. For the majority of the parameters, both significant

increases and significant decreases were seen within the same drug treatment level. For example, as shown in Table 2a, in one experiment there was a significant difference between the mean control cell perimeter ($170 \pm 11.7 \mu\text{m}$) and the mean 0.75 mM VPA-treated cell perimeter ($126 \pm 14.3 \mu\text{m}$) ($p \leq 0.0001$). In another experiment comparison of the mean control cell perimeter ($166 \pm 5.6 \mu\text{m}$) and the mean 0.75mM VPA-treated cell perimeter ($209 \pm 1.8 \mu\text{m}$) was found to also be significantly different ($p \leq 0.0001$).

Overall, area and maximum width were the most consistently decreased parameters for all drug-treated groups. Perimeter and maximum length were generally decreased for all drug-treated groups with the exception of the 2.0 mM treatment, which was generally increased. There was little consistency or significance in the differences between control and drug-treated cells for migration velocity, but dynamic change in area and perimeter were decreased overall, and all significant differences ($p \leq 0.05$) were decreases.

For cells treated with 0.75mM VPA, migration velocity, dynamic change in area, and dynamic change in perimeter were consistently significantly lower than controls ($p \leq 0.05$). For cells treated with 1.5 mM VPA, area, perimeter, maximum width, dynamic change in area, and dynamic change in perimeter showed consistently significantly lower levels than controls ($p \leq 0.05$). For cells treated with 2.0 mM VPA, significant increases in circularity were found ($p \leq 0.05$), while migration velocity, dynamic change in area, and dynamic change perimeter had significant differences from control that were consistently lower ($p \leq 0.05$). For cells treated with 3.0 mM VPA, area, dynamic change in area and dynamic change in perimeter were consistently significantly lower than

controls($p \leq 0.05$). Photographs of control and 2.0 mM VPA-treated cells are shown in Figures 6a-6b.

Figure 6a Example of control cells ready for video image analysis with Optimas. Migrating cells are spread and irregular in shape, showing many characters of typical motile behavior. Magnification 200X.



Figure 6b Example of 2.0 mM VPA-treated cells just prior to video image analysis with Optimas. These migrating cells look similar to controls but are less spread on culture surface and have fewer processes. Arrow indicates a cell outlined for morphometry and motility data analysis with Optimas. Magnification 200X.

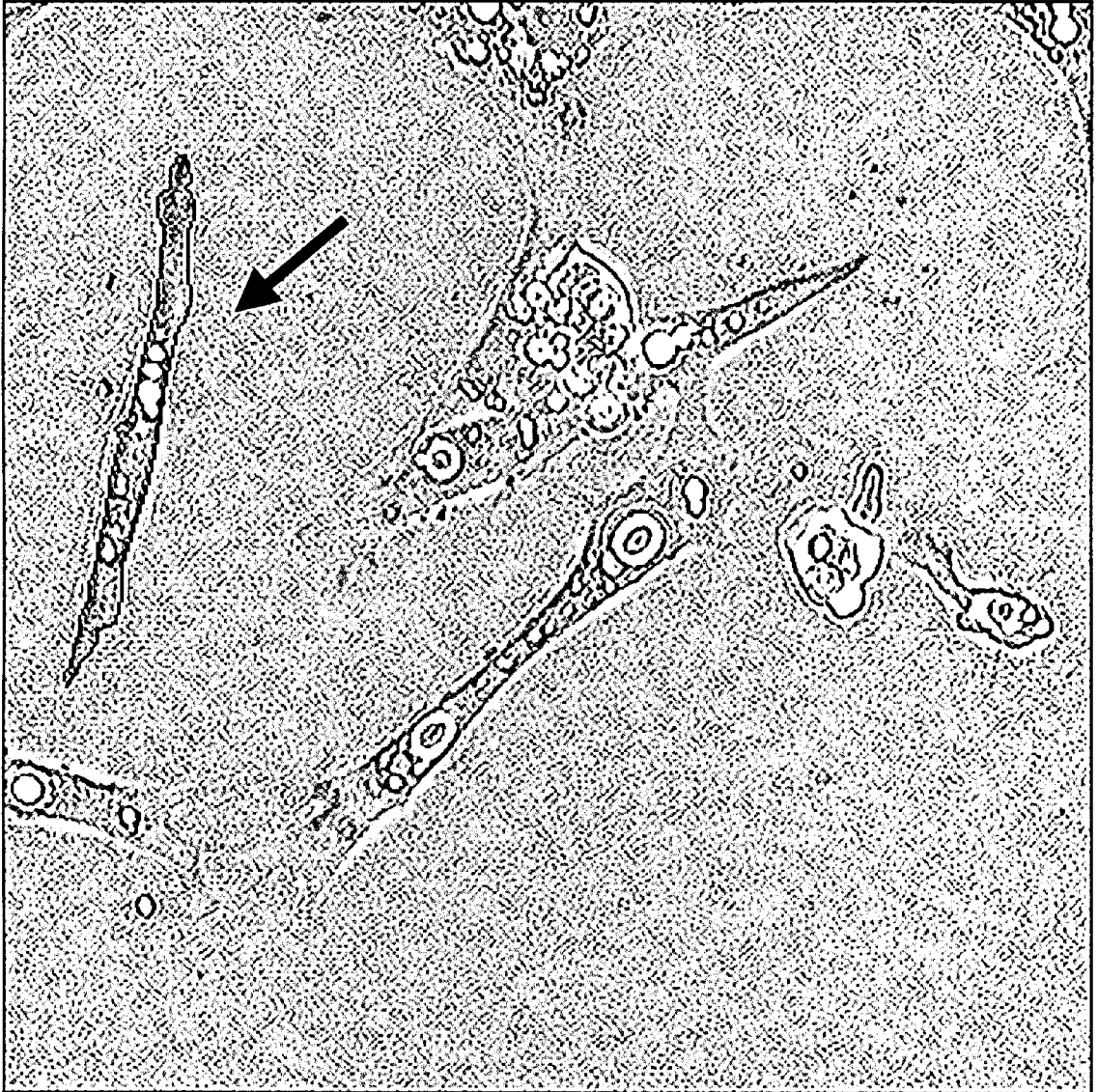


Table 2a The effect of 0.75mM VPA on NCC morphometry parameters. Data from each experiment are given as mean \pm standard deviation, and median with range as determined by video image analysis.

	Area (μm^2)	Perimeter (μm)	Circularity	Elongation Index	M. Length (μm)	M. Width (μm)
Control	626 \pm 34.8	170 \pm 11.7	55 \pm 4.2	0.51 \pm 0.10	61 \pm 6.3	29 \pm 4.0
	629, 570-705	169, 153-191	54, 51-68	0.54, 0.38-0.63	59, 52-71	30, 23-33
	1369 \pm 44	264 \pm 11.2	49 \pm 6.0	0.46 \pm 0.02	90 \pm 2.9	38 \pm 1.3
	1368, 1293-1455	259, 250-290	47.3, 42-61	0.46, 0.44-0.48	89, 86-94	37, 35-39
	647 \pm 40.0	187 \pm 15.9	56 \pm 7.3	0.47 \pm 0.048	66 \pm 6.8	28 \pm 1.3
	633, 603-745	179, 170-218	54, 49-71	0.49, 0.40-0.54	63, 59-79	28, 24-29
	753 \pm 30.8	173 \pm 5.7	42 \pm 2.6	0.56 \pm 0.049	58 \pm 2.3	31 \pm 2.0
	749, 697-799	173, 165-183	43, 37-45	0.55, 0.50-0.66	57, 28-34	31, 28-34
	723 \pm 66.7	183 \pm 13.4	49 \pm 3.6	0.55 \pm 0.033	61 \pm 3.9	32 \pm 3.4
	733, 616-823	183, 159-202	50, 42-55	0.54, 0.49-0.61	62, 53-67	32, 28-37
	606 \pm 55.3	166 \pm 5.6	48 \pm 2.2	0.50 \pm 0.042	56 \pm 1.8	26 \pm 0.62
	598, 513-694	173, 120-189	50, 29-58	0.50, 0.44-0.57	56, 42-66	25, 22-30
	602 \pm 48.4	184 \pm 15.6	58 \pm 6.9	0.45 \pm 0.04	59 \pm 4.2	26 \pm 1.6
	619, 487-651	188, 150-200	59, 45-68	0.48, 0.43-0.54	65, 60-70	28, 28-32
0.75mM VPA	613 \pm 69.0	126 \pm 14.3	28 \pm 4.5	0.68 \pm 0.03	43 \pm 4.7	27 \pm 2.1
	620, 483-702	123*, 101-150	26*, 22-35	0.67*, 0.61-0.75	40*, 35-50	27, 23-30
	516 \pm 20	124 \pm 4.2	31 \pm 1.7	0.69 \pm 0.05	40 \pm 2.0	26 \pm 1.7
	519*, 468-543	124*, 116-130	30*, 28-33	0.69*, 0.61-0.77	39*, 36-43	26*, 23-29
	784 \pm 51.7	203 \pm 15.1	54 \pm 6.1	0.48 \pm 0.04	67 \pm 2.2	30 \pm 2.4
	783*, 725-866	202*, 184-233	55, 45-64	0.48, 0.43-0.56	67*, 62-70	29*, 27-34
	583 \pm 34.7	142 \pm 6.4	36 \pm 3.9	0.49 \pm 0.016	53 \pm 2.4	25 \pm 1.1
	581*, 545 -646	140*, 134-154	36*, 32-39	0.50, 0.46-0.51	52*, 48-56	24*, 22-25
	576 \pm 23.9	154 \pm 5.2	43 \pm 2.4	0.51 \pm 0.022	54 \pm 1.7	26 \pm 0.94
	584*, 523-610	156*, 143-162	43, 41-49	0.51*, 0.47-0.55	54*, 51-57	26*, 24-27
	762 \pm 26.6	182 \pm 5.0	45 \pm 2.1	0.50 \pm 0.296	62 \pm 2.5	30 \pm 1.4
	762, 171-802	181, 175-191	45*, 40-48	0.50*, 0.46-0.54	61, 58-68	29, 28-32
	889 \pm 42.1	209 \pm 1.8	62 \pm 5.4	0.50 \pm 0.02	65 \pm 0.58	31 \pm 0.29
	888*, 809-945	211*, 200-220	55*, 46-85	0.50, 0.48-0.54	64*, 62-69	31*, 29-32
	834 \pm 40.3	195 \pm 9.9	50 \pm 5.4	0.48 \pm 0.033	66 \pm 2.8	29 \pm 1.1
	843*, 738-886	197*, 175-210	50*, 38-56	0.48, 0.43-0.54	65*, 60-70	28*, 28-32

*Significantly different from control, $p \leq 0.05$, Wilcoxon rank sum test

Table 2b The effect of 1.5 mM VPA on NCC morphometry parameters. Data from each experiment are given as mean \pm standard deviation, and median with range as determined by video image analysis.

	Area (μm^2)	Perimeter (μm)	Circu- larity	Elongation Index	M. Length (μm)	M. Width (μm)
Control	1129 \pm 43.9	226 \pm 7.3	48 \pm 3.7	0.47 \pm 0.078	80 \pm 3.7	35 \pm 4.3
	1122, 1078-1216	224, 215-236	49, 41-54	0.46, 0.33-0.60	81, 75-88	36, 28-41
	1072 \pm 41.5	244 \pm 7.8	58 \pm 4.4	0.45 \pm 0.031	83 \pm 2.7	34 \pm 2.3
	1069, 1013-1130	248, 231-254	58, 51-66	0.05, 0.39-0.50	83, 79-87	35, 30-38
	1169 \pm 28.2	253 \pm 9.1	56 \pm 4.5	0.47 \pm 0.023	83 \pm 1.9	37 \pm 1.3
	1176, 1125-1205	255, 238-266	57, 48-64	0.46, 0.42-0.50	83, 81-87	38, 35-39
	1221 \pm 40.0	225 \pm 8.4	46 \pm 3.9	0.48 \pm 0.024	82 \pm 3.5	35 \pm 1.1
	1236, 1151-1289	223, 214-243	44, 42-57	0.48, 0.43-0.52	81, 77-89	35, 33-37
	1021 \pm 43.7	314 \pm 9.4	104 \pm 5.6	0.36 \pm 0.070	111 \pm 4.7	35 \pm 5.0
	1020, 951-1097	314, 297-335	105, 96-115	0.46, 0.41-0.52	112, 102-117	35, 29-43
	1209 \pm 45.0	265 \pm 7.3	60 \pm 4.2	0.51 \pm 0.055	79 \pm 3.5	40 \pm 2.8
	1208, 1115-1276	265, 251-280	60, 53-68	0.51, 0.44-0.62	78, 74-85	40, 35-45
1.5 mM VPA	1038 \pm 110.0	213 \pm 15.9	48 \pm 3.1	0.45 \pm 0.020	75 \pm 4.5	33 \pm 2.0
	1051*, 821-1172	217*, 178-237	47, 42-54	0.46*, 0.41-0.49	75, 66-82	33, 27-35
	867 \pm 26.7	202 \pm 7.5	49 \pm 4.1	0.58 \pm 0.019	64 \pm 2.2	36 \pm 0.953
	865*, 818-917	203*, 187-215	50*, 40-56	0.57*, 0.55-0.62	64*, 60-67	36, 34-39
	1015 \pm 126	255 \pm 11.7	67 \pm 5.5	0.43 \pm 0.027	95 \pm 3.7	34 \pm 2.6
	1064*, 823-1150	256, 239-274	65*, 61-79	0.43*, 0.38-0.47	97*, 89-100	34*, 28-38
	976 \pm 61.9	234 \pm 13.8	59 \pm 3.7	0.40 \pm 0.028	88 \pm 2.5	30 \pm 3.3
	965*, 892-1095	231, 216-256	59*, 52-67	0.38*, 0.35-0.44	88*, 84-93	29*, 26-37
	895 \pm 36.7	257 \pm 8.4	77 \pm 5.8	0.47 \pm 0.033	82 \pm 5.0	36 \pm 1.2
	889*, 829-954	258*, 245-272	77*, 68-89	0.47*, 0.41-0.53	83*, 72-91	36, 33-37
	497 \pm 52.0	157 \pm 23.6	52 \pm 10.9	0.55 \pm 0.040	52 \pm 6.2	26 \pm 4.2
	486*, 406-594	157*, 119-200	54*, 32-72	0.54, 0.49-0.63	51*, 42-61	25*, 20-36
	829 \pm 42.4	230 \pm 8.3	69 \pm 7.8	0.47 \pm 0.045	76 \pm 3.62	34 \pm 2.60
	848*, 765-888	229*, 211-246	68*, 55-87	0.47, 0.39-0.55	76, 72-84	35*, 29-38

*Significantly different from control, $p \leq 0.05$, Wilcoxon rank sum test

Table 2c The effect of 2.0 mM VPA on NCC morphometry parameters. Data from each experiment are given as mean \pm standard deviation, and median with range as determined by video image analysis.

	Area (μm^2)	Perimeter (μm)	Circu- larity	Elongation Index	M. Length (μm)	M. Width (μm)
Control	1250 \pm 39	241 \pm 7.4	47 \pm 2.4	0.46 \pm 0.032	83 \pm 2.0	36 \pm 2.4
	1253, 1177-1307	241, 233-259	48, 44-52	0.46, 0.40-0.51	83, 80-88	36, 33-41
	706 \pm 73.6	178 \pm 12.1	48 \pm 4.9	0.59 \pm 0.049	56 \pm 1.9	32 \pm 2.9
	720, 560-793	180, 156-193	47, 38-56	0.59, 0.50-0.65	56, 53-59	32, 28-36
	845 \pm 97.6	210 \pm 21	57 \pm 6.4	0.46 \pm 0.033	73 \pm 5.4	32 \pm 3.8
	863, 689-968	210, 171-247	58, 45-70	0.46, 0.41-0.51	73, 62-81	33, 24-36
	903 \pm 41.7	223 \pm 14.1	58 \pm 5.3	0.53 \pm 0.041	76 \pm 4.6	36 \pm 2.7
	911, 811-960	226, 198-245	57, 48-65	0.51, 0.48-0.62	76, 68-83	36, 31-39
2.0 mM VPA	661 \pm 33	172 \pm 7.6	47 \pm 3.6	0.45 \pm 0.024	64 \pm 3.6	25 \pm 0.99
	676*, 595-692	173*, 156-182	49, 40-51	0.45, 0.40-0.48	64*, 57-69	26*, 23-27
	617 \pm 28	190 \pm 10.2	61 \pm 5.0	0.44 \pm 0.030	66 \pm 2.2	27 \pm 1.5
	623*, 573-653	191*, 171-202	62*, 52-66	0.45*, 0.37-0.49	66*, 60-69	27*, 24-29
	657 \pm 47.0	188 \pm 16.7	59 \pm 7.8	0.47 \pm 0.049	66 \pm 5.3	28 \pm 3.2
	652*, 581-736	186, 165-213	60*, 48-73	0.45*, 0.38-0.52	66*, 58-74	28*, 22-33
	560 \pm 47.7	181 \pm 12.2	62 \pm 6.2	0.52 \pm 0.650	58 \pm 3.6	27 \pm 3.5
	555*, 487-637	180*, 162-203	58, 55-74	0.53*, 0.44-0.68	58*, 51-64	27*, 22-33
	919 \pm 58.0	219 \pm 15.0	55 \pm 5.1	0.51 \pm 0.051	71 \pm 2.0	35 \pm 4.0
	901, 849-1033	213, 202-253	55, 49-67	0.50*, 0.44-0.60	71, 69-75	34, 30-42
	1394 \pm 48.4	271 \pm 12.7	56 \pm 4.6	0.48 \pm 0.027	90 \pm 4.7	40 \pm 1.7
	1411*, 1286-1449	271*, 238-292	56, 47-66	0.48*, 0.44-0.53	91*, 76-94	40*, 37-43
	933 \pm 52.0	276 \pm 14.8	89 \pm 5.5	0.33 \pm 0.033	105 \pm 5.2	29 \pm 2.8
	943, 858-1006	283*, 245-293	89*, 77-97	0.33*, 0.25-.040	106*, 95-113	29*, 25-33

*Significantly different from control, $p \leq 0.05$, Wilcoxon rank sum test.

Table 2d The effect of 3.0 mM VPA on NCC morphometry parameters. Data from each experiment are given as mean \pm standard deviation, and median with range as determined by video image analysis.

	Area (μm^2)	Perimeter (μm)	Circu- larity	Elongation Index	M. Length (μm)	M. Width (μm)
Control	906 \pm 26.3	212 \pm 11.6	55 \pm 5.8	0.48 \pm 0.027	77 \pm 4.7	31 \pm 1.7
	904, 863-945	211, 198-232	55, 47-64	0.49, 0.45-0.54	76, 71-83	31, 28-35
	1657 \pm 96.0	283 \pm 9.5	52 \pm 2.8	0.61 \pm 0.034	81 \pm 2.7	47 \pm 2.0
	1683, 1501-1767	282, 271-297	52, 48-57	0.61, 0.55-0.67	80, 78-86	48, 44-51
	1719 \pm 49.6	292 \pm 14.7	53 \pm 3.9	0.49 \pm 0.025	93 \pm 3.1	44 \pm 2.8
	1719, 1652-1844	290, 271-323	52, 47-59	0.50, 0.45-0.53	92, 89-98	43, 41-50
	1176 \pm 150.3	288 \pm 18.1	73 \pm 3.2	0.39 \pm 0.028	105 \pm 4.6	37 \pm 3.1
	1137, 998-1402	280, 268-317	74, 68-78	0.39, 0.35-0.44	103, 98-114	36, 33-42
	861 \pm 35.7	227 \pm 7.5	66 \pm 6.1	0.39 \pm 0.048	86 \pm 3.7	26 \pm 1.3
	867, 812-912	227, 218-243	67, 57-78	0.41, 0.31-0.45	85, 82-93	26, 24-28
3.0 mM VPA	774 \pm 28.9	252 \pm 5.3	95 \pm 5.8	0.55 \pm 0.377	86 \pm 2.8	40 \pm 2.8
	768*, 742-819	249*, 246-263	93*, 87-107	0.55*, 0.50-0.60	87*, 80-89	39*, 36-44
	954 \pm 75	224 \pm 13.0	55 \pm 3.7	0.53 \pm 0.04	73 \pm 6.1	37 \pm 2.7
	986*, 795-1046	228*, 196-243	56*, 48-61	0.53*, 0.46-0.60	74*, 61-80	38*, 33-43
	631 \pm 38.0	173 \pm 8.2	50 \pm 3.1	0.46 \pm 0.040	65 \pm 3.5	25 \pm 1.2
	617*, 581-698	176*, 162-187	49, 47-55	1.45*, 0.40-0.52	66*, 60-70	25*, 23-28
	913 \pm 95	191 \pm 19.9	43 \pm 5.8	0.53 \pm 0.027	66 \pm 5.8	31 \pm 2.6
	897*, 746-1040	198*, 155-214	44*, 33-49	0.52*, 0.49-0.59	69*, 55-71	32*, 27-35
	820 \pm 95.2	174 \pm 20.9	38 \pm 5.3	0.57 \pm 0.37	59 \pm 7.0	30 \pm 3.5
	808, 688-980	171*, 145-203	39*, 30-47	0.57*, 0.52-0.65	56*, 51-68	31*, 24-35

*Significantly different from control, $p \leq 0.05$, Wilcoxon rank sum test.

Table 3a The effect of 0.75mM VPA on NCC motility parameters. Data from each experiment are given as mean \pm standard deviation, and median with range as determined by video image analysis.

	Dynamic Change in Area (μm^2)	Dynamic Change in Perimeter (μm)	Migration Velocity ($\mu\text{m per min}^2$)
Control	107 \pm 38.9	32 \pm 11.4	0.03 \pm 0.009
	97.3, 59.8-161.8	29, 17-52	0.03, 0.02-0.04
	217 \pm 146.9	36 \pm 16.7	0.03 \pm 0.011
	138, 84-549	32, 14-73	0.03, 0.01-0.05
	105 \pm 18.3	38 \pm 43.0	0.03 \pm 0.012
	105, 79-136	28, 16-172	0.02, 0.02-0.05
	83 \pm 20.1	18 \pm 4.2	0.03 \pm 0.007
	86, 49-124	18, 12-25	0.02, 0.02-0.04
	111 \pm 35.4	27 \pm 8.8	0.02 \pm 0.007
	113, 62-177	25, 15-47	0.02, 0.02-0.03
	165 \pm 60.6	39 \pm 3.6	0.04 \pm 0.012
	127, 85-275	36, 23-57	0.04, 0.02-0.07
	149 \pm 41.3	38 \pm 9.9	0.03 \pm 0.013
	136, 107-253	37, 25-58	0.03, 0.02-0.07
0.75 mM VPA	102 \pm 28.4	21 \pm 8.4	0.03 \pm 0.012
	96, 61-156	21*, 9-38	0.03, 0.02-0.06
	104 \pm 39.5	22 \pm 8.6	0.03 \pm 0.010
	101*, 50-184	20*, 13-40	0.03, 0.01-0.05
	125 \pm 48.9	32 \pm 10.9	0.04 \pm 0.021
	124, 57-241	34, 13-49	0.03, 0.02-0.09
	113 \pm 43.8	23 \pm 7.8	0.02 \pm 0.010
	104, 64-184	24, 13-33	0.02, 0.01-0.04
	73 \pm 17.9	20 \pm 5.1	0.02 \pm 0.009
	70, 43-109	20, 12-28	0.02, 0.02-0.05
	112 \pm 23.7	23 \pm 7.3	0.02 \pm 0.008
	114, 68-143	26, 10-30	0.02, 0.01-0.04
	209 \pm 103	27 \pm 10.3	0.02 \pm 0.010
	159, 73-371	24*, 16-54	0.02*, 0.01-0.03
	150 \pm 55.3	26 \pm 7.6	0.02 \pm 0.013
	138, 65-265	30*, 15-37	0.02*, 0.01-0.06

*Significantly different from control, $p \leq 0.05$, Wilcoxon rank sum test.

Table 3b The effect of 1.5 mM VPA on NCC motility parameters. Data from each experiment are given as mean \pm standard deviation, and median with range as determined by video image analysis.

	Dynamic Change in Area (μm^2)	Dynamic Change in Perimeter (μm)	Migration Velocity ($\mu\text{m per min}^2$)
Control	290 \pm 130	38 \pm 11.9	0.03 \pm 0.009
	317, 102-497	38, 22-61	0.02, 0.01-0.04
	180 \pm 99.3	40 \pm 20.4	0.3 \pm 0.011
	134, 52-368	31, 21.5-79	0.03, 0.01-0.05
	124 \pm 42.9	28 \pm 7.8	0.02 \pm 0.010
	114, 76-200	28, 19-44	0.02, 0.01-0.05
	269 \pm 134.3	30 \pm 9.8	0.02 \pm 0.006
	322, 115-502	29, 20-56	0.02, 0.01-0.04
	125 \pm 69	30 \pm 8.4	0.03 \pm 0.015
	99, 59-284	31, 18-46	0.02, 0.01-0.05
	188 \pm 88.8	45 \pm 16.7	0.02 \pm 0.008
	211, 57-371	45, 23-76	0.02, 0.01-0.04
1.5 mM VPA	137 \pm 48.0	25 \pm 8.8	0.02 \pm 0.006
	120*, 74-248	24*, 16-41	0.02, 0.01-0.03
	155 \pm 80	31 \pm 13.8	0.02 \pm 0.011
	154, 45-267	26, 17-54	0.03, 0.01-0.04
	124 \pm 52.4	27 \pm 8.1	0.02 \pm 0.011
	133, 50-222	27, 15-44	0.02, 0.01-0.04
	196 \pm 91	37 \pm 12.9	0.02 \pm 0.008
	183, 71-374	38, 21-54	0.02, 0.02-0.04
	130 \pm 47.6	34 \pm 13.7	0.04 \pm 0.012
	112, 70-226	34, 14-58	0.03, 0.02-0.06
	129 \pm 31.6	44 \pm 12.3	0.05 \pm 0.01
	123, 84-198	45, 25-64	0.05*, 0.03-0.07
	126 \pm 48.8	23 \pm 7.6	0.02 \pm 0.007
	129, 65-245	22*, 13-37	0.02, 0.02-0.04

*Significantly different from control, $p \leq 0.05$, Wilcoxon rank sum test.

Table 3c The effect of 2.0 mM VPA on NCC motility parameters. Data from each experiment are given as mean \pm standard deviation, and median with range as determined by video image analysis.

	Dynamic Change in Area (μm^2)	Dynamic Change in Perimeter (μm)	Migration Velocity ($\mu\text{m per min}^2$)
Control	189 \pm 76.4	36 \pm 17.9	0.02 \pm 0.009
	194, 79-316	39, 19-53	0.02, 0.01-0.04
	142 \pm 52.8	29 \pm 5.7	0.03 \pm 0.011
	133, 54-230	28, 17-40	0.03, 0.01-0.05
	266 \pm 116.2	46 \pm 14.9	0.04 \pm 0.016
	247, 138-498	46, 20-76	0.05, 0.01-0.07
	214 \pm 68	47 \pm 16.7	0.04 \pm 0.012
	196, 121-329	45, 25-77	0.04, 0.02-0.07
2.0 mM VPA	169 \pm 66	49 \pm 41.3	0.03 \pm 0.01
	129*, 54-87	35, 26-176	0.03, 0.02-0.06
	122 \pm 72.0	40 \pm 22.3	0.03 \pm 0.016
	95, 57-294	31, 20-108	0.03, 0.02-0.07
	142 \pm 86	33 \pm 16.0	0.02 \pm 0.013
	105, 73-351	35, 10-58	0.02, 0.01-0.06
	115 \pm 39.1	34 \pm 9.3	0.03 \pm 0.136
	116*, 51-192	32*, 17-48	0.03, 0.01-0.06
	167 \pm 92.5	30 \pm 12.9	0.03 \pm 0.008
	141*, 46-332	25*, 15-54	0.03*, 0.02-0.04
	266 \pm 147.2	41 \pm 18.2	0.02 \pm 0.010
	235, 108-634	38, 18-78	0.02, 0.01-0.05
	111 \pm 35.1	25 \pm 12.4	0.04 \pm 0.016
	111*, 63-165	23*, 11-54	0.04, 0.02-0.07

*Significantly different from control, $p \leq 0.05$, Wilcoxon rank sum test.

Table 3d The effect of 3.0 mM VPA on NCC motility parameters. Data from each experiment are given as mean \pm standard deviation, and median with range as determined by video image analysis.

	Dynamic Change in Area (μm^2)	Dynamic Change in Perimeter (μm)	Migration Velocity ($\mu\text{m per min}^2$)
Control	139 \pm 48.5	31 \pm 9.8	0.03 \pm 0.008
	151, 64-222	30, 19-49	0.03, 0.01-0.04
	239 \pm 128.8	38 \pm 15.6	0.02 \pm 0.009
	201, 97-436	38, 16-60	0.02, 0.01-0.04
	364 \pm 219.0	48 \pm 24.4	0.02 \pm 0.006
	313, 90-768	50, 12-93	0.02, 0.01-0.03
	101 \pm 41	30 \pm 19.0	0.03 \pm 0.012
	91, 55-197	27, 7-69	0.02, 0.01-0.05
	100 \pm 70.4	25 \pm 13.6	0.03 \pm 0.132
	77, 26-301	22, 12-54	0.02, 0.01-0.05
3.0 mM VPA	86 \pm 33	35 \pm 41	0.03 \pm 0.014
	80*, 50-145	23, 13-136	0.03, 0.01-0.05
	100 \pm 22.7	24 \pm 6.0	0.03 \pm 0.007
	97*, 63-155	26*, 16-34	0.03, 0.02-0.05
	73 \pm 20.8	19 \pm 9.4	0.02 \pm 0.009
	67*, 37-107	13*, 10-39	0.02, 0.01-0.04
	90 \pm 30.9	20 \pm 8.4	0.03 \pm 0.009
	77, 46-147	19, 11-36	0.03, 0.02-0.05
	92 \pm 40	17 \pm 7.5	0.02 \pm 0.012
	85, 37-169	15, 9.6-35	0.01, 0.01-0.04

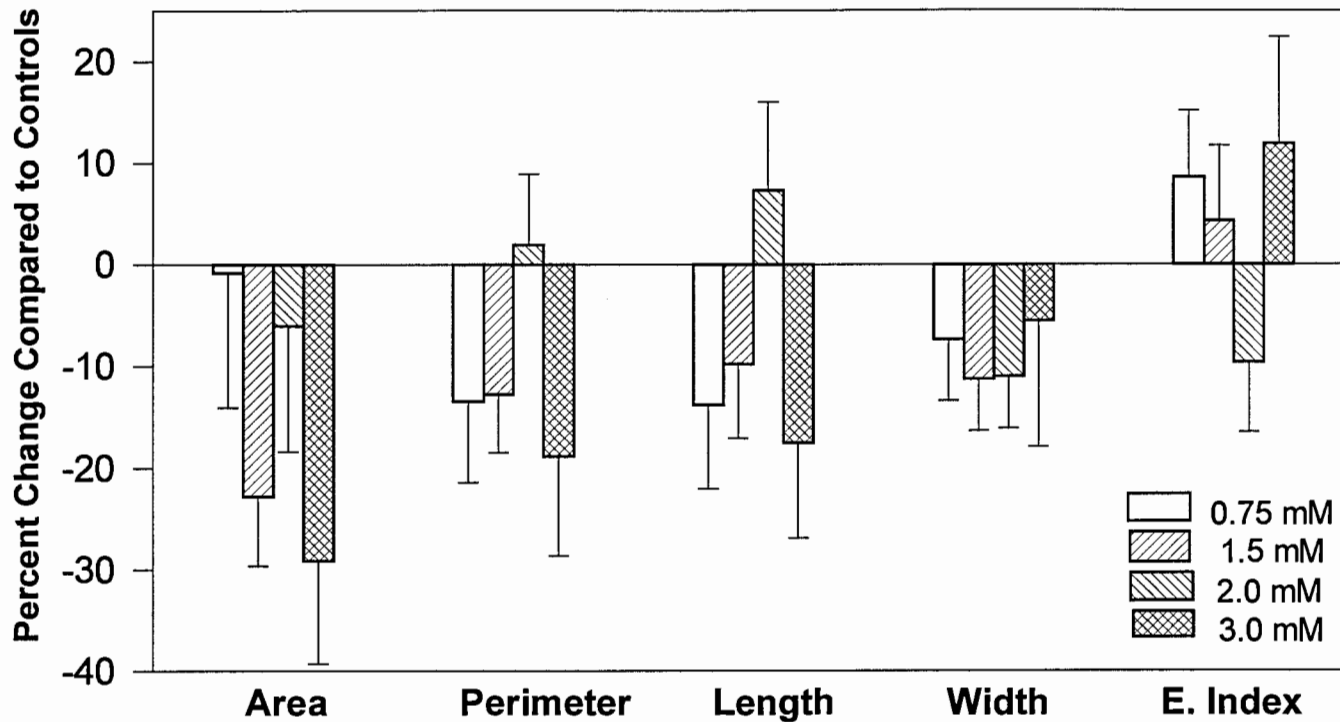
*Significantly different from control, $p \leq 0.05$, Wilcoxon rank sum test.

In order to more clearly display the effects of VPA on the NCCs' morphometry and motility behaviors, the mean percent change \pm standard error from control was calculated using the medians for each experiment. These values were then plotted in two bar graphs, one for cell morphometry (Figure 7) and one for cell motility parameters (Figure 8). Area overall was decreased for all groups from 6 to 29% of the control area. The effect of VPA appeared to be dose responsive, although the data at 2.0 mM does not fit. Perimeter was also decreased to 13-19% of control level with the exception of 2.0 mM VPA, which had a mean increase of 2%. Maximum length data looked very similar to that of perimeter, with a decrease of 10-18% of controls for all treatments except 2.0 mM, with an increase of 7% over controls. Maximum width was most affected at 1.5 mM and 2.0 mM, an 11% decrease from controls. At 0.75 and 3.0 mM VPA, similar decreases of 6% and 7% from control respectively, were seen. Consistent with the length and width data, the elongation index was 4%-12% higher (cells less elongated) than controls for all treatments except 2.0 mM, which was 10% lower (cells more elongated) than controls.

Migration velocity was not consistently changed from controls, and showed a large amount of standard error. For 3.0 mM VPA, the mean was an 8% increase from controls, but the standard error was 19.6%. Dynamic change in area seemed to demonstrate a dose response curve, with 0.75mM, 1.5mM, 2.0mM, and 3.0mM all showing decreases (4%, 20%, 29% and 28% respectively) compared to controls. Dynamic change in perimeter also indicated a possible dose response curve, with 0.75mM, 1.5mM, 2.0mM, and 3.0mM all showing decreases of 14%, 10%, 16%, and

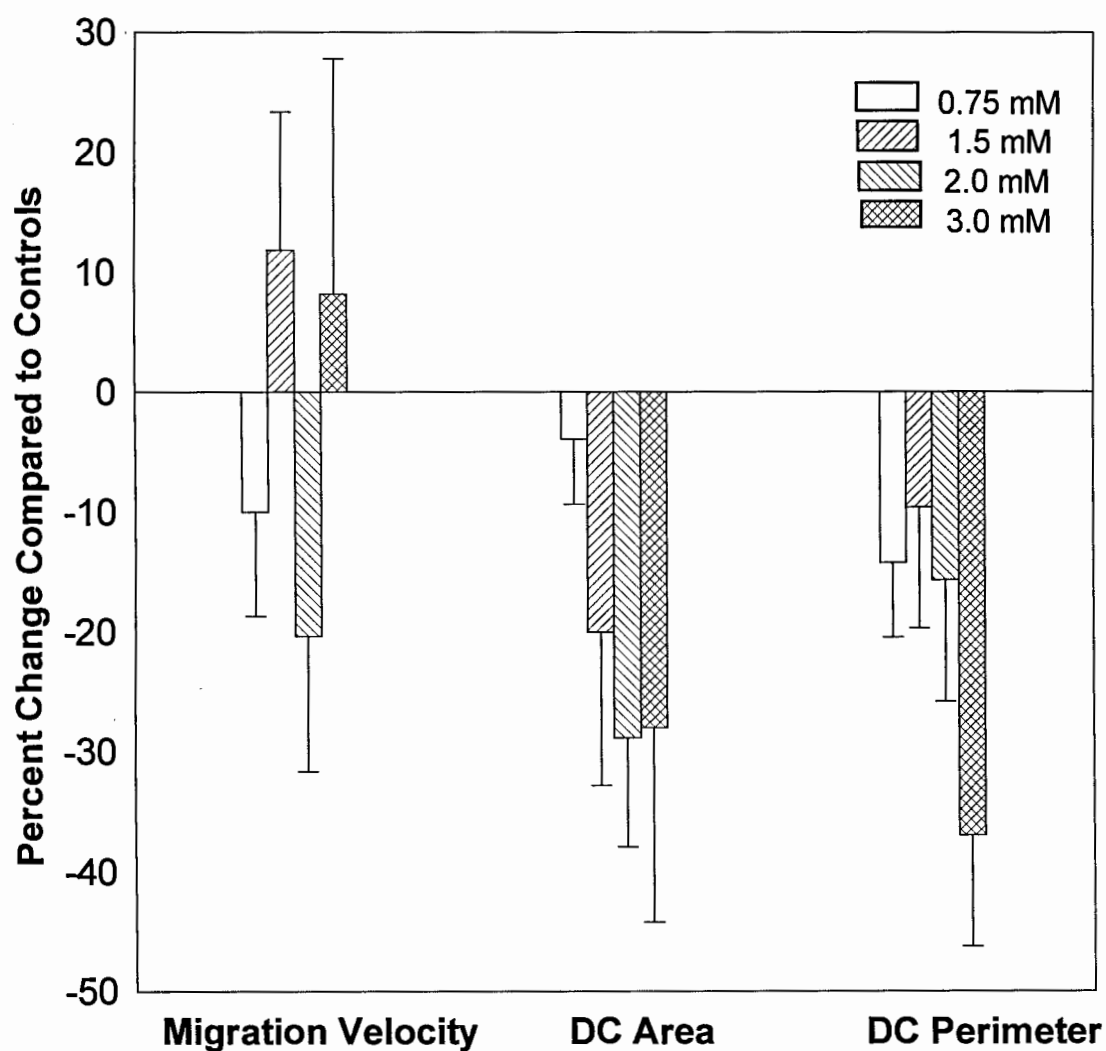
37% respectively. Taken as a whole, the data suggests that VPA-treated cells are smaller or less spread, and much less actively changing their shape than control cells. The effect of VPA was usually stronger as its concentration was increased. This data suggests that these cells are less actively migrating since they are more rounded and not producing as many filopodia or cellular extensions, but the migration velocity data is not fully consistent with this finding.

Figure 7. Mean percent increase or decrease from control in median* value for morphometry parameters \pm standard error.



*Medians are from 5-8 14 frame image sequences with 6-14 cells per frame. A total of 48-96 control cells and 42-94 drug treated cells are represented.

Figure 8. Mean percent increase or decrease from control in median* value for motility parameters \pm standard error.



*Medians are from 5-8 14 frame image sequences with 6-14 cells per frame. A total of 48-96 control cells and 42-92 drug treated cells are represented.

The Effect of VPA on Cell Proliferation

As a measure of cell viability and proliferative status, the relative BrdU incorporation rates of control and the four VPA-treated groups were assessed (Table 4). After 24 hours in culture, appropriate BrdU containing media was exchanged for the original media followed by a two-hour incubation. During this time, mitotic cells would incorporate the BrdU in place of thymidine during the process of DNA replication. By detecting the proportion of BrdU positive cells with a commercially available kit, the relative proliferative rate of the populations could be determined and statistically compared using a Student's T-test. A total of 512 of 1923 cells from nine control explants had positively stained nuclei. The mean percent per explant with positive nuclei was 25.9 (range, 8.1-42.1). A total of 757 of 1960 cells from nine explants cultured in 0.75 mM VPA were BrdU positive. The mean percent per explant with positively stained nuclei was 35.1 (range, 17.9-55.6). The difference between this group and control was not statistically significant. A total of 1008 of 1978 cells from eight explants were positive for BrdU in those treated with 1.5 mM VPA, where the mean percent per explant with positively stained nuclei was 32.1 (range, 0.0-66.7). No statistically significant difference was found between this group and controls. A total of 153 of 934 2.0 mM VPA exposed cells from eight explants were BrdU positive, where the mean percent per explant with positively stained nuclei was 14.7 (range, 6.4-30.7). This difference from the control group was statistically significant ($P \leq 0.05$). Finally, from eight explants cultured in 3.0 mM VPA, 0 of 939 cells were positive for BrdU. This was a statistically significant reduction from the control ($p \leq 0.001$).

Table 4. Proliferation assay results of BrdU incorporation into nuclei[†] of dividing NCCs in culture.

VALPROIC ACID CONCENTRATION	TOTAL NUMBER OF EMIGRATED CELLS	MEAN PERCENT OF EMIGRATED CELLS STAINED
0.00 mM	1923	25.9
0.75 mM	1960	35.1
1.50 mM	1978	32.1
2.00 mM	934	14.7*
3.00 mM	939	0.0**

[†] For 2 hours following 24 hour culture of explants from stage 10 embryos; n = 8-9 explants in each group.

* Significantly different from control, $p < 0.05$

** Significantly different from control, $p < 0.001$

The Effect of VPA on N-Cadherin (A-CAM) Expression

Monoclonal Anti-A-Cell Adhesion Molecule (A-CAM) antibody (Sigma, St. Louis, MO) was used to visualize A-CAM at cell junctions in explants in control and all VPA concentrations after 24 hours in culture. The primary antibody was visualized with CY-3-conjugated streptavidin and images of the explants were captured with both fluorescence and phase-contrast optics.

In control and all VPA-treated explants (Figures 9b-11b) there were high amounts of fluorescence within the attached explant, indicating high A-CAM expression in adherens junctions among cells still in contact within the original tissue. The fluorescence was evenly distributed throughout the complex multilayered network within the explant. In all cases the explant was several times brighter than the surrounding positive areas. In all treatments, independent migratory cells not in contact with any other cells did not exhibit any fluorescence (Figures 9b-11b). This implies that A-CAM was no longer present at the surface of these cells. In control (no VPA) dishes, cells in clusters did not exhibit any fluorescence. There were no epithelial sheets seen in any of the control dishes.

In some of the 0.75 mM VPA-treated dishes (Figure 9a), epithelial sheets were present and had low amounts of discontinuous fluorescence in what appeared to be areas of cell-cell contact close to the explants (Figure 9b), indicating the presence of A-CAM. The other cells in contact in the sheet did not indicate any A-CAM expression with fluorescence, despite appearing to be in full contact with one another.

In some 1.5 mM VPA-treated dishes containing cells in an epithelial arrangement, differentiation between explant and the epithelial sheet was not easily determined using phase contrast optics (Figure 10a). The A-CAM staining (Figure 10b) facilitated identification of the structures. There was high fluorescence in the area of the original explant, with a decreasing gradient of fluorescence in the attached epithelial sheet. The areas of staining are clearly at the boundaries of cellular contact within the sheet indicating the presence of A-CAM in adherens junctions.

In the 2.0 mM VPA-treated dishes (Figure 11a), explant morphology was similar to that seen in 1.5 mM. The level of A-CAM staining, however, was constant from the explant to the edge of the sheet at the cell junctions (Figure 11b). There also appeared to be additional diffuse staining in addition to the junctions. Possibly, there were two layers of cells in the sheet, and the lower levels of staining seen are from the junctions in the second layer, below the first.

In 3.0 mM treated dishes, there was high staining in attached explants, but no emigrated cells in sheets or individually were present. Therefore, no immunostaining of emigrated cells could be assessed.

Figure 9a Phase contrast image of explant cultured in 0.75 mM VPA. The explant (A) is attached to the culture surface and cells are emigrating outward while maintaining contact with one another in an epithelial sheet (E) or individually (arrow). Magnification 100X

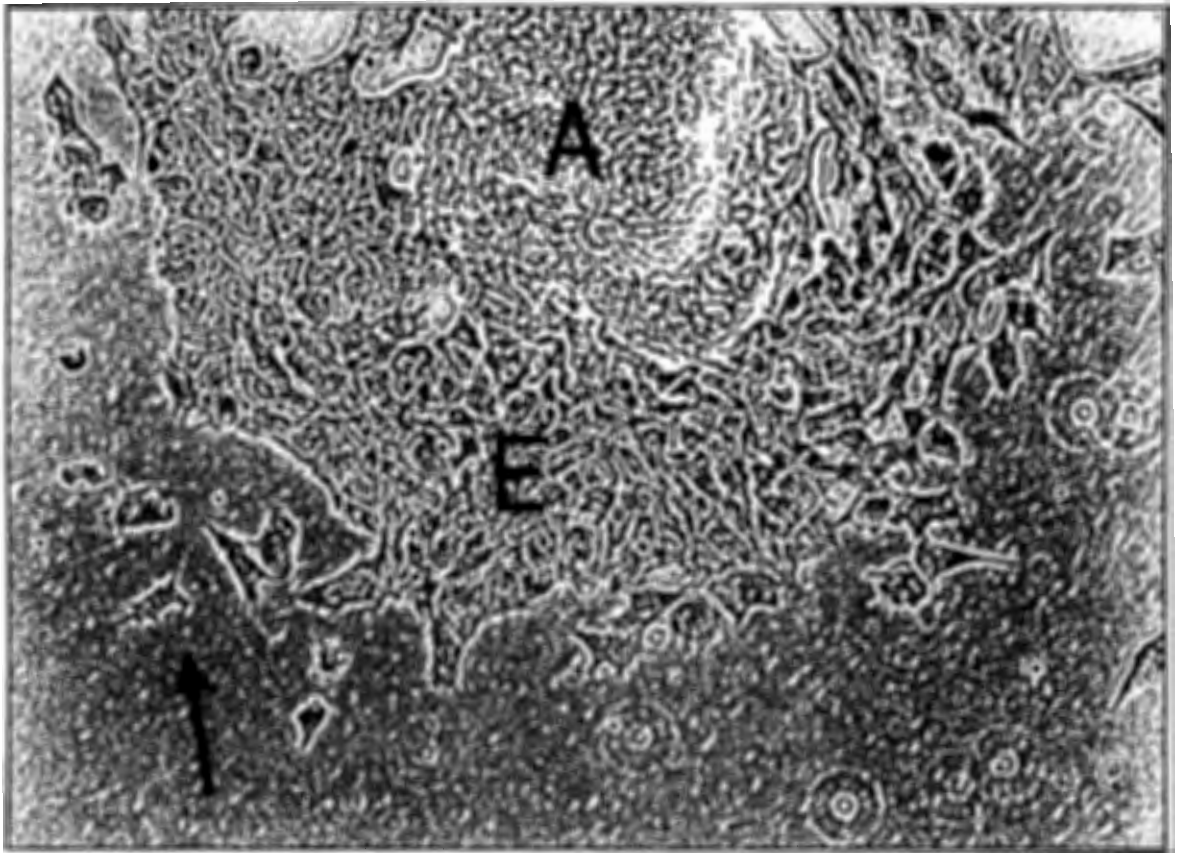


Figure 9b Explant cultured in 0.75 mM VPA, primary antibody to A-CAM detected with a Cy-3 fluorescent label. In the multilayered explant (A), high amounts of A-CAM immunostaining are seen at the cell junctions. Very low levels of scattered staining are observed in part of the epithelial sheet flanking the explant (arrow). The antigen is no longer expressed in the rest of the sheet or on individual cells. Magnification 100X

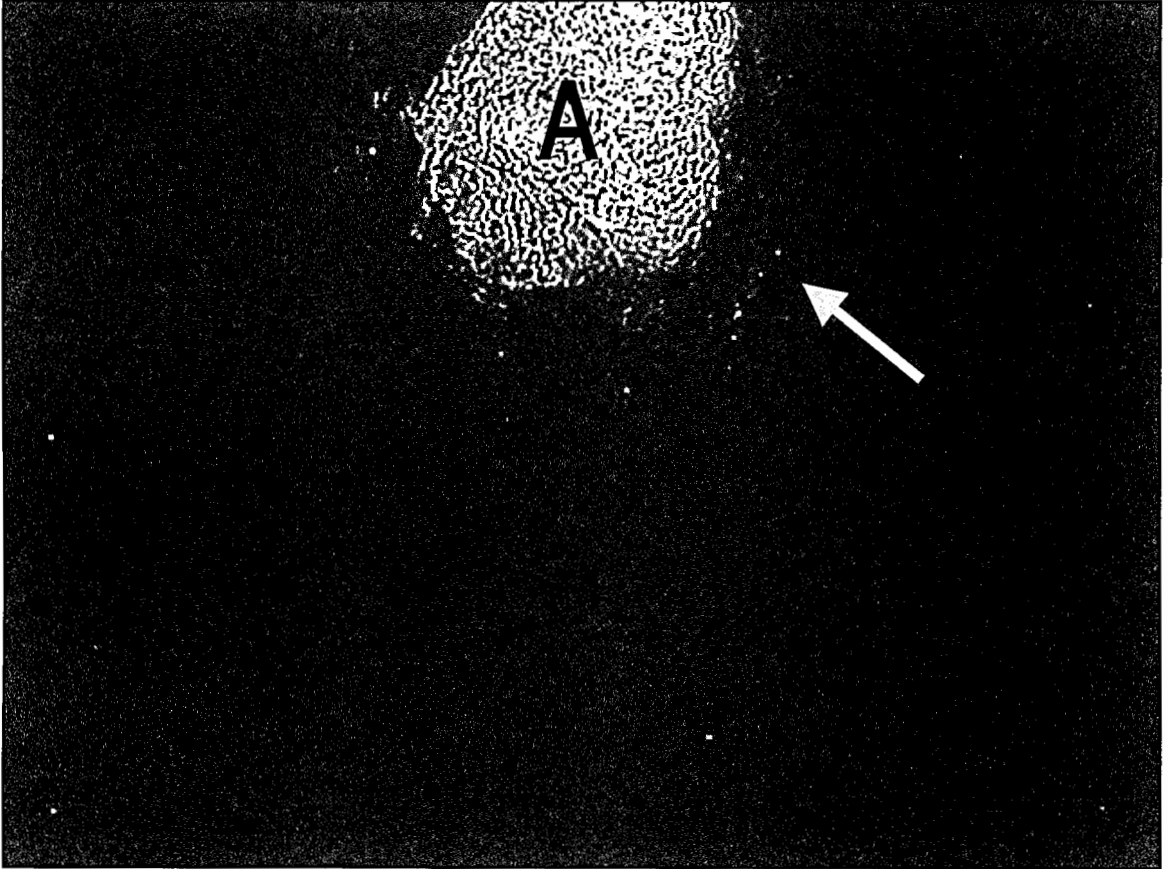


Figure 10a Phase contrast image of explant cultured in 1.5 mM VPA. The explant (A), is attached to the culture surface and cells are emigrating outward while maintaining contact with one another in an epithelial sheet (E), or individually (arrow). Magnification 100X

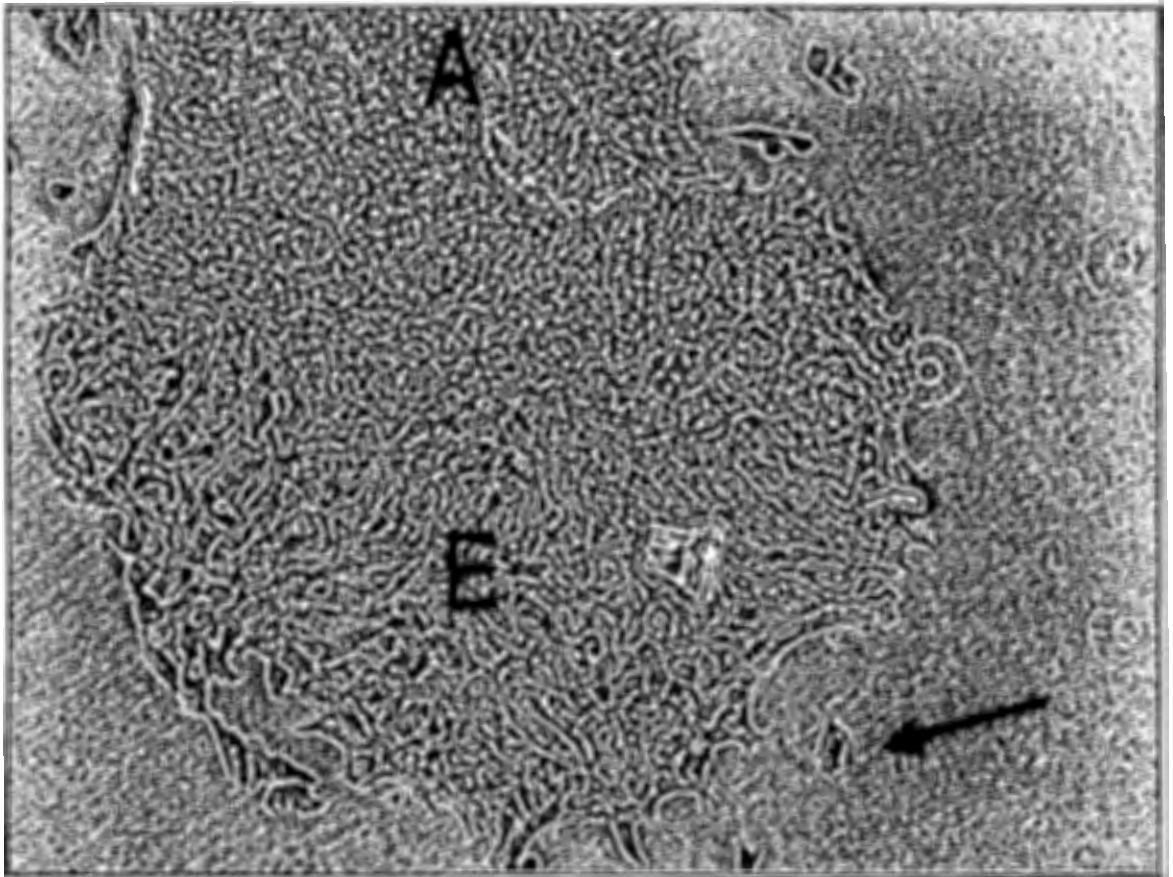


Figure 10b Explant cultured in 1.5 mM VPA, immunostained with primary antibody to A-CAM and detected with a Cy-3 fluorescent label. In the multilayered explant (A), high amounts of A-CAM staining are seen at the cell junctions. In the epithelial sheet (E), expression is seen at the regions of cell junctions and appears to decrease gradually as the distance from the explant increases. Staining is no longer observed in individual cells (arrow). Magnification 100X

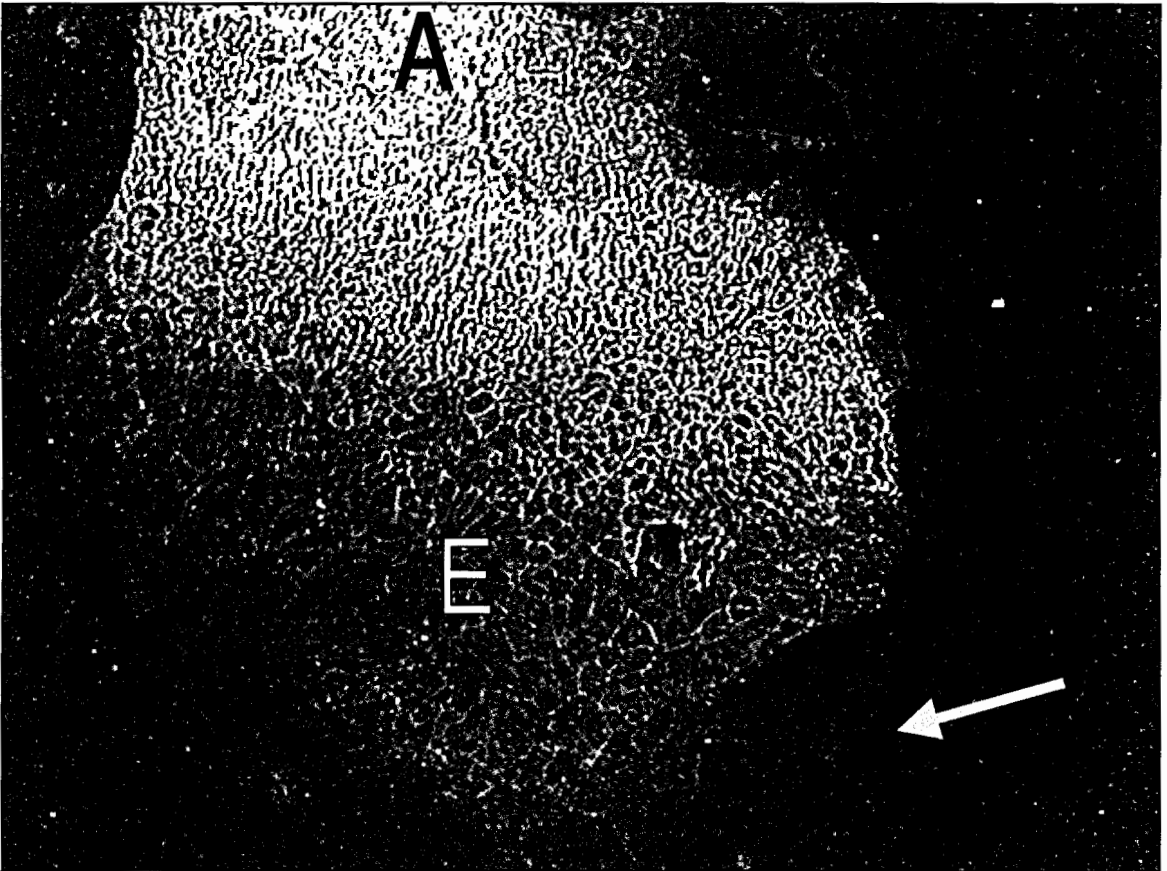


Figure 11a Phase contrast image of explant cultured in 2.0 mM VPA. The explant (A), is attached to the culture surface and cells are emigrating outward while maintaining contact with one another in an epithelial sheet (E), or individually (arrow). Magnification 100X

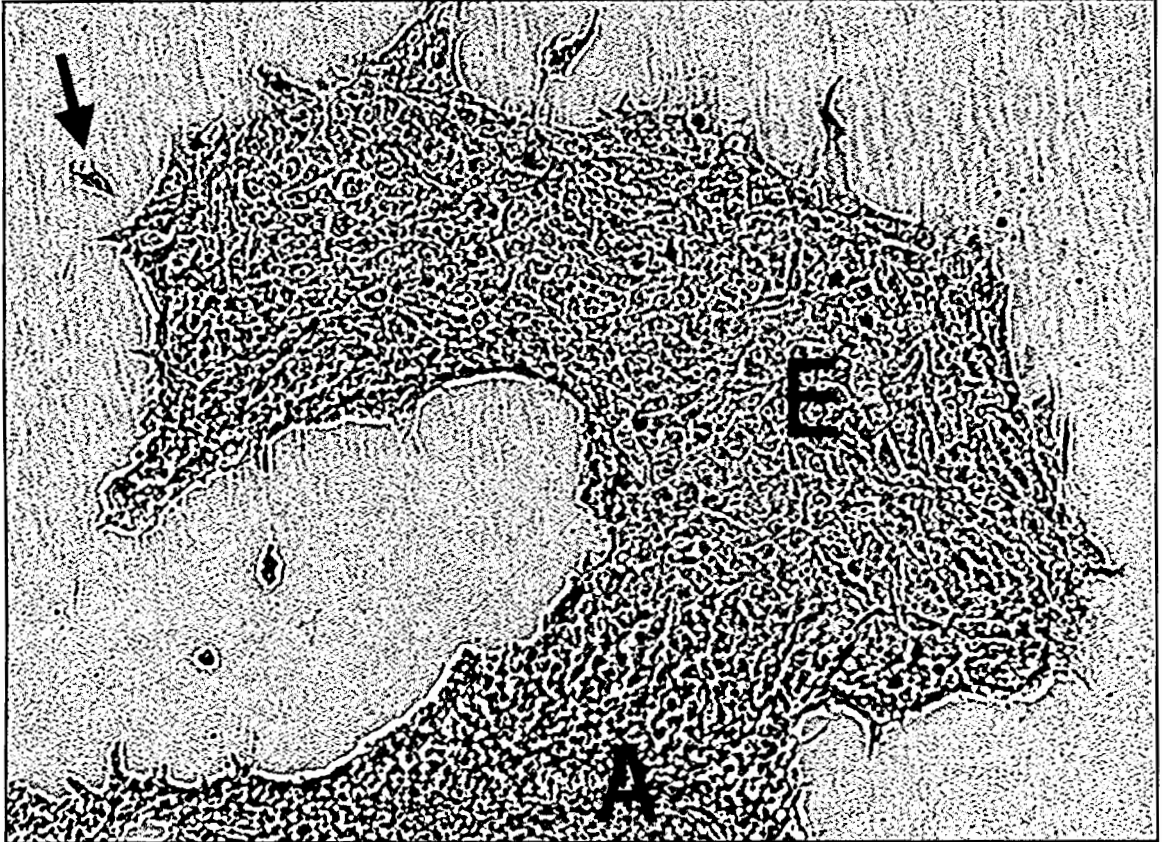
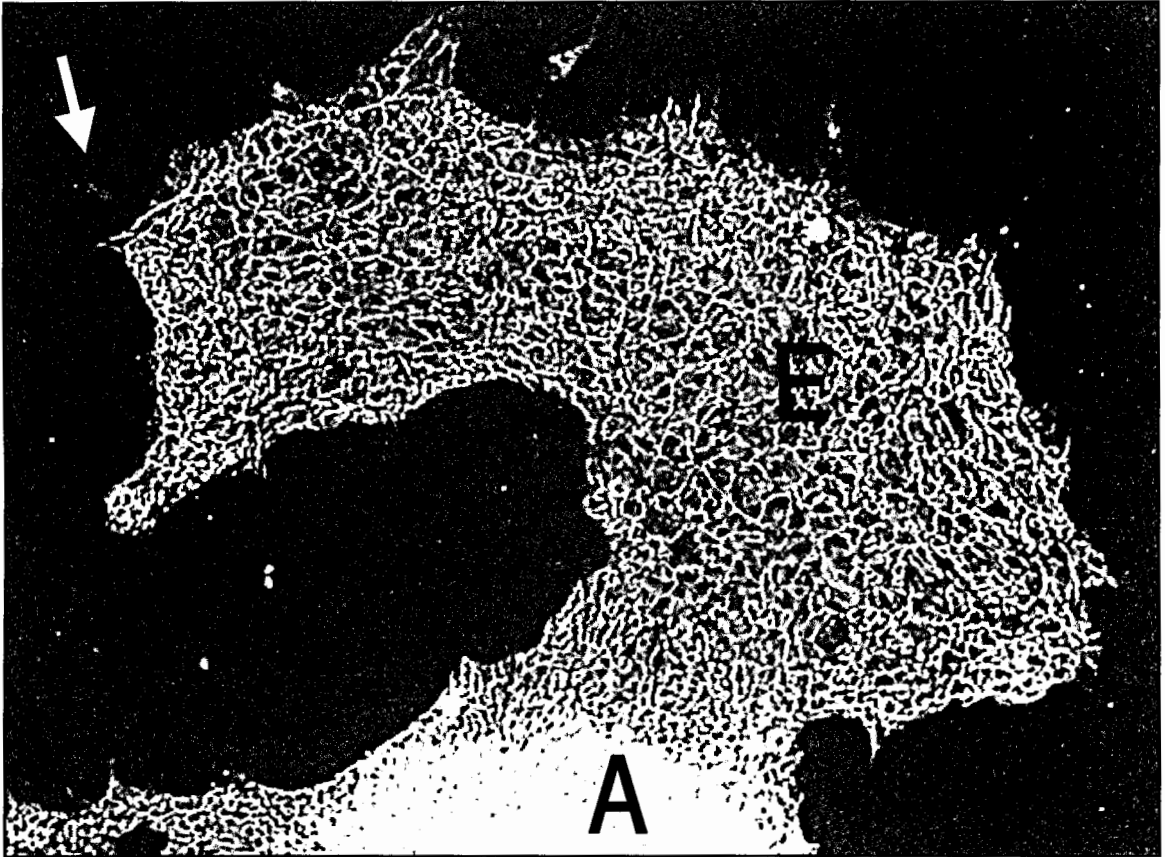


Figure 11b Explant cultured in 2.0 mM VPA, immunostained with primary antibody to A-CAM and detected with a Cy-3 fluorescent label. In the multilayered explant (A), high amounts of A-CAM staining are seen at the cell junctions. In the epithelial sheet (E), staining is seen in the regions of cell junctions and does not appear to be down regulated as the distance from the explant increases as seen in 1.5 mM explants. Staining is no longer observed in individual cells (arrow). Magnification 100X



The Effect of VPA on Stress Fiber Distribution

Fluorescein isothiocyanate (FITC)-labeled phalloidin, which binds and stabilizes filamentous actin (F-actin), was used to reveal the F-actin in NCC cultures. In control cultures (Figure 12), immunostained F-actin was concentrated in organized, multidirectional stress fibers and cortical areas of individual cultured NCCs. Staining in these areas was most intense in control cultures. In contrast, staining appeared to decrease in a manner that was somewhat dose-dependent in VPA-containing cultures. This suggests F-actin is decreased in the presence of VPA, possibly dose dependantly.

At the VPA concentration of 0.75 mM, the stress fibers appeared finer, and stained less intensely. Cortical area staining appeared as thick as in control cells, but also became less intense as VPA concentration increased. The distribution of staining was similar to that of controls. There was no detectable difference in appearance between 0.75 mM (Figure 13) and 1.5 mM (Figure 15) VPA-treated cells with regard to stress fiber distribution and orientation or cortical actin staining in individual, spread NCCs.

In 2.0 mM VPA-treated dishes (Figure 18), the stress fibers and cortical areas were predictably less intensely stained, however in a small proportion of spread cells there was an irregular, globular distribution of intense (bright) staining. This pattern was also seen in many rounded cells. This suggests a high amount of small actin filament fragments collecting in these cells. It is unlikely that this is an accumulation of globular actin, because phalloidin possesses a high affinity to filamentous, not globular, actin.

In 3.0 mM VPA-treated dishes (Figure 19), there were few cells migrating outwardly, but those that were appeared to have a generally homogeneous pattern of

fluorescence, only slightly brighter in nuclear and cortical areas. There were no prominent stress fibers.

Epithelial sheet morphology was seen in control, 0.75, and 1.5 mM VPA treatment conditions (Figures 14, 16, and 17). In control (not pictured) and 1.5 mM VPA treatment, where the explant had usual morphology, (explant edge easily distinguished from the pavement of cells), stress fibers within cells were multidirectional, numerous, and also appeared to continue from cell to cell. There were however some sheets that continued from explants that had lost their integrity, where the edge of the explant and sheet were not distinguishable. In these cases, the F-actin staining was markedly different in distribution. It appeared that only cortical areas of the cells were stained. The overall appearance was similar to the A-CAM staining of the same types of explant/sheet morphology.

Figure 12 NCCs cultured in control medium, immunostained with FITC-conjugated phalloidin. Staining was seen concentrated in the cortical areas of spread lamellapodia (black arrow). Staining was also seen in stress fibers, which radiate in several directions in spread cells and appear to be thick in diameter (white arrow). Epithelial sheet formation seen (E) with mass of stress fibers appearing to extend from cell to cell. Magnification 200X



Figure 13 NCCs cultured in 0.75 mM VPA, immunostained with FITC-conjugated phalloidin. Staining was seen concentrated in the cortical areas of spread lamellapodia (white arrow) similar to that seen in control cells. Staining was also seen in stress fibers, which appear to be less pronounced than in control cells (black arrow). Magnification 200X

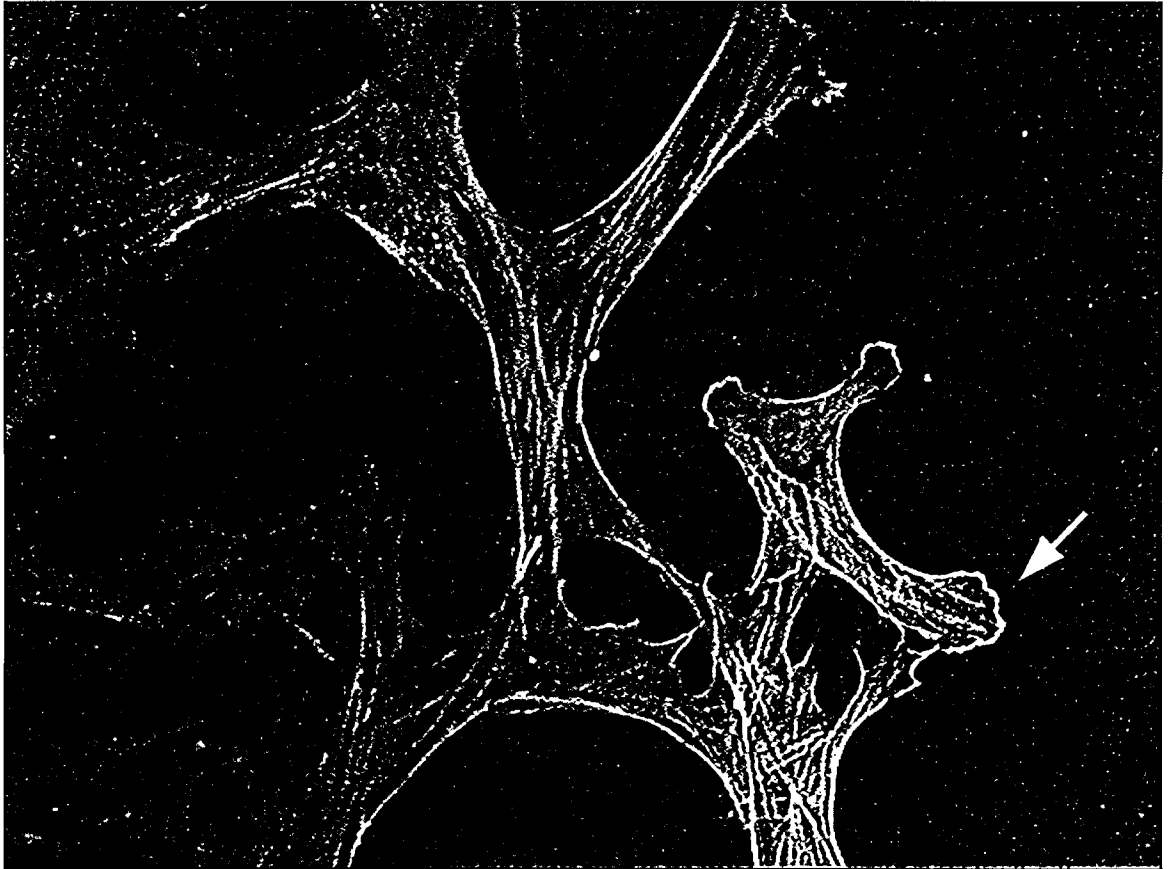


Figure 14 Explant cultured in 0.75 mM VPA, immunostained with FITC-conjugated phalloidin. Sheet formation seen in a single culture. Staining appears to be at cell-cell borders (black arrow). Magnification 100X

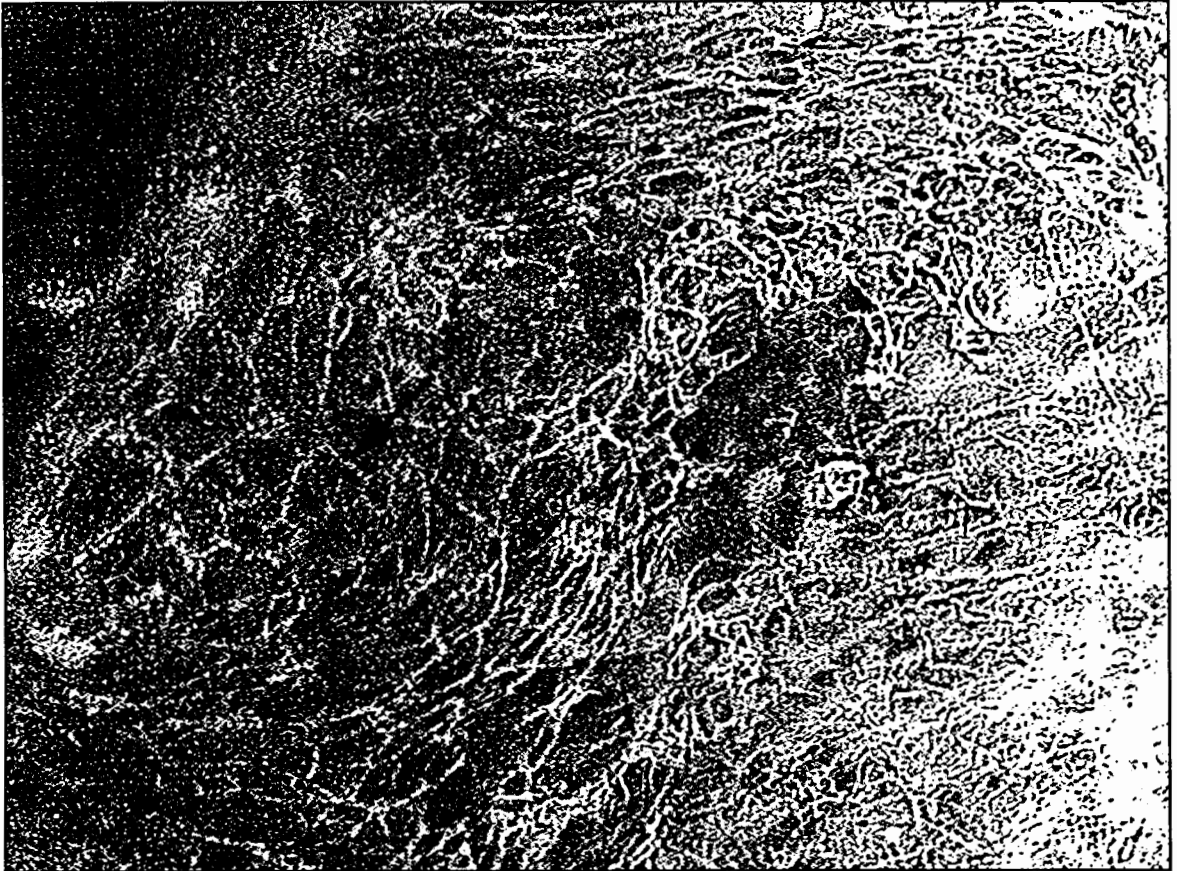


Figure 15 NCCs cultured in 1.5 mM VPA, immunostained with FITC-conjugated phalloidin. Staining was seen in the cortical areas of spread lamellapodia (black arrow) but appeared to be less intense than in controls. Staining was also seen in stress fibers, which radiate in several directions in spread cells (white arrow). Magnification 200X



Figure 16 NCCs cultured in 1.5 mM VPA, immunostained with FITC-conjugated phalloidin. Epithelial sheet formation seen (E) with mass of stress fibers appearing to extend from cell to cell as in control. Note explant (A) edge is easily distinguished (black arrows). Magnification 100X

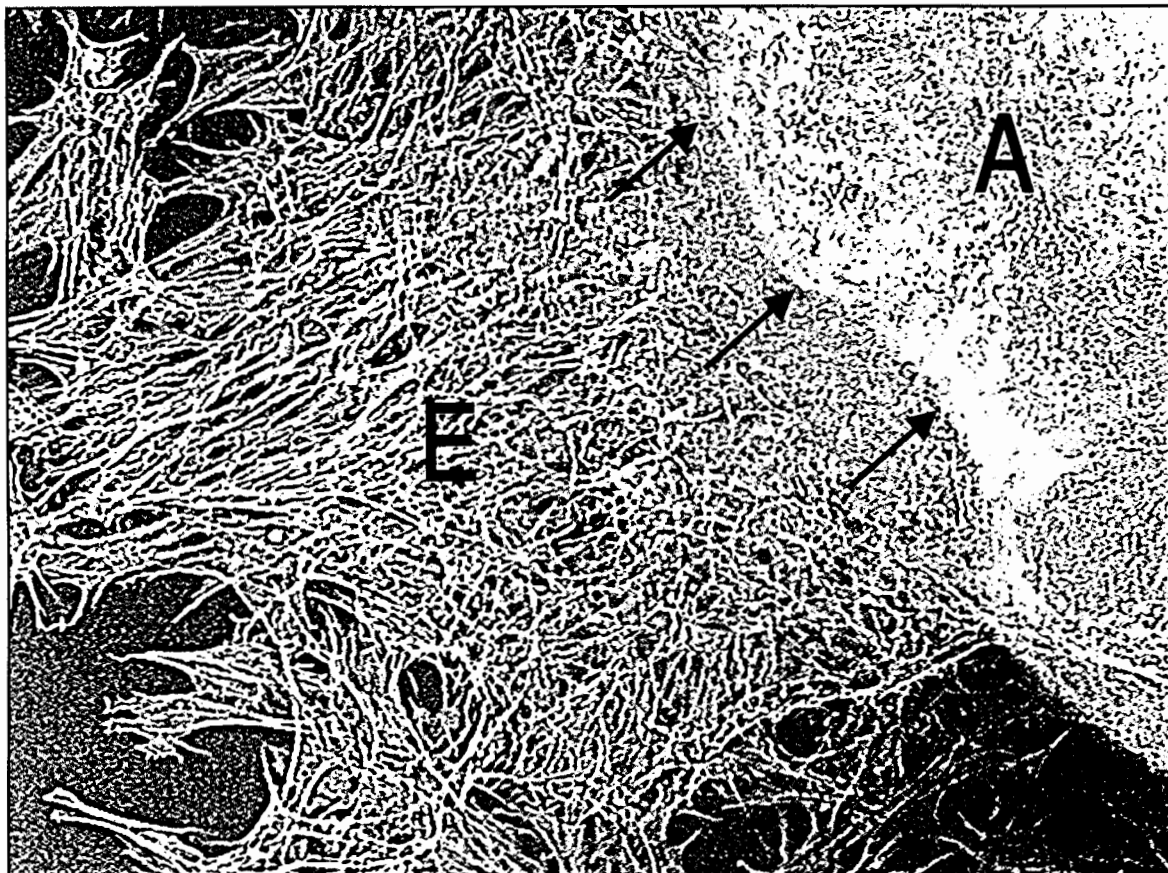


Figure 17 NCCs cultured in 1.5 mM VPA, immunostained with FITC-conjugated phalloidin. Epithelial sheet formation seen (E) with staining localized only to cortical areas of cells. Note that the explant (A) edge is not easily distinguished, having the rolled out appearance seen in multiple cultures. Individual cells (black arrow) are positive for actin, but stress fibers are not apparent. Magnification 100X

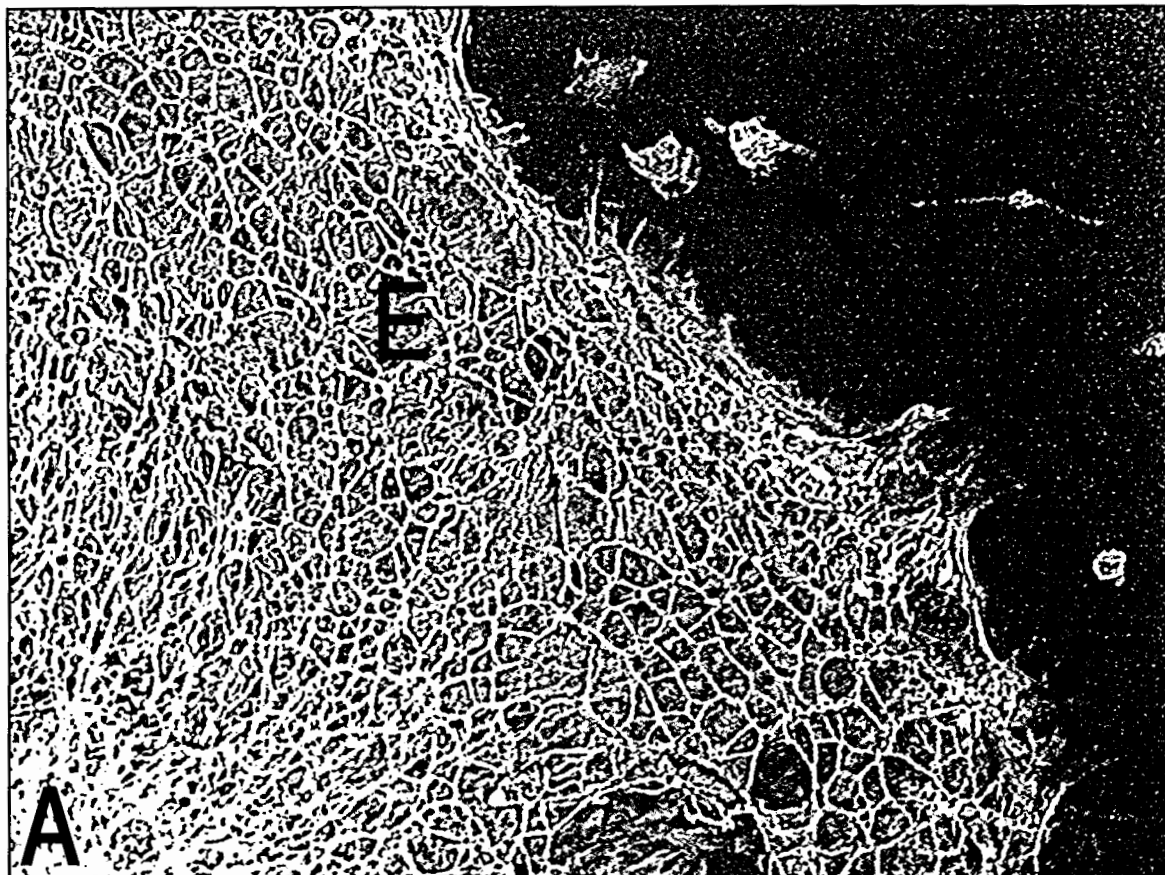


Figure 18 NCCs cultured in 2.0 mM VPA, immunostained with FITC-conjugated phalloidin. Staining was seen in the cortical areas and in stress fibers of spread cells (A and B, black arrows) but appeared to be less intense than in controls. Some individual cells appearing that had diffuse, clumped staining in all or part of the cell body (A and B, white arrows). In B, a group of cells independent of the explant (G) is seen displaying unusual actin distribution. Magnification 200X

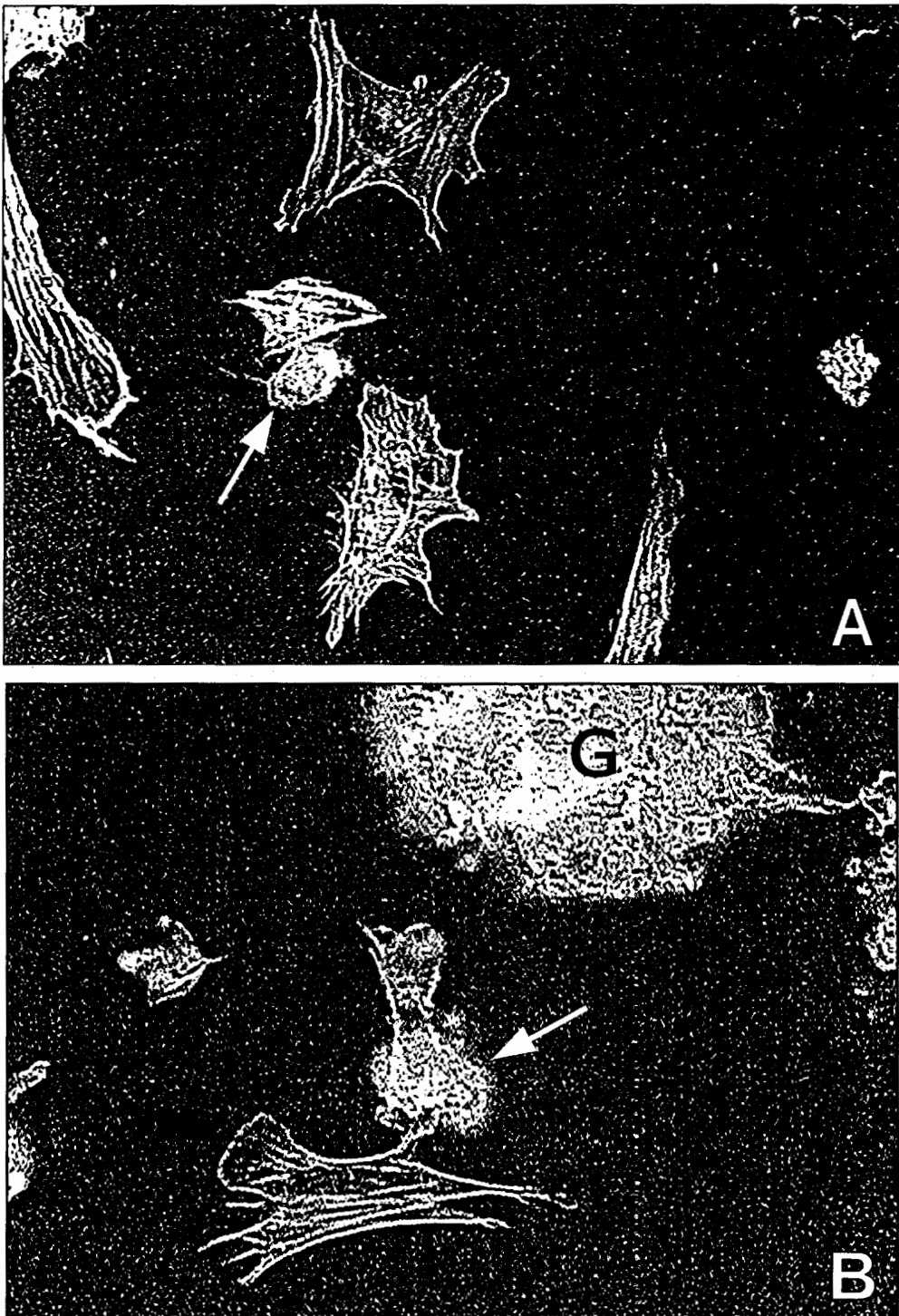
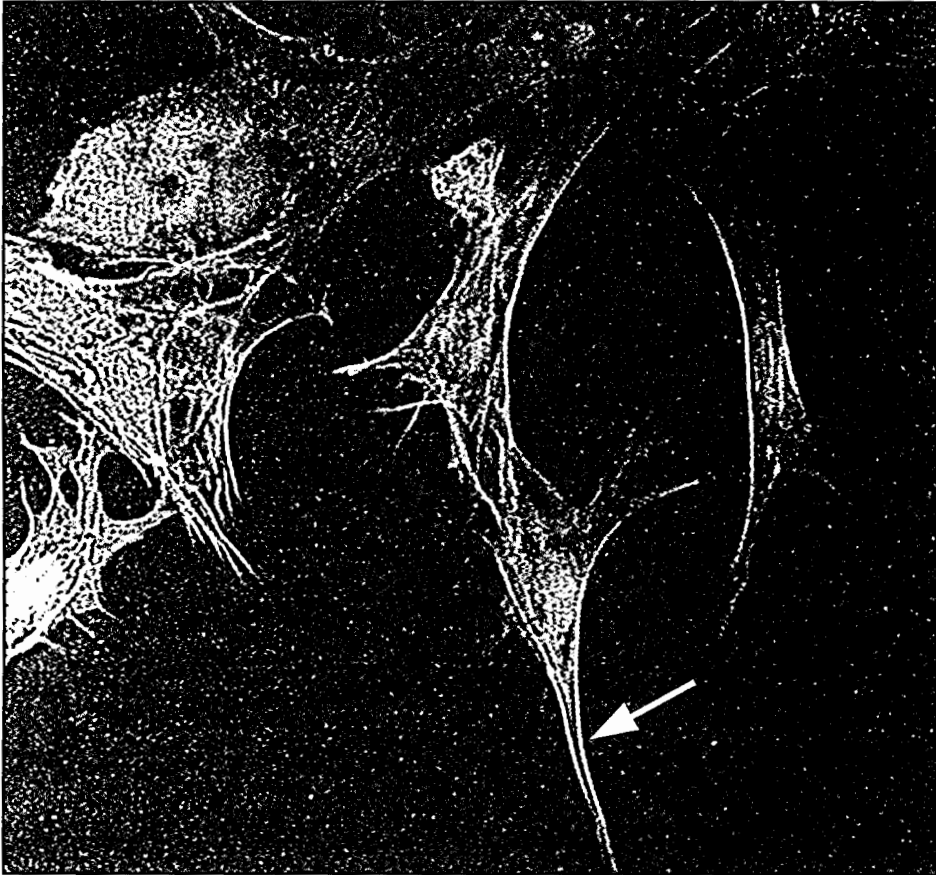


Figure 19 NCCs cultured in 3.0 mM VPA, immunostained with FITC-conjugated phalloidin. Staining was seen concentrated in some cortical areas of cellular extensions as in lower drug concentrations and control (white arrow). Overall, staining is evenly distributed throughout the cell, prominent stress fibers are not seen (black arrow). Magnification 200X



CHAPTER 4

DISCUSSION

Neural crest cells are a distinct group of multipotent cells first recognizable as they emerge from the neural tube as the neural folds rise up and fuse. These cells actively migrate outward over long distances using various extracellular guidance cues encountered in their varying environments. They cease migration in a variety of embryonic locations where they terminally differentiate into cartilage, bone, endocrine, connective, neural and pigment cell types (Erickson and Perris 1993; Bronner-Fraser 1993).

Valproic acid is a simple eight carbon branched chain fatty acid originally approved by the FDA in 1978 for the treatment of absence seizures (Lammer and others 1987). Its usefulness has now been demonstrated in a wide variety of neurological disorders including schizophrenia, bi-polar disorder, and migraine prophylaxis (Citrome and others 2000; Mitchell 2000). Weak teratogenicity in laboratory species was established by Whittle in 1976, and the first data supporting a causal relationship between VPA and NTDs became known in 1982 from Robert and Guibaud. A series of anomalies termed fetal valproate syndrome was described by Clayton-Smith and Donnai in 1995. These included neural tube defects (spina bifida), and congenital heart defects. Spina bifida, the most commonly noted birth defect, was calculated to be 1-2% more frequent in embryos exposed to valproate than not. Spina bifida has a variety of origins, and the overall mechanism of this defect is not clearly understood. Failure of the neural folds to completely fuse along any portion of the neural tube can result in this NTD. Altered

levels of extracellular matrix molecules, cell adhesion molecules, and cell proliferation have been found to contribute to the incidence of NTDs (Newgreen and others 1997; Bennett and others 2000).

The Effect of VPA on Explant Attachment

In this study, VPA affected the ability of explanted neural fold tissues to attach to the culture surface in a dose-dependant manner. As the concentration of drug increased, consistently lower percentages of explants were able to adhere to the substratum. In addition, 3.0 mM VPA highly impaired the ability of the NCCs to migrate outward as very few explants overall had more than 100 cells visible, whereas in controls and at lower concentrations, the mean numbers of emigrated cells were over 200.

The Effect of VPA on NCC Morphology in Culture

Valproic acid has been shown to increase mean cell area of fibroblastoid mouse L-cells (Berezin and others 1996). In this study, however, the mean cell area of migrated cells was not consistently increased or decreased. Significant increases and decreases were seen in separate experiments within the same drug concentration. Generally, more decreases in area values were noted than increases within each VPA treatment level. With 1.5 and 3.0 mM VPA exposure, the mean percent changes in median area values from control were 20-30% lower overall, and with 2.0 mM VPA exposure median area value was lowered about 6%. However, the effect of VPA on migrated cell area lacked consistency.

In general, when compared to controls, the 0.75, 1.5 and 3.0 mM treated cells appeared more rounded with lower length and width measurements and higher elongation

index values, but there were no clear trends. The lower area values and more rounded appearance of the NCCs supports previous observations of cells that are less migratory, such as those in preparation for division. It is known that migrating cells, in preparation for mitosis, become less spread out in shape and decrease the number of substratum contacts, giving them a more rounded appearance.

The Effect of VPA on NCC Motility on Culture

It might be expected, based on the overall morphology of NCCs cultured in VPA, that migration rates would be lower for VPA exposed cells. Dose-dependant decreases in the migration speed of L929 cells, together with an increase in persistence of direction have been seen in the presence of VPA (Walmod and others 1998). In the present study with chick NCCs, migration velocity was highly variable with large amounts of standard error within experimental groups. Both significant increases and decreases in migration rate were seen within experiments at all drug levels when compared to controls. Overall, there were no clear effects of VPA exposure seen on migration rates of these cells. The dynamic activity of the cell calculated by determining changes in area and perimeter over time, however, did appear to be consistently lowered as VPA concentration increased. These cell's lamellapodia may not be as active. Possibly, this is a result of internal cytoskeletal changes in the actin network responsible for membrane protrusion and retraction.

VPA concentrations of 3 mM have previously been found to change cytoskeletal organization and increase the presence of focal adhesions (Walmod and others 1998). In addition, microspikes were found to be missing in VPA-treated cells (Walmod and others

1998). In our study, median perimeter values were lower for the 0.75, 1.5 and 3.0 mM treated groups, suggesting a lower number of membrane protrusions.

The Effect of VPA on the Actin Cytoskeleton

Confocal micrographs of fluorescence staining of microtubules, F-actin, and selected focal adhesion proteins compiled by Walmod and others (1998) demonstrated that VPA-exposure caused enhanced focal adhesion formation. This was accompanied by a rearrangement of F-actin reflected in an increase in stress fiber formation in L929 cells. A decrease was seen in the amount of cortical F-actin. Stress fibers in VPA-treated cells were found in a predominantly perinuclear organization rather than in a cortical mesh as in control cells, and the relative amount of F-actin per cell was significantly higher (23%) for treated cells (Walmod and others 1998). In our study, F-actin was immunolocalized to stress fibers and cortical areas of individual cultured NCCs. Staining in these areas was most intense in control cultures. As VPA concentration increased, the stress fibers appeared more fine and stained less intensely. Cortical areas appeared to have the same amount of intensity relative to the stress fibers for control through 2.0 mM VPA. There was no difference in appearance between 0.75 mM and 1.5 mM VPA-treated cells with regard to stress fibers or cortical actin staining in individual spread NCCs.

In 2.0 mM VPA-treated dishes, the inverse correlation between VPA concentration and F-actin staining in stress fibers and cortical areas was still apparent. However, in a small proportion of spread cells there was an irregular, globular distribution of staining. This was also seen in many rounded cells. This suggests a high

amount of small actin filament fragments collecting in these cells. It is unlikely that this is an accumulation of globular actin, because phalloidin possesses a high affinity to filamentous, not globular actin. Walmod and others (1998) showed that after VPA treatment, the distribution of gelsolin was altered. They reported that it was found in a diffuse perinuclear pattern (where stress fibers were) unlike the pattern in control cells where it was found in the peripheral membrane ruffles. VPA also altered gelsolin so that it responded insignificantly to the addition of the PIP₂-binding gelsolin-peptide. This is interesting because gelsolin is a compact actin binding protein found in many vertebrate cells which blocks lengthening of actin filaments, and can also sever them by breaking bonds between actin monomers. An alteration of gelsolin production or distribution by VPA in NCCs may account for the disturbed F-actin destitution seen in the 2.0 mM VPA cultures. Further investigation including staining for gelsolin could help clarify this mystery.

In 3.0 mM VPA-treated dishes, there were few cells migrating outwardly. Those that were appeared to have a low amount of F-actin fluorescence, slightly increased in cortical areas unlike controls, which had very bright staining in both stress fibers and cortical areas. There were no prominent stress fibers seen in the 3.0 mM-treated cultures. This is unlike results seen with the L929 cells exposed to 3.0 mM VPA. It is yet to be determined what causes these two different results in these differing cell types. Differing mechanisms of action, or roles that VPA may play in normal cell function could be explored. It would be interesting to immunolocalize G-actin in migrating NCCs exposed

to 3.0 mM VPA to investigate whether actin was being prohibited from filament formation.

The Effect of VPA on Epithelial Sheet Morphology

Epithelial sheet morphology was seen in neural fold explants cultured in control, 0.75, and 1.5 mM VPA treatment conditions. In control and 1.5 mM VPA, the explant had usual morphology, with the explant edge easily distinguished from the pavement of cells. Stress fibers within the cells were multidirectional, numerous, and also appeared to continue between multiple cells. There were however some sheets that continued from explants that had lost their integrity, where the edge of the explant and sheet were not distinguishable. In these cases, the F-actin staining was markedly different in distribution. It appeared that only cortical areas of cells were stained, and not stress fibers. This appears to be the first observations of this phenomenon.

The Effect of VPA on Cell-Substratum and Cell-Cell Contacts

Walmod and others (1998) showed that VPA increased the presence of focal adhesions indicated by a higher proportion of paxillin, vinculin, and FAK staining in treated than in control cells. We did not investigate the presence of focal adhesion proteins, however based on the smaller areas and generalized cell rounding seen in our VPA-treated cultures; it seems probable that their presence would be reduced overall.

In mice with abnormally high levels of the cell adhesion molecule N-CAM, NCCs fail to migrate from segments of the neural tube, and resulting embryos display spina bifida (Moase and Trasler 1990, 1991). In human neuroblastoma cells, N-CAM expression is upregulated in the presence of VPA (Cinatl Jr. and others 1996). In avian

neural crest cells, A-CAM is not present in migrating cells, but is seen in premigratory cells in culture (Delannet and Duband 1992).

In this study, A-CAM (N-cadherin) was immunolocalized in the NCC cultures and visualized with a fluorescent label. Cells in all treatment levels independently migrating did not demonstrate A-CAM expression. Cells within the explant, and any cells appearing to be part of an epithelial sheet where it was continuous with the explant, did localize the antibody at the borders of the cells within the sheet. This staining pattern appeared to be most intense proximal to the explant, and decrease in intensity toward the edge of the sheet. The highest intensity levels were seen in the 2.0 mM VPA group (3.0 mM was not tested because of the lack of emigrated cells). If cells appeared to be grouped but were not in contact with the explant, no A-CAM staining was seen. The Ras GTPase *RhoB* has been demonstrated to be expressed in the dorsal neural tube. It also is transiently expressed in migrating NCCs. When *rho* activity is blocked, they are prevented in their delamination from the dorsal neural tube, suggesting a role for *rhoB* in this step. NCCs have a more elongated morphology overall when *rho* activity is blocked, but no significant changes were noted in migration (Liu and Jessell 1998).

The receptors for factors that can induce epithelial-to-mesenchymal transition (EMT) are protein tyrosine kinases (PTKs) (Komada and Kitamura 1993). Tyrosine kinase inhibitors have been shown to elevate cadherin levels at cell adhesions and increase NCC-cell adhesion (Monier-Gavelle and Duband 1995). The presence of VPA in the embryonic system may modify regulation of expression or enzyme activity of particular protein tyrosine phosphatases (PTPases) and PTKs thereby altering

maintenance of cell-cell adhesion and dynamic substrate adhesion through these enzymes. When serine-threonine kinases, tyrosine kinases, and phosphotyrosine phosphatases are inhibited, aggregates of cells form with tight cell-cell cohesion among cells accompanied by A-CAM accumulation in the areas of intercellular contacts. This indicates that a complex cascade of intracellular signals involving kinases and phosphatases elicited by surface receptors may be the mechanism of A-CAM-mediated interactions. Agents that interfere with fibronectin-to-integrin surface interactions cause rapid A-CAM-mediated cell-cell aggregations. This process is mediated through incorporation of A-CAM molecules from cytoplasmic pools into adherens junctions, which are associated with cytoskeletal elements (Monier-Gavelle and Duband 1997). VPA appears to effect the epithelial-mesenchymal transition necessary for NCCs to begin proper migration. Alteration of A-CAM expression or regulation may strengthen these cell junctions in a manner that is keeping the cells from releasing from one another. If neural crest cells are being prevented from leaving the neural tube, NTDs might result from an overcrowding of cells in localized areas. Other malformations may result from reduced numbers of NCC derivatives in their needed locations in the embryo.

Induction of neural crest and neural tube defects is a general effect of N-methyl-D-aspartate (NMDA) receptor antagonists. Proteins involved in functional NMDA receptors are present as early as stage 10 in the chick. Evidence from later stages of development indicates the NMDA receptor is a regulator of neuronal cell migration, cell-cell adhesion, and apoptosis (Komuro and Rakie 1993; Rashid and Cambray-Deakin 1992; Balazs and others 1989). The NMDA receptor antagonists ethanol, homocysteine,

and VPA have been identified as possibly contributing to NTDs by competitive inhibition. In avian embryos, homocysteine induces neural tube, conotruncal, and orofacial malformations similar to those found in VPA exposed embryos. Ethanol is responsible for 'fetal alcohol syndrome', characterized by maxillo-facial, heart, and other systemic defects. Due to the similarity of deformations caused by these three antagonists, similar teratogenic mechanisms involving the NMDA receptor may be at work. When the balance of NMDA receptor agonists and antagonists is disrupted during development by the addition of VPA or another antagonist, congenital defects of the neural crest and neural tube derivatives may result.

The Effect of VPA on Cell Proliferation

Another contributing factor for NTD development may be altered cell proliferation. A lowered rate of cell proliferation appears to be a mechanism of NTD pathogenesis in curly tail embryos (Copp 1988). One mM VPA has been shown to achieve 50% inhibition of C6 glioma cell proliferation in culture, with higher concentrations completely arresting the cell cycle (Martin and Regan 1997). Other agents found to inhibit this cell line have been associated with neural tube defects (Regan and others 1990). In the present study, 0.75 mM and 1.5 mM VPA actually increased the number of cells that incorporated BrdU 6-9%. NCC exposure to 2.0 mM VPA significantly lowered their proliferation rate by 12%. At 3.0 mM, no uptake of BrdU was detected, suggesting that this concentration arrested NCC DNA synthesis. Altering cell proliferation lowers the number of cells available to contribute to tissues within the embryo that are dependent on NCCs.

Summary

In summary, alterations in the overall cell activity and cytoskeletal actin filament distribution or maintenance may mediate the teratogenicity of VPA through alteration of neural crest cell migration in embryos exposed to it. Increased cell-cell adhesion, possibly through A-CAM and lowered or terminated cell proliferation through exposure to VPA might alter the integrity of the neural tube, allowing the development of NTDs such as spina bifida, and also contribute to other defects seen in VPA-exposed fetuses through the lowered levels of NCCs able to contribute to derivatives of the neural crest. Altered cell proliferation rates are a result of VPA exposure, and have been found to contribute to NTDs in a variety of animal models. VPA appears to have multiple effects on the developing embryo, interfering with multiple activities of embryonic cell biology. Further studies investigating the internal cytoskeletal effects of VPA on focal adhesion proteins and actin-binding proteins such as gelsolin, as well as rescuing experiments with folic acid or methionine, or competitive inhibitors of the NMDA receptor should be the next steps in discovering the teratogenic mechanisms of VPA.

LITERATURE CITED

- Akitaya T and Bronner-Fraser M. 1992. Expression of cell adhesion molecules during initiation and cessation of neural crest cell migration. *Dev Dyn* 194:12-20
- Anderson D. 1997. Cellular and molecular biology of neural crest cell lineage determination. *TIG* 13:276-280.
- Aulthouse A and Hitt D. 1994. The teratogenic effects of valproic acid in human chondrogenesis in vitro. *Teratology* 49:208-217.
- Balazs R, Hack N, Jorgensen O, and Cotman C. 1989. N-methyl-D-aspartate promotes the survival of cerebellar granule cells: pharmacological characterization. *Neurosci Lett* 101:241-246.
- Barnes GL, Mariani BD and Tuan RS. 1996. Valproic acid-induced somite teratogenesis in the chick embryo: relationship with Pax-1 gene expression. *Teratology* 54:93-102.
- Basler K, Edlund T, Jessell T, and Yamada T. 1993. Control of cell pattern in the neural tube: regulation of cell differentiation by dorsalin-1, a novel TGF beta family member. *Cell* 73:687:702.
- Basu A and Wezeman FH. 2000. Developmental toxicity of valproic acid during embryonic chick vertebral chondrogenesis. *Spine* 25:2158-2164.
- Baynash AG, Hosoda K, Giaid A, Richardson JA, Emoto N, Hammer RE, Yanagisawa M. 1994. Interaction of endothelin-B receptor is essential for development of epidermal melanocytes and enteric neurons. *Cell* 79:1277-1285.
- Bennett G, Wlodarczyk B, Calvin J, Craig J, and Finnell R. 2000. Valproic acid induced alterations in growth and neurotrophic factor. *Rep Toxicol* 14:1-11.
- Berezin V, Kawa A, Bojic U, Foley A, Nau H, Regan C, Edvarsen K, and Bock E. 1996. Teratogenic potency of valproate analogues evaluated by quantitative estimation of cellular morphology in vitro. *Toxicol In Vitro* 10:585-594.
- Bergman M, Joukov V, Virtanen I, and Alitalo K. 1995. Overexpressed Csk tyrosine kinase is localized in focal adhesions, causes reorganization of alpha v beta 5 integrin, and interferes with HeLa cell spreading. *Mol Cell Biol* 15:711-722.
- Bjerkedal R, Czeizel A, Goujard J, Kallen P, Mastroiacova N, Nevin G, Oakley Jr, and Robert E. 1982. Valproic acid and spina bifida. *Lancet* 2:1096.

- Bray D. 1992. Cell Movements. New York: Garland Publishing, Inc. p 143-155
- Brennan H, Smith S, and Stoker A. 1999. Phosphotyrosine signalling as a regulator of neural crest cell adhesion and motility. *Cell Motil Cytoskeleton* 42:101-113.
- Bronner-Fraser M. 1993. Neural crest cell migration in the developing embryo. *Trends Cell Biol* 3:392-397.
- Bronner-Fraser M. 1995. Origins and developmental potential of the neural crest. *Exp Cell Res* 218:405-417.
- Bronner-Fraser M. 1998. Inductive Interactions Underlie Neural Crest Formation. *Adv Pharmacol* 142:883-886.
- Browne TR. 1980. Valproic Acid. *Medical Intelligence* 302:661-666.
- Buehler B, Rao V, and Finnell R. 1994. Biochemical and molecular teratology of fetal hydantoin syndrome. *Neurol Clin* 4:741-747.
- Burridge K, Turner C, and Romer L. 1992. Tyrosine phosphorylation of paxillin and pp125PTK accompanies cell adhesion to extracellular matrix: a role in cytoskeletal assembly. *J Cell Biol* 119:893-903.
- Buta J. 1975. Spina bifida occulta and spina bifida cystica and related manifestations. *Michigan Medicine* 74:451-454.
- Campbell L, Dayton D, and Sohal G. 1986. Neural tube defects: a review of human and animal studies on the etiology of neural tube defects. *Teratology* 34:171-187.
- Cary L, Chang J, and Guan J. 1996. Stimulation of cell migration by over expression of focal adhesion kinase and its association with Src and Fyn. *J Cell Sci* 109:1787-1794.
- Citrome L, Levine J, and Allingham B. 2000. Changes in the use of valproate and other mood stabilizers for patients with schizophrenia from 1994 to 1998. *Psychiatr Serv* 51:634-8.
- Clarke DO and Brown NA. 1987. Valproic acid teratogenesis and embryonic lipid metabolism. *Arch Toxicol Suppl* 11:143-147.
- Clayton-Smith J and Donnai D. 1995. Fetal valproate syndrome. *J Med Genet* 32:724-727.

- Copp A, Brook F, Estileiro J, Shum A, and Cockroft D. 1990. The embryonic development of mammalian neural tube defects. *Prog Neurobiol* 35:363-403.
- Copp A, Brook F, and Roberts H. 1988. A cell-type-specific abnormality of cell proliferation in mutant (curly tail) mouse embryos developing spinal neural tube defects. *Development* 104:285-295.
- Craig JC, Bennett GD, Miranda RC, Mackler SA, and Finnell RH. 2000. Ribonucleotide reductase subunit R1: a gene conferring sensitivity to valproic acid-induced neural tube defects in mice. *Teratology* 61:305-313.
- Davis LL, Ryan W, Adinoff B, and Petty F. 2000. Comprehensive review of the psychiatric uses of valproate. *J Clin Psychopharmacol* 20:1s-17s.
- Debby-Brafman A, Burstyn-Cohen T, Klar A, and Kalcheim C. 1999. F-spondin, expressed in somite regions avoided by neural crest cells, mediates inhibition of distinct somite domains to neural crest migration. *Neuron* 22:475-488.
- Delannet M and Duband J-L. 1992. Transforming growth factor- β control of cell-substratum adhesion during avian neural crest cell emigration in vitro. *Development* 116:275-287.
- Desban N and Duband J-L. 1997. Avian neural crest cell migration on laminin: interaction of the $\alpha 1\beta 1$ integrin with distinct laminin-1 domains mediates different adhesive properties. *J Cell Sci* 110:2729-2744.
- DeSesso J, Scialli A, and Holson J. 1999. Apparent lability of Neural tube Closure in Laboratory animals and Humans. *Am J Med Genet* 87:143-162.
- Dodge JC, Illig AM, Snyder PJ, and Badura LL. 2000. GABA levels within the medial preoptic area: effects of chronic administration of sodium valproic acid. *Psychoneuroendocrinology* 25:519-534.
- Donovan SJ, Stewert JW, Nunes EV, Quitkin FM, Parides M, Daniel W, Susser E, and Klein DF. 2000. Divalproex treatment for youth with explosive temper and mood lability: a double blind, placebo-controlled crossover design. *Am J Psychol* 157:818-820.
- Duband D, Volberg T, Sabanay T, Thiery J, and Geiger B. 1988. Spatial and temporal distribution of the adherens junction-associated adhesion molecule A-CAM during avian embryogenesis. *Development* 103:325-344.
- Ehlers K, Sturje H, Merker H-J, and Nau H. 1992. Spina bifida aperta induced by valproic acid and by all-trans-retinoic acid in the mouse: distinct differences in morphology and periods of sensitivity. *Teratology* 46:117-130.

- Eikholt B, Mackenzie S, Graham A, Walsh F, and Doherty P. 1999. Evidence for collapsin-1 functioning in the control of neural crest cell migration in both trunk and hindbrain regions. *Development* 126:2181-2189.
- Erickson C and Perris R. 1993. The role of cell-cell and cell-matrix interactions in the morphogenesis of the neural crest. *Dev Biol* 159:60-74.
- Erickson C and Reedy M. 1998. Neural crest development: the interplay between morphogenesis and cell differentiation. *Curr Top Dev Biol* 40:177-209.
- Failla A, Wernig M, Consalez G, Hostick U, Hofmann C, Hustert E, Boncinelli E, Balling R, and Nadeau J. 2000. A mouse model for valproate teratogenicity: parental effects, homeotic transformations, and altered HOX expression. *Hum Mol Genet* 9:227-236.
- Fleming A and Copp AJ. 2000. A genetic risk factor for mouse neural tube defects: defining the embryonic basis. *Hum Mol Genet* 9:575-581.
- Garcia-Castro M and Bronner-Fraser M. 1999. Induction and differentiation of the neural crest. *Curr Opin in Cell Biol* 11:695-698.
- Garcia-Castro M, Veilmetter E, and Bronner-Fraser M. 2000. N-Cadherin, a cell adhesion molecule involved in establishment of embryonic left-right asymmetry. *Science* 288:1047-1051.
- Gofflot F, Nassogne MC, Etzion T, van Maele-Fabry G, Evrard P, and Picard JJ. 1995. In Vitro neuroteratogenicity of valproic acid and 4-en-VPA. *Neurotoxicol Teratol* 17:425-435.
- Gofflot F, van Maele-Fabry G, and Picard JJ. 1996. Cranial nerves and ganglia are altered after in vitro treatment of mouse embryos with valproic acid (VPA) and 4-en-VPA. *Dev Brain Res* 93:62-69.
- Gumbiner B. 2000. Regulation of Cadherin Adhesive Activity. *J Cell Biol* 148:399-403.
- Hall A. 1998. Rho GTPases and the actin cytoskeleton. *Science* 279:509-514.
- Hamburger V. and Hamilton H. 1951. A series of normal stages of development of the chick embryo. *J Morph* 88:49-92.
- Hanold K. 1984. Teratogenic potential of valproic acid. *JOGNN* Mar/Apr 1986 111-116.

Henderson D and Copp A. 1997. Role of the extracellular matrix in neural crest cell migration. *J Anat* 191:507-515.

Henderson D, Ybot-Gonzales P, and Copp A. 1997. Over expression of the chondroitin sulphate proteoglycan versican is associated with defective neural crest cell migration in the Pax-3 mutant mouse (Splotch). *Mech Dev* 69:39-51.

Hishida R and Nau H. 1998. VPA-induced neural tube defects in mice. I. Altered metabolism of sulfur amino acids and glutathione. *Teratogenesis Carcinog Mutagen* 18:49-61.

Hori H, Terao T, Shiraishi Y, and Nakamura J. 2000. Treatment of Charles Bonnet syndrome with valproate. *Int Clin Psychopharmacol* 15:117-119.

Horwitz A and Parsons J. Cell Migration—Movin' On. *Science* 286:1102-1103.

Huttenlocher A, Palecek SP, Lu Q, Zhang W, Mellgren RL, Lauffenburger DA, Ginsberg MH, Horwitz AF. 1997. Regulation of cell migration by the calcium-dependent protease calpain. *J Biol Chem* 272:32719-22.

Ichiyama T, Okada K, Lipton JM, Matsubara T, Hayashi T, and Furukawa S. 2000. Sodium valproate inhibits production of TNF-alpha and IL-6 and activation of NF-kappaB. *Brain Res* 857:246-251.

Ilc D, Furuta Y, Kanazawa S, Takeda N, Sobue K, Nakatsuji N, Nomura S, Fujimoto J, Okada M, Yamamoto T and others. 1995. Reduced cell motility and enhanced focal adhesion contact formation in cells from FAK-deficient mice. *Nature* 377:539-544.

Ingber D. 1993. Cellular Tensegrity: Defining new rules of biological design that govern the cytoskeleton. *J Cell Sci* 104:467-475.

Johannessen CU. 2000. Mechanisms of action of valproate: a commentary. *Neurochem Int* 37:103-110.

Kelly P and Regan C. 1992. Studies on valproate-induced perturbations of neuralation in the explanted chick embryo. *Toxicology* 71:137-144.

Kerr RS and Newgreen DF. 1997. Isolation and characterization of chondroitin sulfate proteoglycans from embryonic quail that influence neural crest cell behavior. *Dev Biol* 192:108-124.

Klemke R, Yebra M, Bayna E, and Cheresch D. 1994. Receptor tyrosine kinase signaling required for integrin alpha v beta 5-directed cell motility but not adhesion on vitronectin. *J Cell Biol* 127:859-866.

- Klinghoffer RA, Sachsenmaier C, Cooper JA, Soriano P. 1999. Src family kinases are required for integrin but not PDGFR signal transduction. *EMBO J* 18:2459-71.
- Komada M and Kitamura N. 1993. The cell dissociation and motility triggered by scatter factor/hepatocyte growth factor are mediated through the cytoplasmic domain of the c-Met receptor. *Oncogene* 8:2381-2390.
- Komuro H and Rakie P. 1993. Modulation of neuronal migration by NMDA receptors. *Science* 260:95-97.
- Kornberg L, Earp H, Parsons J, Schaller M and Juliano R. 1992. Cell adhesion or integrin clustering increases phosphorylation of a focal adhesion-associated tyrosine kinase. *J Biol Chem* 267:23439-23442.
- Krätke R and Kirschbaum F. 1996. Effects of the antiepileptic drug valproic Acid on the development of the axolotl (*Ambystoma mexicanum*): Histological investigations. *Teratogenesis Carcinog Mutagen* 16:149-167.
- Krull C. 1998. Inhibitory Interactions in the Patterning of Trunk Neural Crest Migration. *Ann N Y Acad Sci* 857:13-22.
- LaBonne C and Bronner-Fraser M. 1998. Induction and Patterning of the Neural Crest, a Stem Cell Like Precursor Population. *J Neurobiol* 36:175-189.
- Lammer EJ, Sever LE, and Oakley GP. 1987. Teratogen Update: Valproic Acid. *Teratology* 35:465-473.
- Landolt R, Vaughan L, Winterhalter K, and Zimmerman D. 1995. Versican is selectively expressed in embryonic tissues that act as barriers to neural crest cell migration and axon outgrowth. *Development* 121:2303-2312.
- Lennkh C, and Simhandl C. 2000. Current aspects of valproate in bipolar disorder. *Int Clin Psychopharmacol* 15:1-11.
- Lewis D, Van Dyke DC, Stumbo P, and Berg M. 1998. Drugs and Environmental Factors Associated with Adverse Pregnancy Outcomes. *Ann Pharmacother* 32:802-817.
- Li H, Leung T, Hoffman S, Balsamo J, and Lilien J. 2000. Coordinate Regulation of Cadherin and Integrin Function by the Chondroitin Sulfate Proteoglycan Neurocan. *J Cell Biol* 149:1275-1288.

- Liem K Jr, Tremml G, and Jessell T. 1997. A role for the roof plate and its resident TGFbeta-related proteins in neuronal patterning in the dorsal spinal cord. *Cell* 91:127-138.
- Liem K Jr, Tremml G, Roelink H and Jessell T. 1995. Dorsal differentiation of neural plate cells induced by BMP-mediated signals from epidermal ectoderm. *Cell* 82:969-979
- Lipfert L, Haimovich B, Schaller M, Cobb B, Parsons J and Brugge J. 1992. Integrin-dependent phosphorylation and activation of the protein tyrosine kinase pp125FAK in platelets. *J Cell Biol* 119:905-912.
- Liu J-P and Jessell T. 1998. A role for rhoB in the delamination of neural crest cells from the dorsal neural tube. *Development* 125:5055-5067.
- Loscher W. 1993. In vivo administration of valproate reduces the (synaptosomal) activity of GABA aminotransferase in discrete brain nerve terminal areas of rats. *Neurosci Lett* 160:177-80.
- Martin M and Regan C. 1997. The anticonvulsant valproate teratogen restricts the glial cell cycle at a defined point in the mid G-1 phase. *Brain Res* 554:223-228.
- Minichiello J, Ben-Ya'acov A, Hearn C, Needham B, and Newgreen D. 1999. Induction of epithelial-mesenchymal transformation of quail embryonic neural cells by inhibition of atypical protein kinase-C. *Cell Tissue Res* 295:195-206.
- Mitchell PB. 1999. The place of anticonvulsants and other putative mood stabilisers in the treatment of bipolar disorder. *Aust N Z J Psychiatry* 33 Suppl:99-107.
- Moase C and Trasler D. 1990. Delayed neural crest cell emigration from Sd and Sd^d mouse neural tube explants. *Teratology* 42:171-182.
- Moase C and Trasler D. 1991. N-CAM alterations in splotch neural tube defect mouse embryos. *Development* 113:1049-1058.
- Monier-Gavelle F and Duband J-L. 1995. Control of N-cadherin mediated intercellular adhesion in migrating neural crest cells in vitro. *J Cell Sci* 108:3839-3853.
- Monier-Gavelle F and Duband J-L. 1997. Cross Talk between Adhesion Molecules: Control of N-Cadherin Activity by Intracellular Signals Elicited by $\beta 1$ and $\beta 3$ Integrins in Migrating Neural Crest Cells. *J Cell Biol* 137:1663-1681.
- Nakagawa S and Takeichi M. 1995. Neural crest cell-cell adhesion controlled by sequential and subpopulation-specific expression of novel cadherins. *Development* 12:1321-1332.

- Narotsky MG, Francis EZ, and Kavvlock RJ. 1994. Developmental toxicity and structure-activity relationships of aliphatic acids, including dose-response assessment of valproic acid in mice and rats. *Fun Appl Tox* 22:251-265.
- Nau H. 1985. Teratogenic valproic acid concentrations: Infusion by implanted minipumps vs. conventional injection regimen in the mouse. *Toxicol Appl Pharmacol* 80:243-250.
- Nau H. 1986a. Transfer of valproic acid and its main active unsaturated metabolite to the gestational tissue: correlation with neural tube defect formation in the mouse. *Teratology* 33:21-27.
- Nau H. 1986b. Valproic acid teratogenicity in mice after various administration and phenobarbital-pretreatment regimens: The parent drug and not one of the metabolites assayed is implicated as teratogen. *Fun Appl Tox* 6:662-668.
- Nau H. 1994. Valproic acid-induced neural tube defects. Neural tube defects. Ciba Foundation Symposium 181 144-160.
- Nau H, Hauck R-S, and Ehlers K. 1991. Valproic-acid induced neural tube defects in mouse and human: aspects of chirality, alternative drug development, pharmacokinetics and possible mechanisms. *Pharm Tox* 69:310-321.
- Newgreen D, Kerr R, Minichiello J, and Warren N. 1997. Changes in cell adhesion and extracellular matrix molecules in spontaneous spinal neural tube defects in avian embryos. *Teratology* 55:15-207.
- Nulman I, Laslo D, and Koren G. 1999. Treatment of epilepsy in pregnancy. *Drugs* 57:535-544.
- Orris AS, Banicky LC, and Wiens DJ. 1999. Isotretinoin alters morphology, polarity, and motility of neural crest cells in culture. *Rep Tox* 13:45-52.
- Otoom SA and Alkadhi KA. 1999. Valproic acid intensifies epileptiform activity in the hippocampal pyramidal neurons. *Neurosci Res* 35:299-307.
- Perris R, Krotoski D, and Bronner-Fraser M. 1991. Collages in avian neural crest development: distribution *in vivo* and migration-promoting ability *in vitro*. *Development* 113:969-984.
- Perris R, Perissinotto D, Pettway Z, Bronner-Fraser M, Morgelin M and Kimata K. 1996. Inhibitory effects of PGH/aggreacan and PG-M/versican on avian neural crest cell migration. *FASEB* 10:293-301.

- Rashid N and Cambray-Deakin M. 1992. N-methyl-D-aspartate effects on the growth, morphology, and cytoskeleton of individual neurons *in vitro*. *Brain Res Dev Brain Res* 67:301-308.
- Regan CM, Gorman AM, and Larsson OM. 1990. In vitro screening for anticonvulsant – induced teratogenesis in neural primary cultures and cell lines. *Int J Develop Neurosci* 8:143-150.
- Richardson A and Parsons J. 1995. Signal transduction through integrins: a central role for focal adhesion kinase? *Bioessays* 17:229-236.
- Ring C, Hassell J, and Halfter W. 1996. Expression pattern of collagen IX and potential role in the segmentation of the peripheral nervous system. *Dev Biol* 180:41-53.
- Rosenquist T, Ratashak S, and Selhub J. 1996. Homocysteine induces congenital heart and neural tube defects. Effect of folic acid. *Proc Natl Acad Sci USA* 93:15227-15232.
- Rosenquist T, Schneider A, and Monaghan D. 1999. N-methyl-D-aspartate receptor agonists modulate homocysteine-induced developmental abnormalities. *FASEB J* 13:1523-1531.
- Sands SA, Guerra V, and Morilak DA. 1999. Changes in tyrosine hydroxylase mRNA expression in the rat locus coreuleus following acute or chronic treatment with valproic acid. *Neuropsychopharmacology* 22:27-35.
- Sato M, Shirota M, and Nagao T. 1995. Pantothenic acid decreases valproic acid-induced neural tube defects in mice. *Teratology* 52:143-148.
- Schaller M, Borgman C, Cobb B, Vines R, Reynolds A, and Parsons J. 1992. pp125FAK a structurally distinctive protein-tyrosine kinase associated with focal adhesions. *Proc Natl Acad Sci USA* 89:5192-5196.
- Selleck M and Bronner-Fraser M. 1996. The genesis of avian neural crest cells: a classic embryonic induction. *Proc Natl Acad Sci* 93:9352-9357.
- Serbedzija G, Bronner-Fraser M, and Fraser S. 1994. Developmental potential of trunk neural crest cells in the mouse. *Development* 120:1709-1718.
- Shah N, Groves A, and Anderson D. 1996. Alternative neural crest cell fates are instructively promoted by TGF beta superfamily members. *Cell* 85:331-343.
- Sieber-Blum M and Zhang J. 1997. Growth factor action in neural crest cell diversification. *J Anat* 191:493-499.

- Sieg DJ, Hauck CR, Schlaepfer DD. 1999. Required role of focal adhesion kinase (FAK) for integrin-stimulated cell migration. *J Cell Sci* 112:2677-91.
- Stemple D, and Anderson D. 1992. Isolation of a stem cell factor for neurons and glia from the mammalian neural crest. *Cell* 71:973-985.
- Stossel T. 1993. On the crawling of animal cells. *Science* 260:1086-1094.
- Tamura T, Aiso K, Johnston K, Black L, and Faught E. 2000. Homocysteine, folate, vitamin B-12 and Vitamin B-6 in patients receiving antiepileptic drug monotherapy. *Epilepsy Res* 40:7-15.
- Tennyson V, Payette R, Rothman T and Gershon M. 1990. Distribution of hyaluronic acid and chondroitin sulfate proteoglycans in the presumptive aganglionic bowel of *ls/ls* fetal mice: An ultrastructural analysis. *J Comp Neurol* 291:345-362.
- Testaz S, Delannet M, and Duband J. 1999. Adhesion and migration of avian neural crest cells on fibronectin require the cooperating activities of multiple integrins of the $\beta 1$ and $\beta 3$ Families. *J Cell Sci* 112:4715-4728.
- Tucker R, Hagios, Chiquet-Ehrismann R, Lawler J, Hall R and Erickson C. 1999. Thrombospondin-1 and Neural Crest Cell Migration. *Dev Dyn* 214:312-322.
- Tunnicliff G. 1999. Actions of sodium valproate on the central nervous system. *J Physiol Pharmacol* 50:347-65.
- Vaglia J, and Hall B. 1999. Regulation of neural crest cell populations: occurrence, distribution, and underlying mechanisms. *Int J Dev Biol* 43:95-110.
- Van Aelst L and D'Souza-Schorey C. 1997. Rho GTPases and signaling networks. *Genes Dev* 11:2295-2322.
- Van Straaten H, Janssen H, Peeters M, Copp A, and Hekking J. 1996. Neural tube closure in the chick embryo is multiphasic. *Dev Dyn* 207:309-318.
- Volk T, Volberg T, Sabanay I, Geiger B. 1990. Cleavage of A-CAM by endogenous proteinases in cultured lens cells and in developing chick embryos. *Dev Biol* 139:314-26.
- Walmod P, Foley A, Berezin A, Ellerbeck U, Nau H, Bock E, and Berezin V. 1998. Cell motility is inhibited by the antiepileptic compound, valproic acid and its teratogenic analogues. *Cell Motil Cytoskeleton* 40:220-237.

Walmod P, Skladchikova G, Kawa A, Berezin V, and Bock E. 1999. Antiepileptic teratogen Valproic Acid (VPA) modulates organization and dynamics of the actin cytoskeleton. *Cell Motil Cytoskeleton* 42:241-255.

Wegner C, Drews E, and Nau H. 1990. Zinc concentrations in mouse embryo and maternal plasma. Effect of valproic acid and nonteratogenic metabolite. *Biol Trace Elem Res* 3:211-217.

Wenstrom K. 1996. Understanding how neural tube defects occur—and can be prevented. *Medscape Womens Health* Dec 1:6.

Whittle BA. 1976. Pre-clinical, teratological studies on sodium valproate and other anti-convulsants. In: Legg NJ ed. *Clinical and Pharmacological Aspects of Sodium Valproate In the Treatment of Epilepsy*. Turnbridge Wells, England: MCS consultants, 1976. p. 1976:105-110.

Wiens DJ, Mann TK, Fedderson DE, Rathmell WK, and Frank BH. 1992. Early heart development in the chick embryo: effects of isotretinoin on cell proliferation, alpha-actin synthesis, and development of contractions. *Differentiation* 51:105-112.

Wulf E, Deboben A, Bautz FA, Faulstich H and Wieland T. 1976. Fluorescent phallotoxin, a tool for the visualization of cellular actin. *Proc Natl Acad Sci* 76:4498:4502.

Yerby M. 1994. Pregnancy, Teratogenesis, and Epilepsy. *Pediatric Neurogenetics* 12:749-771.